Master's Thesis of Engineering

Study on Shrinkage Prediction Models and Restraint Crack Formation in Unbonded Post-Tensioned Slabs

비부착 포스트텐션 슬래브의 수축 예측모델과 구속균열 형성에 관한 연구

August 2021

Graduate School of Engineering

Seoul National University

Architecture and Architectural Engineering

Gabriela Renee Martinez Lara

Study on Shrinkage Prediction Models and Restraint Crack Formation in Unbonded Post-Tensioned Slabs

Advisor: Thomas Kang

Submitting a Master's thesis of
Architecture and Architectural Engineering

August 2021

Graduate School of Engineering
Seoul National University
Architecture and Architectural Engineering

Gabriela Renee Martinez Lara

Confirming the Master's thesis written by
Gabriela Renee Martinez Lara

July 2021

Chair Sung-Gul Hong
Vice Chair Thomas Kang
Examiner Cheol Ho Lee

Abstract

Study on Shrinkage Prediction Models and Restraint Crack Formation in Unbonded Post-Tensioned Slabs

Gabriela Renee Martinez Lara[1]
Department of Architecture and Architectural Engineering
College of Engineering
Seoul National University

Most of the time, when developing the structural design of a building, deflection-induced cracking is analyzed and measures to prevent serviceability issues regarding deflection are considered in the design. However, crack formation in concrete structures is also produced by restrain-to-shortening effects induced by volume changes in the members through the passage of time and environmental effects. Therefore, the estimation of creep-and-shrinkage-induced stresses, and the inclusion of restraining crack mitigation details should be included in the slab design process. The first part of this study focuses on the comparison of seven published shrinkage and creep calculation models that

[1] The author of this thesis is a Global Korea Scholarship scholar sponsored by the Korean Government.

aim to predict a concrete member's volume-changing behavior. The second part of this study presents a series of architectural configuration prototypes analyzed through a FEM software, where a shrinkage and creep model strain results from part I are used, to determine the combination of shrinkage-and-creep-induced volumetric changes and restraint configuration that can lead to cracking in unbonded post-tensioned slabs and observe the overall behavior of these slabs.

From the selected shrinkage models, the GL 2000 model (N. J. Gardner & Lockman, 2001) was the one showing the largest creep and shrinkage results and therefore it was the one selected for the analysis. The analysis results show that restraints tend to increase tension and also compression in the slabs, which suggests that they reduce the efficiency and spread of prestressing forces. The results also show that the increase in length does not exert a significant increase in tensile stresses compared to the effect of restraining walls, and that in case of having perimeter walls a partial wall release would be more effective than a pour strip.

Keywords: Shrinkage prediction, Crack formation, Post-tensioning concrete slabs, Restraint crack

Student Number: 2019-28364

Contents

List of Tables

List of Figures

List of Notations

a/c	=	Aggregate-cement ratio
A_s	=	Minimum area of bonded reinforcement in mm^2 or in^2
c	=	Cement content in kg/m^3 or lb/yd^3
E	=	Modulus of elasticity in MPa or psi
E_{cmt0}	=	mean modulus of elasticity of concrete when loading starts at age t_0, MPa or psi
f_c'	=	Concrete specified 28-day strength in MPa or psi
f_t'	=	Tensile splitting strength in MPa or psi
f_y	=	Minimum yield stress MPa or psi
f_u	=	Minimum tensile strength MPa or psi
h	=	Relative humidity in decimals
$J(t,t_0)$	=	compliance at concrete age t when loading starts at age t_0, 1/MPa or 1/psi
k_s	=	Average precompression in MPa or psi
N_c	=	Resultant tensile force in MPa or psi
s	=	Concrete slump in mm or in.
T	=	Temperature in °C or °F
t	=	Concrete age in days
t_0	=	Age at loading in days
t_c	=	Age when drying begins, usually at the end of curing, in days
U	=	Poisson's ratio
V/S	=	Volume-surface ratio in mm or in.
w	=	Water content in kg/m^3 or lb/yd^3
α	=	Coefficient of thermal expansion
α_c	=	Air content in percentage

γ	=	Unit weight in kg/m^3 or lb/yd^3
ΔL	=	Final shortening in mm or in.
ΔT	=	Temperature change in °C or °F
ε_{cr}	=	Final creep strain in mm/mm or in./in.
ε_{es}	=	Elastic strain in mm/mm or in./in.
ε_T	=	Thermal strain in mm/mm or in./in.
ε_{sh}	=	Final shrinkage strain in mm/mm or in./in.
σ	=	Average precompressive stress in MPa or psi
$\varphi(t,t_0)$	=	Creep coefficient (dimensionless)
ψ	=	Fine aggregate percentage

Chapter 1. Introduction

1.1 Introduction

Crack formation in reinforced and prestressed concrete structures can significantly affect the performance and lifespan of buildings. Usually, when developing the structural design of a building, deflection-induced cracking is analyzed and measures to prevent serviceability issues regarding deflection are considered in the design of concrete structures. However, crack formation in concrete structures is developed by other causes apart from deflection effects, such as the case of restrain-to-shortening effects induced by volume changes in the members. Structural engineers can often minimize the importance of accurate creep-and-shrinkage-induced strain estimation and restraining crack mitigation details in their slab design.

The first part of this study focuses on the comparison of seven published shrinkage and creep calculation models that aim to predict a concrete member's volume-changing behavior. The second part of this study presents a series of architectural configuration prototypes analyzed using ETABS 2017, where the most appropriate shrinkage and creep model strain results from part I is used, to determine the combination of shrinkage-and-creep-induced volumetric changes and restraint configuration that can lead to cracking in unbonded post-tensioned slabs.

The shrinkage and creep calculation models to be compared are the ACI 209R-92 (ACI Committee 209, 1992) model, the Bažant-Baweja B3 model (Bazant & Baweja, 1995), CEB MC90-99 model (CEB-FIP, 1999), GL2000 model (N. J. Gardner & Lockman, 2001), the PCI Industry Handbook 6th Edition model (Precast/Prestressed Concrete Institute, 2004), the AASHTO model (Al-Omaishi, Tadros & Seguirant, 2009) and the Bažant B4 model (Bazant, Jirásek,

Hubler & Carol, 2015). Even though these models promise different degrees of accuracy and produce an estimation based on different quantities of parameters, in reality, an accuracy of 50% is considered more than ideal even in the one deemed the most accurate among them, due to the unpredictability of the real site conditions.

Although, in theory, volume-changing behavior in unbonded and bonded slabs should be similar when the slab has the same composition and is subjected to the same environmental conditions and loads, the appearance of cracks can be significantly different. Slabs with bonded reinforcement, when subjected to shrinkage and creep effects, will produce smaller shallow cracks, closer to each other and spread in the central area of the slab span. While slabs that have unbonded reinforcement will produce less cracks with a larger separation between each other, although they will be longer and may be opened throughout the thickness of the slab.

Due to the characteristics of unbonded post-tensioned slabs, creep and shrinkage effects may be greater because of the prestressing forces and because they have less bonded reinforcement. Effects of movements due to creep and shrinkage may require more attention than is normally required for nonprestressed concrete and these movements may increase prestress losses (ACI Committee 318, 2019). Therefore, this study focuses only on the restraint effects occurring in unbonded post-tensioned slabs.

1.2 Scope and Objectives

As mentioned, there are many different shrinkage and creep prediction models that take into account different variables but there is no consensus for the influence that different restraint configurations could have in the slabs when they are subjected to volume-changing effects. The results obtained from these models are for the concrete member observed individually, but do not consider

the restraint actions that can occur between members that are connected. The use of a creep and shrinkage calculation model is just one step of many for the prediction of crack formation in the design of a post-tensioned slab.

Therefore, the goal of this study is to conduct an analysis of the application of these models and determine which model could be more appropriate in the design of unbonded post-tensioned slabs. Then this model is applied in the FEM analysis of restraint effects in different post-tensioned slab configuration prototypes, and through the analysis, it is attempted to determine which of these prototypes could suffer a more significant cracking behavior that could be detrimental to the post-tensioned slab's intended performance.

1.3 Organization

This thesis consists of 5 main chapters. The introduction of the study is shown in Chapter 1. The literature reviews pertaining to the shrinkage and creep calculation models and the previous papers written regarding shrinkage behavior are shown in Chapter 2. In Chapter 3 different available shrinkage prediction models are compared and studied, and one of them is selected for further analysis. Chapter 4 deals with the development of different prototypes where restraint-induced shrinkage effects are studied. Chapter 5 discusses the results obtained through the FEM modeling of the prototypes. The conclusion of the study is finally presented in Chapter 6.

Chapter 2. Literature Review

2.1 Shrinkage and Creep Calculation Models

Throughout the years, several models to predict shrinkage and creep behavior in structural concrete members have been developed, and some of them have been periodically updated thanks to the development of new concrete formulations and admixtures, and the increased amount of analysis and monitoring of shrinkage and creep behavior.

Because there are many factors that influence concrete shortening, and due to their unpredictability monitoring of these in a real construction setup is very difficult, it is normal for a prediction model to have an error percentage of 30 to 50% from the test results (Guo & Joseph, 2013).

Regardless, it is important to account for shrinkage and creep effects during the design process of a concrete member to avoid problems during the building's lifetime, or even during its construction period. There are several considerations for the selection of models, such as how simple or complex should it be, how easy the calculation process is, what data is available at the time of calculation, and how closely it is representing the real behavior.

The selection of the model based on accuracy could be defined by the building's importance, use, complexity, and size. If the building is defined as high on these characteristics, it is usually recommended to dedicate a larger amount of time to the analysis of creep and shrinkage by using a model that considers a larger amount of parameters, and even to accompany this computational analysis with a short-term testing of the concrete to be used.

As mentioned, the models selected for comparison in this study are the ACI 209R-92 (1992) model, the Bažant-Baweja B3 model (1995), CEB MC90-99

model (1999), GL2000 model (2001), the PCI Industry Handbook 6th Edition model (2004), the AASHTO model (2009) and a more recent update to the B3 model, the Bažant B4 model (2015). The parameters considered in each model are listed in **Table 2-1**.

Table 2-1 Model Parameters

Parameters Included in Prediction Models					
Parameters	Imperial	Metric	B3 Model	CEB MC90-99	GL2000
Age of concrete	days				
Age of concrete when drying begins (Environmental exposure)	days		✓	✓	✓
Age of concrete at loading	days		✓	✓	✓
Aggregate content	lb/yd^3	kg/m^3	✓		
Cement content	lb/yd^3	kg/m^3	✓		
Water content	lb/yd^3	kg/m^3	✓		
Cement type	TYPE		✓	✓	
Concrete mean strength at 28 days	MPa	psi	✓	✓	✓
Concrete mean strength at loading	MPa	psi			✓
Modulus of elasticity at 28 days	MPa	psi	✓		✓
Modulus of elasticity at loading	MPa	psi			✓
Curing condition	TYPE		✓		
Relative humidity	Decimal		✓	✓	✓
Shape of specimen			✓		
v/s ratio	in	mm	✓	✓	✓
Concrete slump	in	mm			
Fine aggregate percentage	Percentage				
Air content	Percentage				
Temperature	C°	F°		✓	
Average prestress	MPa	psi			
Type of concrete (Lightweight or normal weight)	TYPE				
Aggregate type	TYPE				
Curing temperature	C°	F°		✓	
Mass density of concrete (In case)	kip/ft^3	kg/m^3			
Admixture type (In case)	TYPE				
Activation energies of moisture and creep (In case)	Joules				
Aggregate stiffness (In case)	Factor (by test)				

Parameters Included in Prediction Models (cont.)						
Parameters	Imperial	Metric	ACI 209	PCI	B4 Model	AASHTO
Age of concrete	days				✓	✓
Age of concrete when drying begins (environmental exposure)	days		✓		✓	✓
Age of concrete at loading	days		✓		✓	✓
Aggregate content	lb/yd^3	kg/m^3			✓	
Cement content	lb/yd^3	kg/m^3	✓		✓	
Water content	lb/yd^3	kg/m^3			✓	
Cement type	TYPE		✓		✓	
Concrete mean strength at 28 days	MPa	psi		✓	✓	✓
Concrete mean strength at loading	MPa	psi				✓
Modulus of elasticity at 28 days	MPa	psi			✓	✓
Modulus of elasticity at loading	MPa	psi				✓
Curing condition	TYPE		✓	✓		✓
Relative humidity	Decimal		✓	✓	✓	✓
Shape of specimen					✓	
v/s ratio	in	mm	✓	✓	✓	✓
Concrete slump	in	mm	✓			
Fine aggregate percentage	Percentage		✓			
Air content	Percentage		✓			
Temperature	C°	F°			✓	✓
Average prestress	MPa	psi		✓		
Type of concrete (lighweight or normalweight)	TYPE			✓		
Aggregate type	TYPE				✓	✓
Curing temperature	C°	F°			✓	
Mass density of concrete	kip/ft^3	kg/m^3			✓	✓
Admixture type (In case)	TYPE				✓	
Activation energies of moisture and creep (In case)	Joules				✓	
Aggregate stiffness (In case)	Factor (by test)					✓

2.1.1 ACI 209R-92 Model

This model was developed by the American Concrete Institute Committee 209 in the year 1992, and it was initially developed for the precast/prestressing industry. Since its release it has not been updated. It has been commonly used in the industry and its advantage is that it is simple to use. However, its disadvantages are limited accuracy and that it calculates creep through creep coefficient rather than compliance. A comparison of this model with the RILEM database (ACI Committee 209, 2008) showed that it overestimates shrinkage at short drying times and overestimates shrinkage at long drying times, and it tends to underestimate creep.

2.1.2 Bažant-Baweja B3 Model

This model was developed by Zdenek Bažant and Sandeep Baweja, through the use of a comprehensive database from RILEM on creep and shrinkage tests. According to Guo and Joseph (2013) it is considered the most accurate model for both shrinkage and creep, and according to Goel, Kumar, and Paul (2007) it is considered the most accurate for shrinkage, even compared to its update, Model B4 in a recent study by Fanourakis (2017). This model's advantages are that it has both a simplified version, therefore allowing for simple or detailed calculation on case of necessity, and a more detailed version accounting for the effects of a wider range of parameters. However, its disadvantage is that it includes parameters that might not be available at the time of calculation. The comparison of this model with the RILEM database (ACI Committee 209, 2008) shows that it has no significant over or underestimation of shrinkage; however, it has a slight underestimation of creep.

2.1.3 CEB MC90-99 Model

This shrinkage and creep model is contained in the CEB-FIP Model Code, developed by the joint associations known as the European Committee for

Concrete and the International Federation for Prestressing, with its last update in the year 1999. It considers autogenous shrinkage and drying shrinkage separately. One of its main disadvantages is that it does not take into account curing condition, which is generally understood as an important parameter for shrinkage prediction. The comparison with the RILEM database (ACI Committee 209, 2008) shows that it tends to underestimate shrinkage and slightly underestimate creep. According to Fanourakis and Ballim (2003) it appears to be less accurate compared to the ACI 209 and B3 models regarding creep.

2.1.4 GL2000 Model

This model developed by N.J. Gardner and M.J. Lockman, is a modification of the previous GZ Atlanta 97 model. This model's main advantage is that it only requires input data easily available at the time of initial design. A comparison with the results from the RILEM database (ACI Committee 209, 2008) show that it does not significantly deviates from shrinkage results and it slightly underestimates creep. Although it uses simple formulas and considers less parameters than many of the other models, according to Fanourakis (2017) and N. Gardner (2004), it appears to be the most accurate among the prediction models, and according to Goel et al. (2007) it appears to be the most accurate for creep and the second most accurate for shrinkage.

2.1.5 PCI Industry Handbook Model

This model was developed by the Precast/Prestressed Concrete Institute and it is included in the PCI Design Handbook (Precast/Prestressed Concrete Institute, 2004). It does not produce results based on equations, rather its modifiers are selected from a series of tables, included in the Handbook, that influence the resulting ultimate shrinkage and ultimate creep values. Although it is a fairly

simple calculation process, this also does not facilitate the plotting of results at different times.

2.1.6 AASHTO Model

Developed by the American Association of State Highway and Transportation Officials, an update of the year 2005 is considered in this study. This later version takes into account high strength concretes and is based on shrinkage analysis performed mainly on prestressed bridge girders. It is highly influenced by the ACI 209R-92 model, but its most recent update was developed thanks to an experimental program conducted at various bridge sites. This model also measures creep strain through the creep coefficient (Al-Omaishi et al., 2009). Because it was developed with results from bridge structures, it might not be accurate for interior slabs, due to the difference in environmental conditions and volumes.

2.1.7 Bažant B4 Model

This model is an update of the B3 model, also developed by Zdenek Bazant. The development of this model considered a more extensive RILEM database of shrinkage tests. This model's main update is the inclusion of the autogenous shrinkage prediction, the consideration of high strength concretes and temperature, and the effects of various admixtures and aggregate types (Bazant et al., 2015). According to a recent study by Fanourakis (2017) it is less accurate than its previous version.

2.2 Previous Studies

2.2.1 Shadravan et al.'s Study

A study by Shadravan, Ramseyer, and Kang (2015) about the volume-changing behavior of concrete slabs-on-ground with different concrete

materials and admixtures in controlled environments was developed. The concrete mixes tested were normal-strength Portland cement concrete (PCC), high-strength concrete (HSC), normal concrete mixes with two types of common shrinkage reducing admixtures (SRA #1 and SRA #2), and normal concrete mixes with two types of calcium sulfo-aluminate cement defined as per ACI Committee 223 (CSA and RSCC). It observed the shrinkage behavior measured from several small-scale specimens following ASTM C 157, ASTM C 878, and shrinkage from time zero test procedures. It also measured the behavior of large-scale slabs-on-ground specimens with the same materials and similar environmental conditions as the small-scale specimens.

The study concluded that the ASTM C 157 specimen method of measuring drying shrinkage is the most accurate for comparison of concrete mix designs; however, it showed over-estimation when compared to the large scale slab-on-ground results, as it can be observed in **Figure 2-1**. This can be attributable to the difference of exposed surface as the specimen has more area exposed compared to the slab-on-ground, and to the difference in volumes.

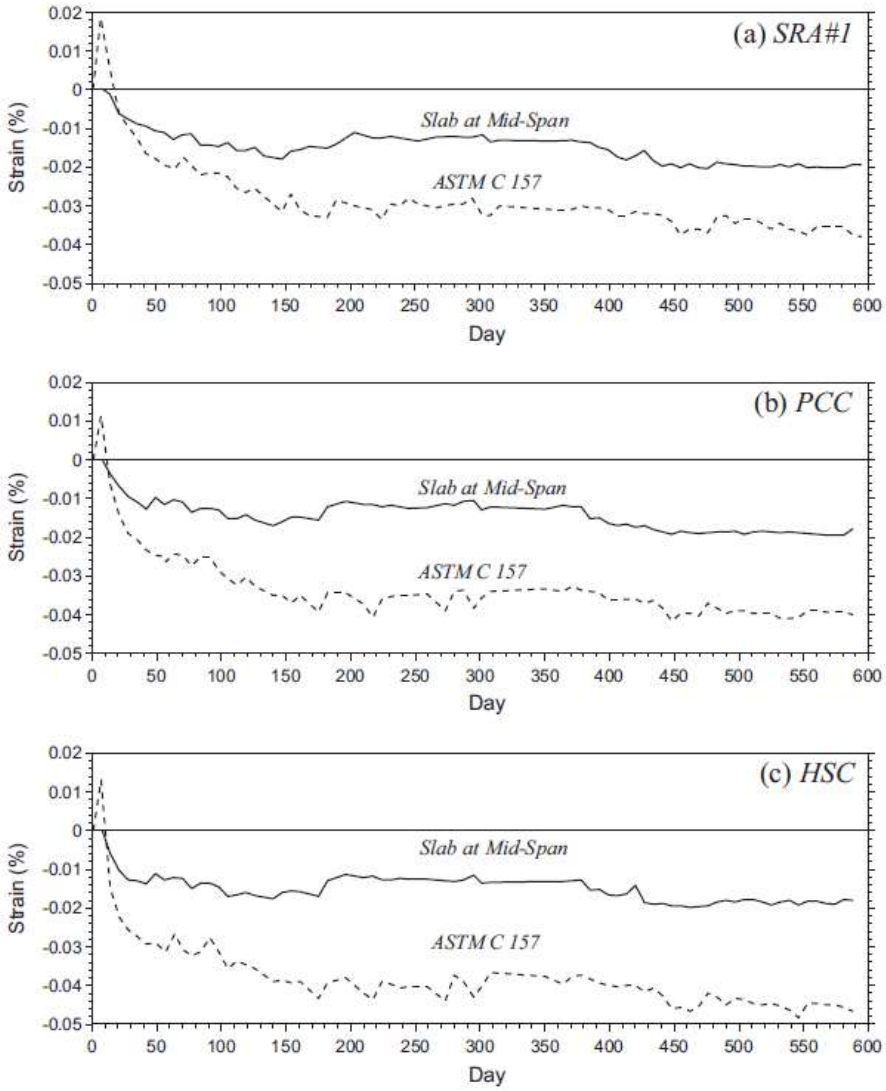

Figure 2-1 Strains of slab-on-ground at mid-span for SRA #1, PCC and HSC in comparison with those obtained from ASTM C 157 test specimens (Shadravan et al., 2015)

It also concluded that, among the tested concrete mixes, high-strength concrete went through the largest shrinkage, while the concrete using calcium sulfo-aluminate cement produced the least shrinkage, as it can be observed in **Figure 2-2** and **Figure 2-3**.

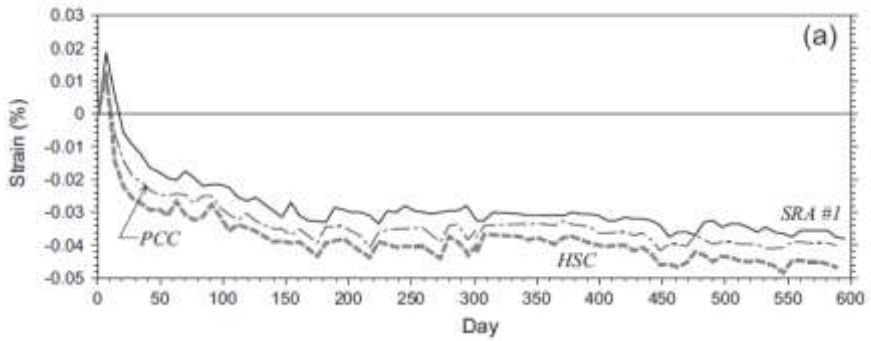

Figure 2-2 Unrestrained expansion ASTM C 157 specimen versus time (PCC, HSC and SRA #1) (Shadravan et al., 2015)

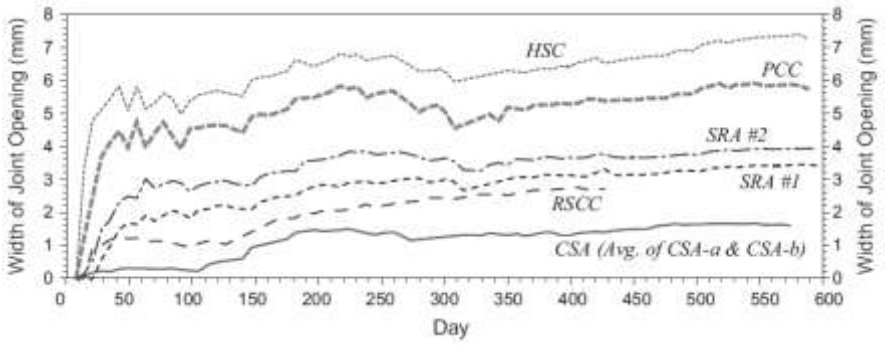

Figure 2-3 Width of slab-on-ground joint opening versus time (Shadravan et al., 2015) (Note: 1 mm = 0.039 in)

2.2.2 Le Roy et al.'s Study

A study by Le Roy, Le Maou, and Torrenti (2016) presents a long-term creep testing of cylinder specimens of high-strength concrete. The tests performed were in compliance with the RILEM TC 107 CSP technical recommendations, with the exception of the weight-loss measurements. The specimens were cylinders with a height of 39 in. (1000 mm) and a diameter of 6.3 in. (160 mm).

The creep results for the specimen B3 can be observed in **Figure 2-4**. This specimen had a specified concrete strength of 13,677 psi (94.3 MPa) and the

applied stress was 4,206 psi (29 MPa). Overall, the majority of concretes tested exhibited a linear long-term behavior when plotted against logarithmic time.

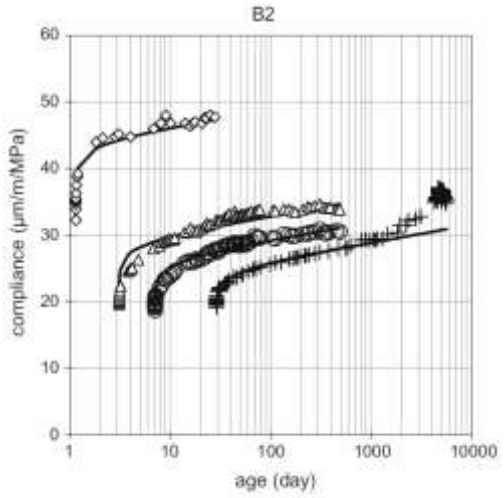

Figure 2-4 Comparison between experimental values and modeling (Le Roy et al., 2016) (Note: 1 mm = 0.039 in.; 1 MPa = 145 psi)

2.2.3 Guo et al.'s Study

A technical paper published in the PTI Journal by Guo, Joseph, and Bieberly (2009) discusses the precompression-reducing and shortening effects of restraints in underground parking slabs and how could these effects be mitigated. A finite element analysis model of an underground parking project with a one-way unbonded post-tensioned slab is presented to analyze the slab precompression loss by restraints in a post-tensioned slab. The framing plan is presented in **Figure 2-5**.

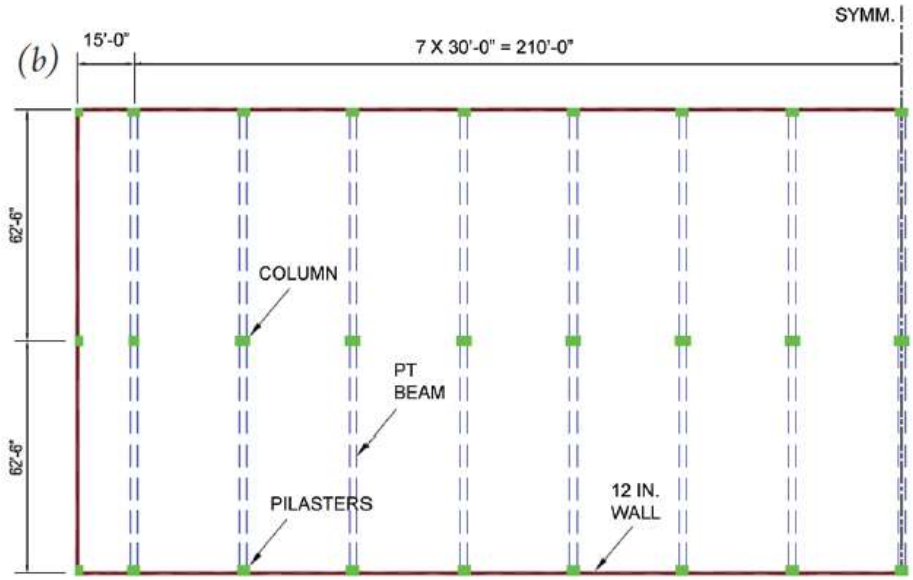

Figure 2-5 Parking structure framing plan. Slab spans numbered sequentially from 1 at left to 8 at right (Guo et al., 2009) (Note: 1 in. = 25.4 mm; 1 ft. = 304.8 mm)

The resulting axial stresses in the longitudinal direction are presented in the paper; Model A (**Figure 2-6**) shows the slab influenced by columns and perimeter walls, Model B (**Figure 2-7**) shows the influence of walls in the short direction and columns, Model C (**Figure 2-8**) shows the influence of only the columns and Model D (**Figure 2-9**) shows the influence of only columns with half of the slab as to simulate the effects of including a pour strip.

Among the presented models, the largest precompression loss is observed in the model that is affected by the walls in both directions of the perimeter, while the least precompression loss is observed in the model that emulates the inclusion of a pour strip.

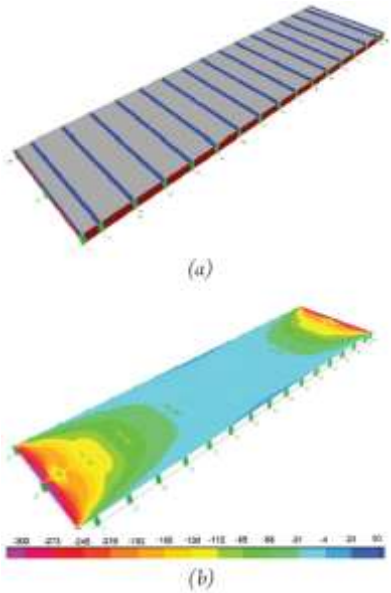

Figure 2-6 Model A with slabs, beams, columns, and perimeter walls: (a) ETABS model; and (b) axial stress from -300 to 50 psi (Guo et al., 2009) (Note: 1 psi = 0.0068 MPa)

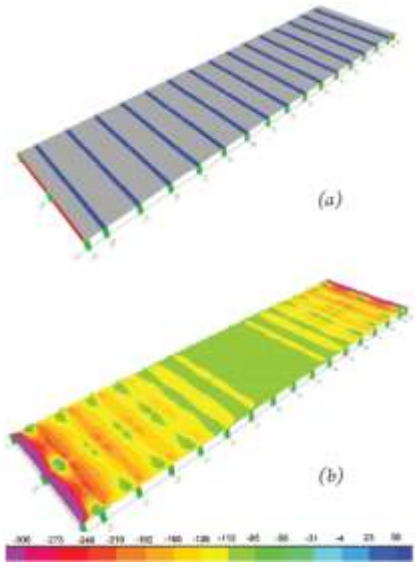

Figure 2-7 Model B with slabs, beams, columns, and walls in short direction: (a) ETABS model; and (b) axial stress from -300 to 50 psi (Guo et al., 2009) (Note: 1 psi = 0.0068 MPa)

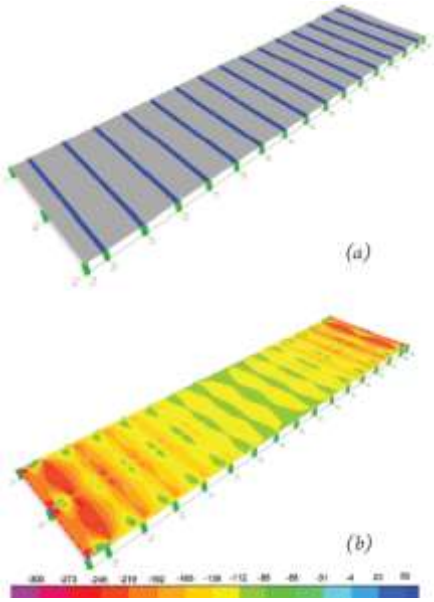

Figure 2-8 Model C with slabs, beams, and columns: (a) ETABS model; and (b) axial stress from -300 to 50 psi (Guo et al., 2009) (Note: 1 psi = 0.0068 MPa)

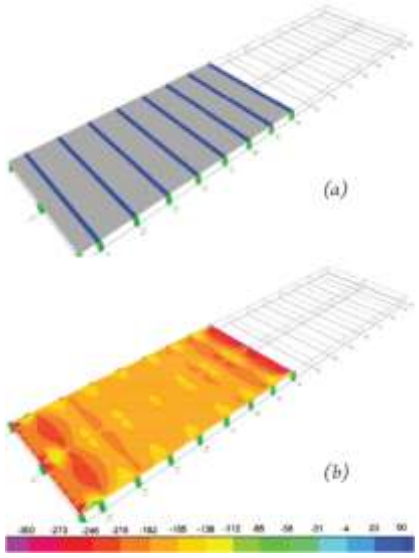

Figure 2-9 Model D with slabs, beams, and columns–half of the building: building: (a) ETABS model; and (b) axial stress from -300 to 50 psi (Guo et al., 2009) (Note: 1 psi = 0.0068 MPa)

Chapter 3. Investigation of Existing Analysis Models

3.1 General Information About Shrinkage in Structural Concrete

Shortening in unbonded post-tensioned slabs is primarily the result of:

- Shrinkage
  - Drying shrinkage
  - Autogenous shrinkage
- Creep
  - Basic creep
  - Drying creep
- Temperature decrease
- Elastic shortening of concrete

According to Aalami and Barth (1988) shrinkage exerts the largest volume-changing behavior, followed by temperature, creep and finally elastic shortening. **Figure 3-1** shows the percentage of each effect observed in a concrete slab at a parking structure in Southern California.

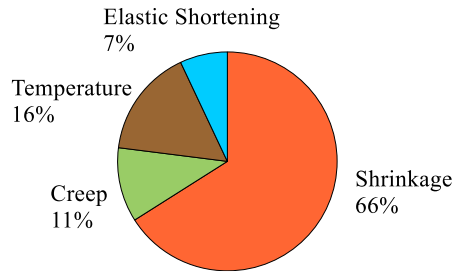

Figure 3-1 Contribution to size-reduction effects according to Aalami and Barth (1988)

The effect of each of the causes for volume-changing behavior is thought to be independent of each other. The final shortening is the summation of the strain for each of the causes multiplied by the length of the concrete slab.

The shrinkage strain ε_{sh} and creep strain ε_{cr} at a determined time can be obtained by any one of the available calculation models.

The creep strain in most of the models is obtained through multiplying the resulting compliance by the stress that is sustained by the member. The compliance $J(t,t_0)$, describes the time-dependent strain at age t, caused by a unit uniaxial load applied since the loading age t_0 and it can be obtained through a series of formulas depending on the selected calculation model.

Another way that creep is reported by some of the models is through the creep coefficient $\varphi(t,t_0)$ which is the ratio of the creep strain at time t to the initial strain at loading time t_0, or the ratio of the creep compliance to the compliance obtained at early ages. To obtain the compliance from the creep coefficient, the following formula can be used:

$$J(t,t_0) = \frac{1}{E_{cmt0}} + \frac{\varphi(t,t_0)}{E_{cmt0}}$$

Where E_{cmt0} represents the mean modulus of elasticity of concrete when loading starts, which can be obtained by formulas included in the selected model.

Regarding thermal strain, it can be calculated by the following formula:

$$\varepsilon_T = \Delta T \cdot \alpha$$

Where ε_T represents the thermal strain, ΔT the temperature change and α the coefficient of thermal expansion.

For this study, and for ordinary thermal stress calculations, when the type of aggregate and concrete degree of saturation are unknown a coefficient of thermal expansion of $\alpha = 5.5 \times 10^{-6}$ /F ($\alpha = 10 \times 10^{-6}$ /C) may be sufficient according to ACI Committee 209 (1992).

The elastic shortening present in prestressed concrete members can be calculated by the following formula:

$$\varepsilon_{es} = \frac{\sigma}{E}$$

Where ε_{es} is the total elastic shortening, σ is the average precompressive stress and E is the modulus of elasticity.

Therefore, the final slab shortening, represented as ΔL, in inches or millimeters, at one of its axis can be determined by the following formula, where L represents the slab length:

$$\Delta L = L(\varepsilon_{sh} + \varepsilon_{cr} + \varepsilon_T + \varepsilon_{es})$$

In post-tensioned slabs in North America, it is common to use pour strips to reduce shortening problems. Pour strips are left open for a certain period of time to allow for the free movement of the two divided sections of the slab. Strip open periods are typically between 30 and 90 days. For this, it is useful to have an estimation of the shortening that will take place at different times.

From the performance experience of post-tensioned slabs, the following guidelines for the provision of closure strips or structural separations may be considered (Nawy, 2008):

- If the slab length is less than 250 ft. (76.2 m), no closure strip or structural separations are necessary, unless the supporting walls are unfavorably placed.

- If the slab length is longer than 250 ft. (76.2 m) but less than 375 ft. (114.3m), provide one centrally located closure strip.
- If the slab length is longer than 375 ft. (114.3m), provide a structural separation.

3.2 Comparison between Models and Test Results

Although there have been several model-vs-tests reports in the past, they have not reached a definitive consensus as to which model is the most accurate. In this study a brief comparison between models and a test is presented.

The test results presented in the study by Shadravan et al. (2015) for the high-strength concrete specimen vs. models' results are presented in **Figure 3-2**, and the results for the slab-on-ground from the same study using high-strength concrete are in **Figure 3-3**, and Portland cement concrete in **Figure 3-4**.

As it can be observed in these graphs, all the models seem to overestimate the shrinkage; however, Model B3 is the one resulting with the shrinkage strain most similar to the test result. This behavior coincides with most of the reviewed papers (Guo & Joseph, 2013; Goel et al., 2017; and Fanourakis, 2017)

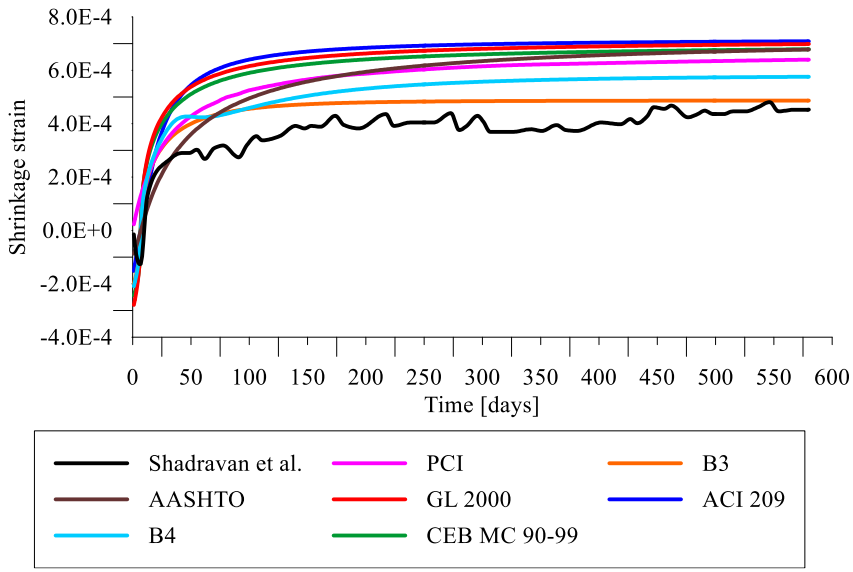

Figure 3-2 Shrinkage strain models' results for HSC specimen in Shadravan et al. study

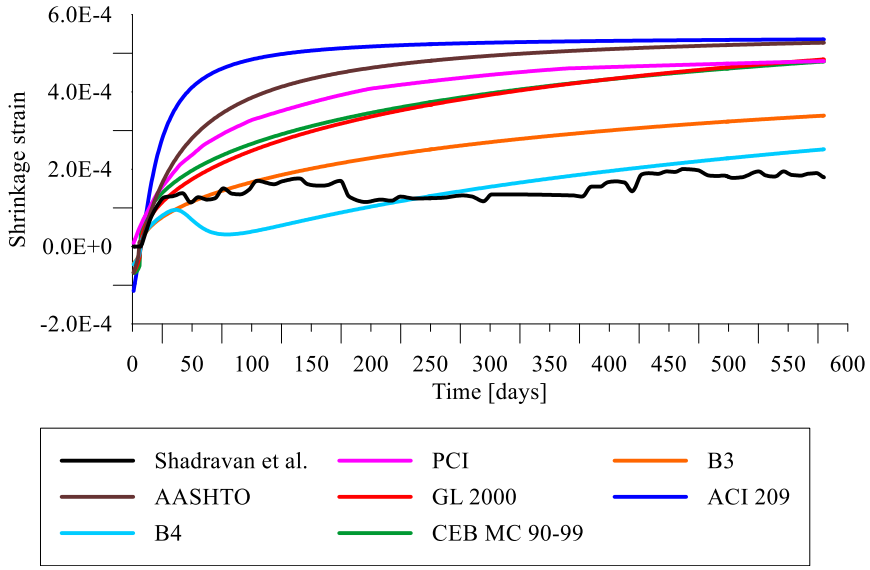

Figure 3-3 Shrinkage strain models' results for HSC slab in Shadravan et al. study

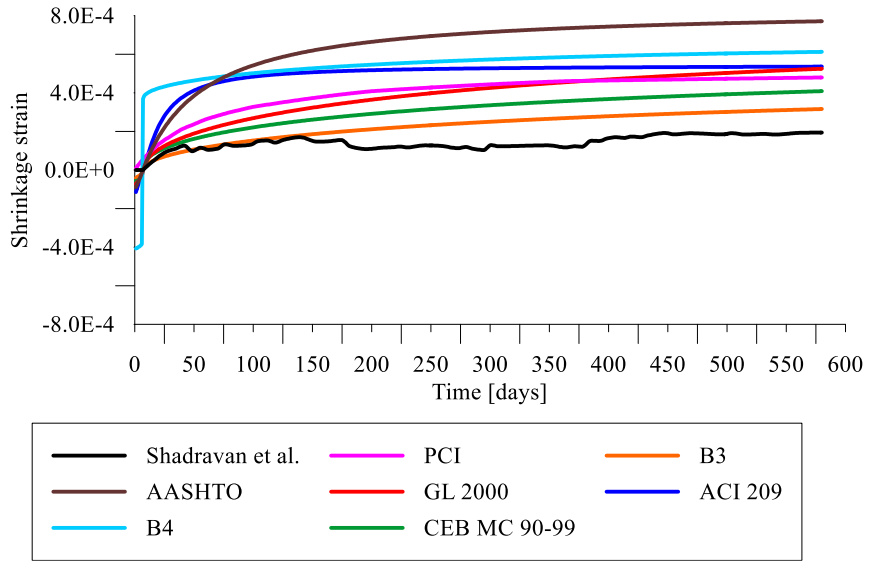

Figure 3-4 Shrinkage strain models' results for PCC slab in Shadravan et al. study

The test results presented in the study by Le Roy et al. (2016) for a high-strength concrete cylinder specimen (B3) vs. the models' results are presented in **Figure 3-5**. As the specified concrete strength of the specimen was 13,677 psi (94.3 MPa) and the applied stress was 4,206 psi (29 MPa), these characteristics are outside of the limitations of the PCI model; therefore, it was not included in the comparison.

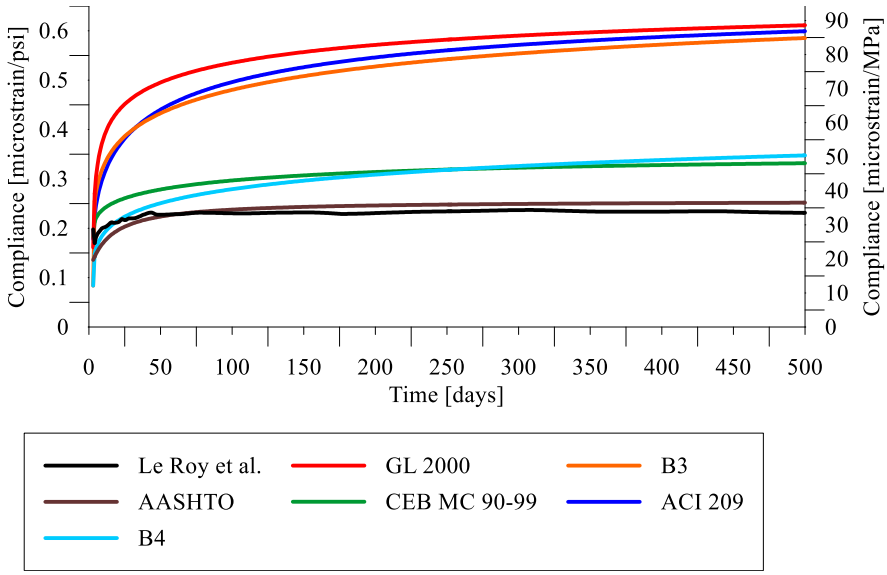

Figure 3-5 Compliance models' results for HSC specimen in Le Roy et al. study (Note: 1 microstrain/psi = 147.06 microstrain/MPa)

In the case of creep there is also a tendency of overestimation of results. The AASHTO model is the closest to the test results overall; however, it underestimates the compliance at earlier stages. The AASHTO model was not considered in the reviewed studies, where the consensus is that the GL 2000 model appears to be the most accurate for creep (Fanourakis, 2017; Gardner, 2004; Goel et al., 2007).

3.3 Selection of Creep and Shrinkage Model

Tendons are typically stressed when concrete reaches a minimum strength of 3,000 psi (20.7 MPa), which also has to be achieved after 3 days of moist curing. This is because post-tensioned anchors are designed to distribute tendon forces at this concrete strength. To fulfill this requirement, high early strength concrete is often used. This concrete usually achieves a compressive strength of 5,000 psi (34.5 MPa) at 28 days.

Therefore, for this calculation, concrete with a specified 28-day strength of 5,000 psi (34.5 MPa) is used and it is specified to be composed of a cement Type III which is defined as high early strength. The estimated concrete mixture according to the guidelines from ACI 318-19(2019) and ACI 211.1-91(2002) is shown below in **Table 3-1**.

Table 3-1 Concrete mixture used in models

Estimated Concrete Mixture			
		SI units	in.-lb units
Cement type		III	III
Maximum aggregate size		20 mm	3/4 in.
Cement content	c =	413.5 kg/m^3	697 lb/yd^3
Water content	w =	201.7 kg/m^3	340 lb/yd^3
Water-cement ratio	w/c =	0.49	
Aggregate-cement ratio	a/c =	4.28	
Fine aggregate percentage	ψ =	40%	
Air content	α_c =	2%	
Slump	s =	75 mm	2.95 in.
Unit weight of concrete	γ_c =	2345 kg/m^3	3953 lb/yd^3

A relative humidity of 70% and an average temperature of 68 °F (20 °C) are considered. In general, the slab prototypes to be analyzed have a volume-to-

surface ratio of 4 in. (100mm) and an average compressive stress of 200 psi (1.38 MPa) due to the tendon forces. The slab is considered as moist-cured during 3 days and immediately subjected to stress due to tendon stressing. **Table 3-2** indicates the mentioned parameters.

Table 3-2 Parameter input in models

Problem Data			
Concrete data:		SI units	in.-lb units
Specified 28-day strength	$f_c' =$	34.5 MPa	5000 psi
Ambient conditions:			
Relative humidity	$h =$	0.7	
Temperature	$T =$	20 °C	68 °F
Specimen:			
Volume-surface ratio	$V/S =$	100 mm	4 in.
Shape		Infinite slab	
Initial curing:			
Curing time (Age when drying begins)	$t_c =$	3 days	
Curing condition		Moist cured	
Concrete at loading:			
Age at loading (Tendon stressing)	$t_0 =$	3 days	
Applied stress (Avg. compressive stress)	$k_s =$	1.38 MPa	200 psi

These parameters were introduced in the formula of each model, and the resulting graph of shrinkage strain vs. time in days can be seen in **Figure 3-6**. The graph shows that the ACI 209 model largely underestimates long-term shrinkage strain compared to the other models, and the AASHTO model shows a tendency to calculate higher shrinkage strains at an earlier age; however, it does not overestimate long-term shrinkage compared to other models. The model that calculated a higher shrinkage strain was the B4 model. The GL 2000 model and the CEB MC 90-99 model show very similar behavior.

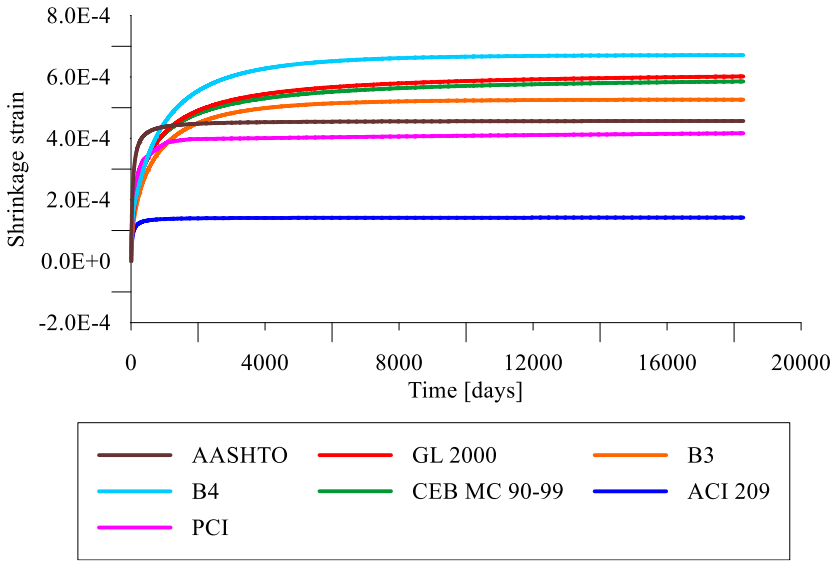

Figure 3-6 Shrinkage strain results per model

The resulting graph of creep strain vs. time in days can be observed in **Figure 3-7**, where all the models produce different final values. The B3 Model gave the largest values, accompanied by the model GL 2000, while the B4 Model produced very small values compared to the others. The AASHTO and ACI 209 models show very similar behavior.

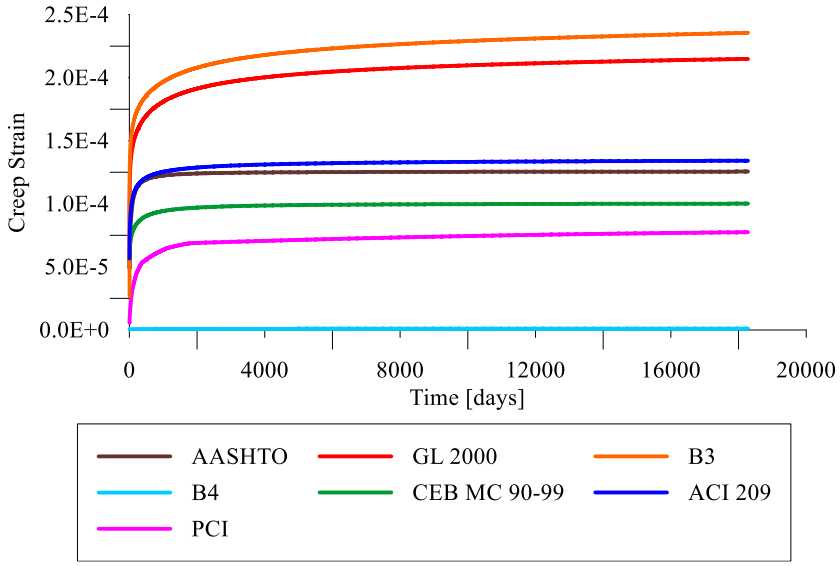

Figure 3-7 Creep strain results per model

The total strain that considers shrinkage, creep, the temperature change and the effects of elastic shortening vs. time can be observed in **Figure 3-8**. When all the effects are considered, the model that registers the largest strain is the GL 2000, followed closely by the B3 model. Here, again, a higher early strain compared with the others can be observed from the AASHTO model. The one that appears to underestimate the overall size-reduction effects compared to the others is the ACI 209 model.

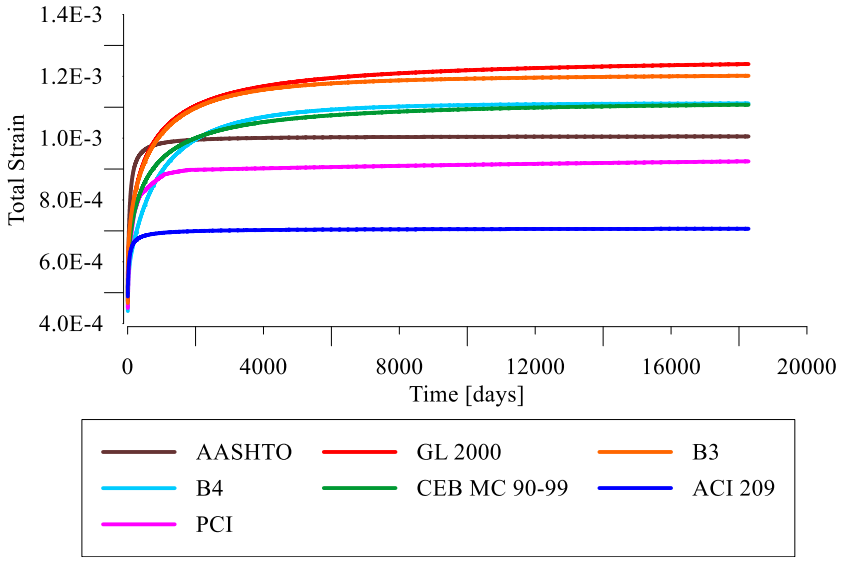

Figure 3-8 Total strain results (Shrinkage, creep, temperature and elastic shortening)

The percentage of contribution from final shrinkage and creep strain obtained with the models, along with the temperature and elastic shortening strain, can be compared in **Figure 3-9**and **Figure 3-10**. Although the amounts could largely differ because of the difference in environmental conditions, the models that show certain coherence with the theorized hierarchy of volume-changing effects presented by Aalami and Barth (1988) are the B3, CEB MC 90-99, GL 2000, PCI and AASHTO models. As observed before, the ACI 209 model shows underestimation of overall shrinkage and creep, while B4 model largely underestimates creep.

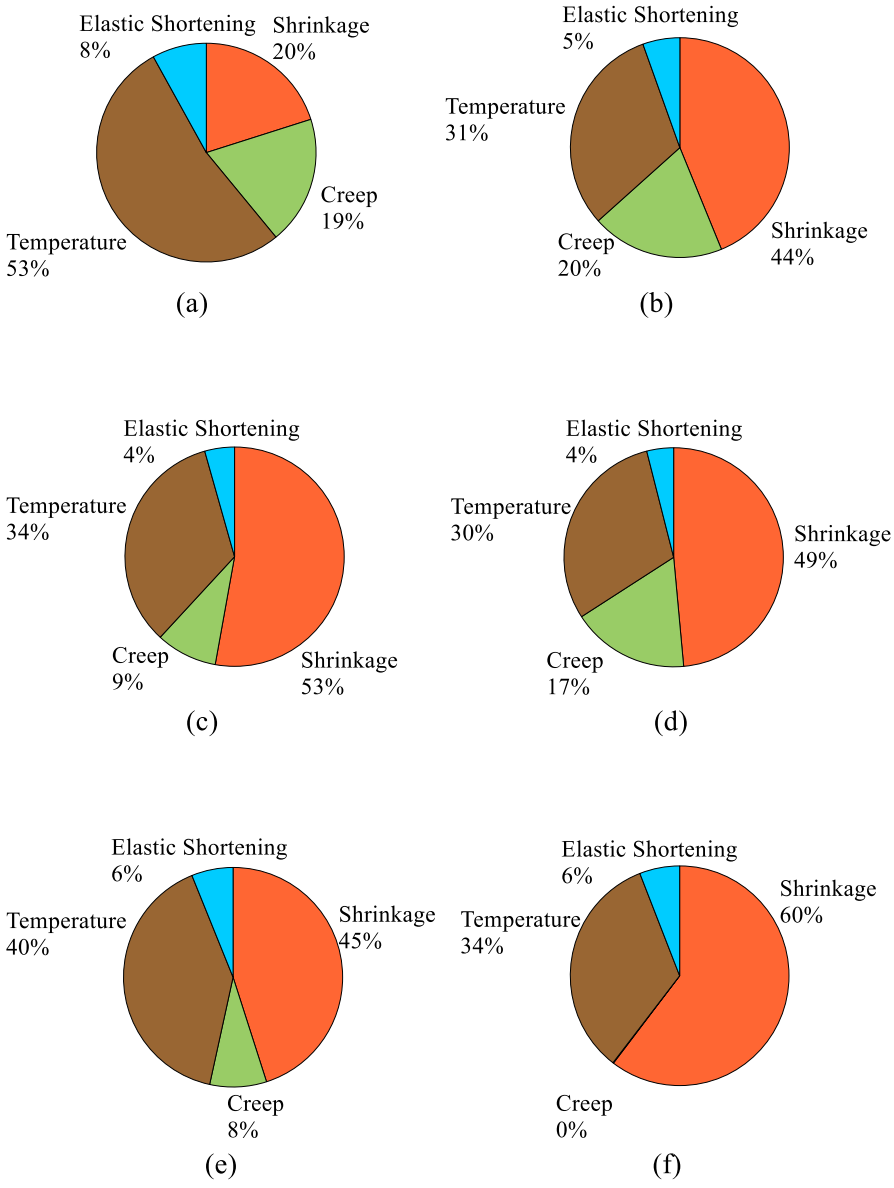

Figure 3-9 Contribution per model: (a) ACI 209; (b) B3; (c) CEB MC 90-99; (d) GL 2000; (e) PCI; (f) B4

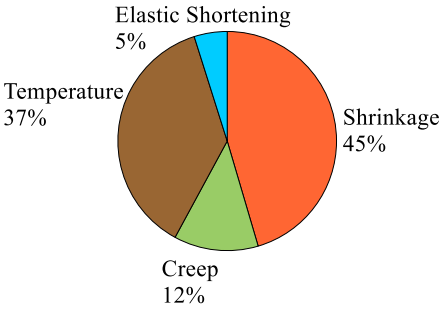

(g)

Figure 3-10 Contribution per model: (g) AASHTO

It is difficult to select only a model based on closeness to the test results, due to the unpredictability of the environmental conditions, as well as the large difference in concrete material compositions available in the industry. The consensus based on the studies is that both the B3 model and the GL 2000 model are the most accurate. However, if the simplicity and ease of use of these models is considered, the model GL 2000 is significantly easier to implement in the design process and requires significantly less parameters to produce calculation. Also, the results for this specific case show that it is the model that calculates the largest total strain between B3 model and GL 2000 model. Therefore, the model GL 2000 will be used in the following analysis.

Chapter 4. Finite Element Modeling

4.1 Selected Architectural Configuration Prototypes

The series of configurations of structural vertical elements (columns and walls) affecting the slabs that were analyzed and the layouts are presented in the following prototype drawings in imperial units, the prototypes not presented in this chapter can be found in Appendix A.

The resulting prototypes are numbered as 1.0 (**Figure 4-1**) to 9.0 (**Figure 4-8**) with some additional variations. The column size considered was 18 in. by 18 in. (457.2 mm by 457.2 mm), two wall thicknesses were considered: 12 in. (304.8 mm) as shown in **Figure 4-2**, and 20 in. (508 mm) as shown in **Figure 4-3** and the slab thickness was 8 in. (228.6 mm).

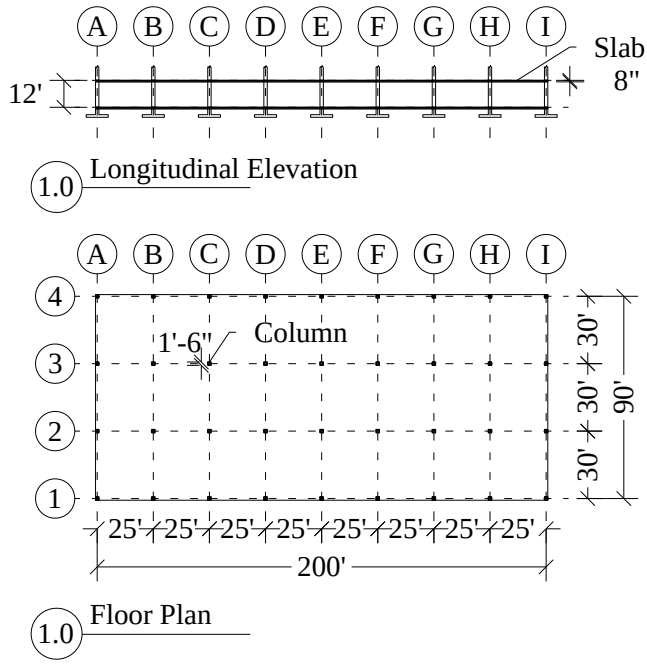

Figure 4-1 Prototype 1.0 reference drawings (Note: 1 in. = 25.4 mm; 1 ft. = 304.8 mm)

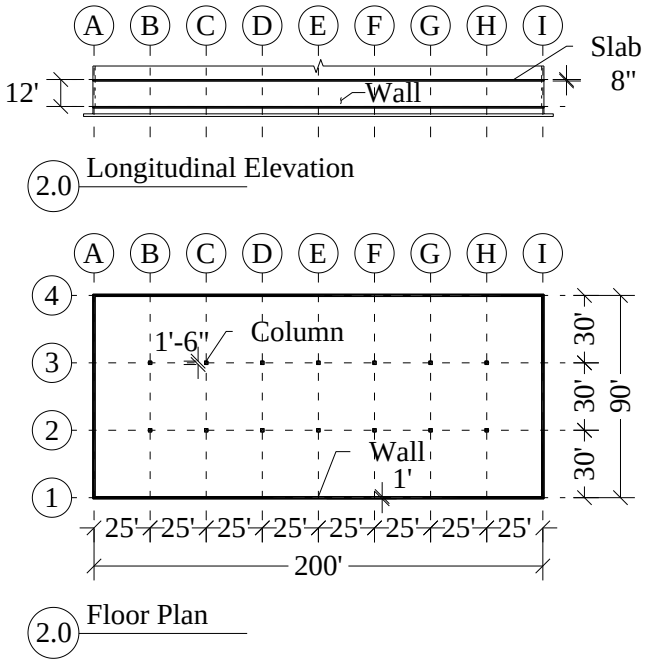

Figure 4-2 Prototype 2.0 reference drawings (Note: 1 in. = 25.4 mm; 1 ft. = 304.8 mm)

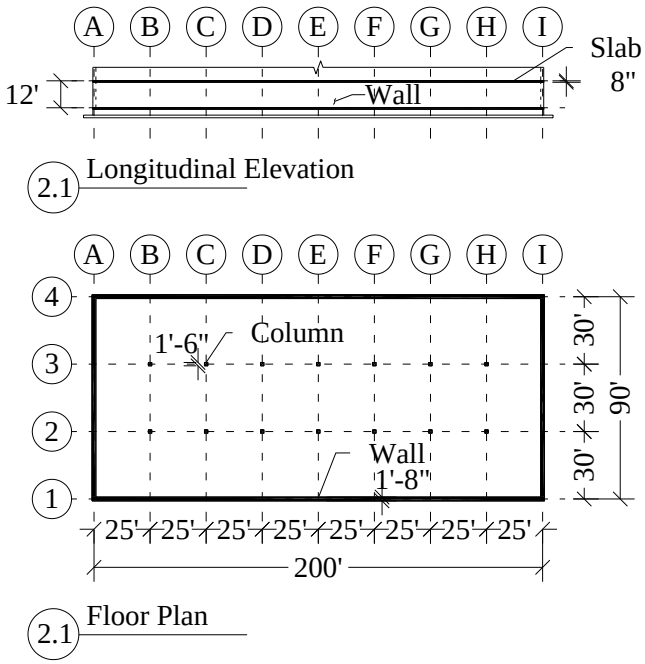

Figure 4-3 Prototype 2.1 reference drawings (Note: 1 in. = 25.4 mm; 1 ft. = 304.8 mm)

A 3 ft. (0.91 m) pour strip was added to what initially are prototype 2.0, 2.2, 4.0 and 5.0, resulting on additional prototypes 2.0.1 (**Figure 4-4**), 2.2.1 (**Figure 4-5**), 4.0.1(**Figure 4-6**), and 5.0.1 (**Figure 4-7**).

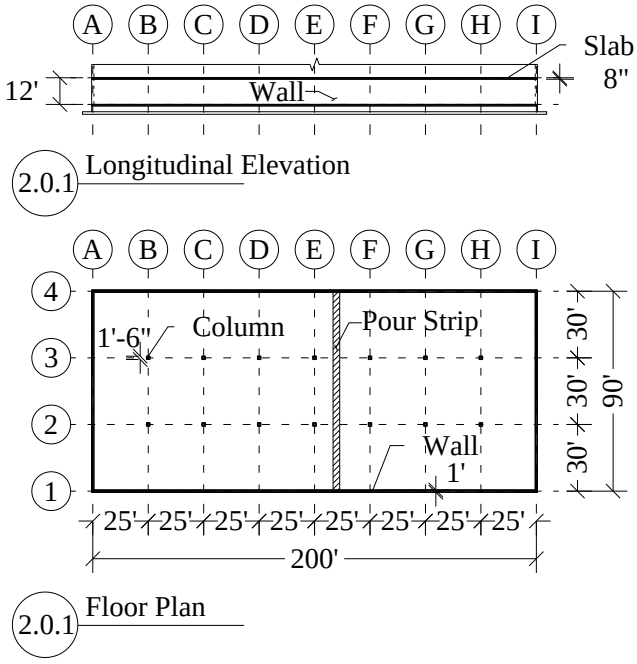

Figure 4-4 Prototype 2.0.1 reference drawings (Note: 1 in. = 25.4 mm; 1 ft. = 304.8 mm)

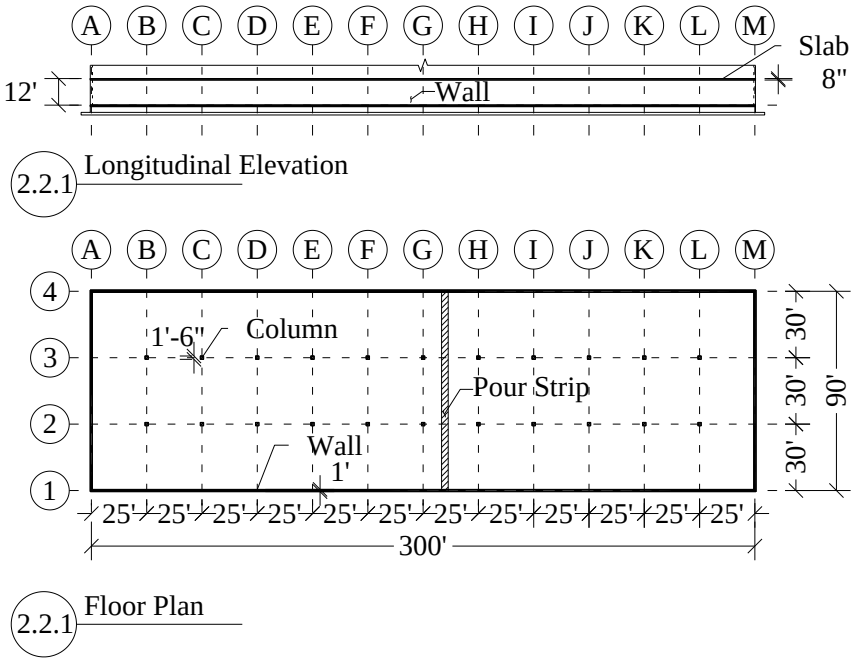

Figure 4-5 Prototype 2.2.1 reference drawings (Note: 1 in. = 25.4 mm; 1 ft. = 304.8 mm)

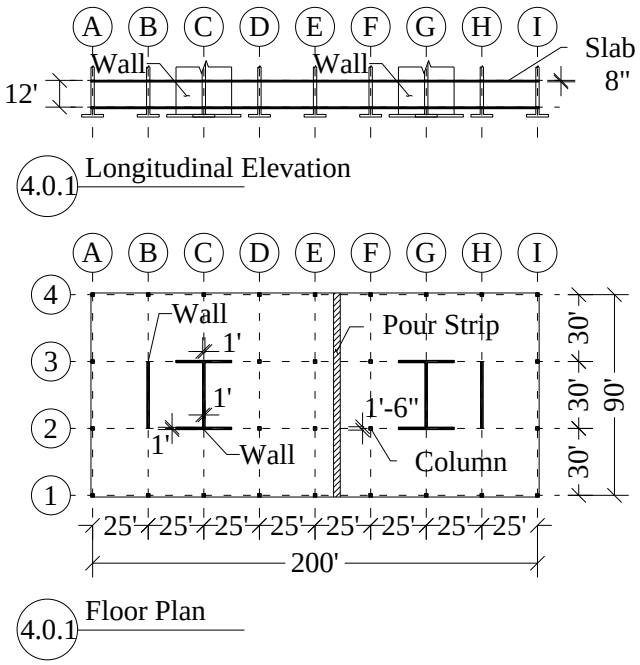

Figure 4-6 Prototype 4.0.1 reference drawings (Note: 1 in. = 25.4 mm; 1 ft. = 304.8 mm)

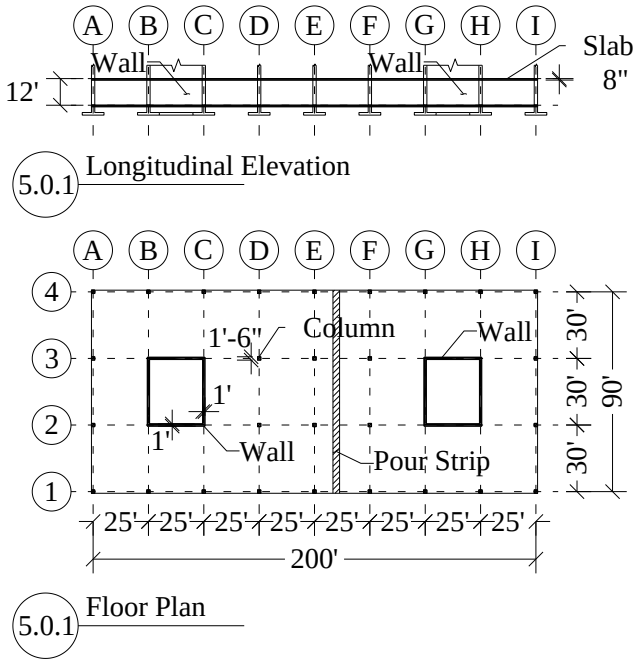

Figure 4-7 Prototype 5.0.1 reference drawings (Note: 1 in. = 25.4 mm; 1 ft. = 304.8 mm)

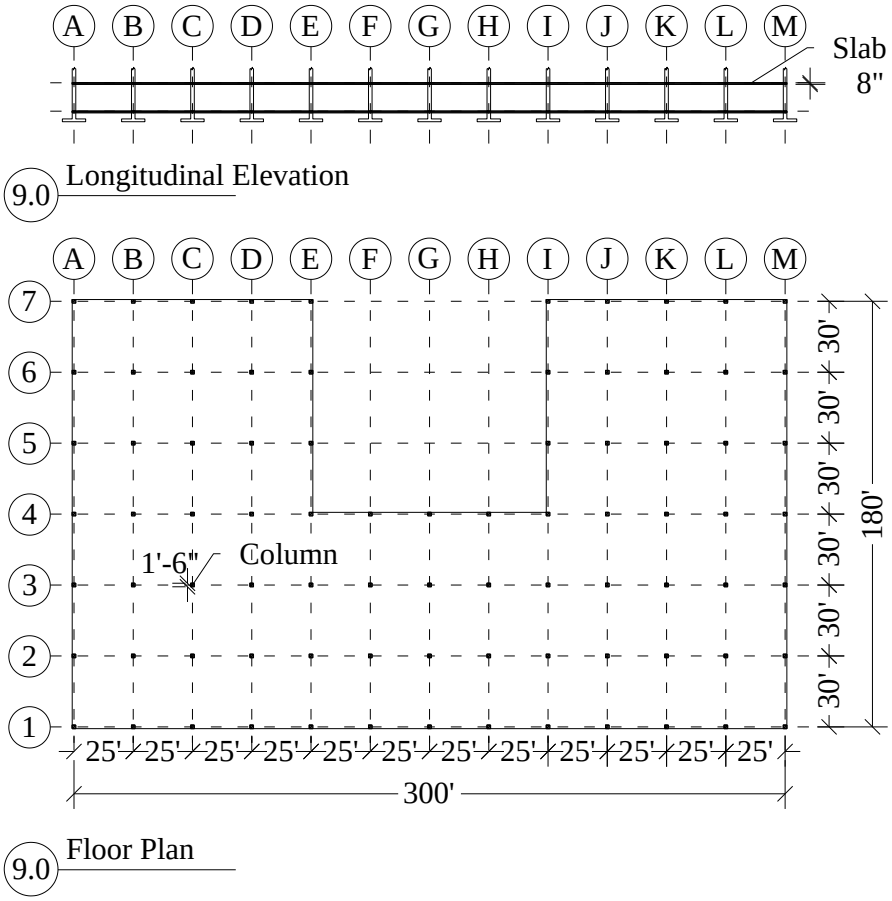

Figure 4-8 Prototype 9.0 reference drawings (Note: 1 in. = 25.4 mm; 1 ft. = 304.8 mm)

4.2 Modeling Information and Process

The axial stresses present in the slabs were analyzed using the finite element analysis software ETABS Ultimate 17.0.1, where the previously presented slabs and vertical members were modeled and the following material conditions were input for the material properties of concrete:

Table 4-1 Material properties of concrete

Material Property Design Data			
Concrete data:		SI units	in.-lb units
Material type		Concrete, Isotropic	
Specified 28-day strength	$f_c' =$	34.5 MPa	5000 psi
Unit weight of concrete	$\gamma =$	2345 kg/m^3	146 lb/ft.^{3}
Modulus of elasticity	$E =$	27,786 MPa	4,030,000 psi
Poisson's ratio	$U =$	0.2	
Coefficient of thermal expansion	$\alpha =$	10 x 10^{-6} 1/°C	5.5 x 10^{-6} 1/°F

These parameters were determined according to ACI Committee 318 (2019), ACI Committee 209 (1992), and ACI Committee 211 (2002).

The shrinkage and creep model selected was the GL 2000 model, which was first manually calculated according to the Guide for Modeling and Calculating Shrinkage and Creep in Hardened Concrete (ACI Committee 209, 2008) using the following parameters:

Table 4-2 Parameters input in GL 2000 model

Problem Data			
Concrete data:		SI units	in.-lb units
Specified 28-day strength	$f_c' =$	34.5 MPa	5000 psi
Cement type		III	
Ambient conditions:			
Relative humidity	$h =$	0.7	
Age of concrete	$t =$	3 to 18,250 days	
Specimen:			
Volume-surface ratio	$V/S =$	100 mm	4 in.
Initial curing:			
Curing time (Age when drying begins)	$t_c =$	3 days	
Concrete at loading:			
Age at loading (Tendon stressing)	$t_0 =$	3 days	
Applied stress (Avg. compressive stress)	$k_s =$	1.38 MPa	200 psi

The resulting strains for shrinkage and creep were as follows:

Table 4-3 Time-dependent strain results from GL 2000 model

Time-dependent Strain Results		
t (days)	Shrinkage Strain (microstrain)	Creep Strain (microstrain)
3	0	4.90×10^{-5}
14	5.90×10^{-5}	1.17×10^{-4}
28	8.85×10^{-5}	1.29×10^{-4}
60	1.32×10^{-4}	1.39×10^{-4}
90	1.61×10^{-4}	1.45×10^{-4}
180	2.22×10^{-4}	1.54×10^{-4}
365	2.98×10^{-4}	1.65×10^{-4}
1,825	4.82×10^{-4}	1.90×10^{-4}
18,250	6.02×10^{-4}	2.15×10^{-4}

Under the time dependent properties of concrete section in ETABS, the preloaded GL 2000 model was selected, where the parameters for relative

humidity, drying age, and cement type were the same as the manually calculated parameters. The time dependence was considered for compressive strength and stiffness, creep and shrinkage, and the creep analysis type was set as full integration. The manually calculated results for creep and shrinkage were compared to the output plot produced by ETABS, which showed concurrence among the results.

The post-tensioning tendons used in this analysis were unbonded, ASTM 416 steel strands, Grade 270, with a strand area of 0.153 $in.^2$ (3.89 mm^2). The input material properties were as follows:

Table 4-4 Tendon material properties

Material Property Design Data			
Tendon data:		SI units	in.-lb units
Material type		Tendon, Uniaxial	
Minimum yield stress	f_y =	1,690 MPa	245,100 psi
Minimum tensile strength	f_u =	1,862 MPa	270,000 psi
Unit weight	γ =	7,849 kg/m^3	490 $lb/ft.^3$
Modulus of elasticity	E =	196,500 MPa	28,500,000 psi

A manual calculation to determine the amount of tendons required for this slab was performed in accordance with the Post-Tensioning Manual (Post-Tensioning Institute, 2006). The design strip width for the longitudinal direction was 30 ft. (9.14 m) and for the transversal direction was 25 ft. (7.62 m). For an average precompressive stress of 200 psi (1.38 MPa), the resulting tendons were 22 for the longitudinal direction and 18 for the transversal direction.

To design the tendons on ETABS, equally spaced design strips were set on each direction and tendons were added in the strips. The design preferences were set as to follow the ACI Committee 318 (2019) code. The tendons were designed as banded with no in the longitudinal direction (X-direction) and distributed

with a separation of 30 in. (762 mm) in the transversal direction (Y-direction) (**Figure 4-9**). The vertical profile of all tendons was set as reverse parabola in the software. A precompression level of 200 psi (1.38 MPa) and a load balancing between 60% and 80% was set on the program. The resulting tendons were same as the manually calculated, and the distributed tendons were grouped in 2 strands per tendon.

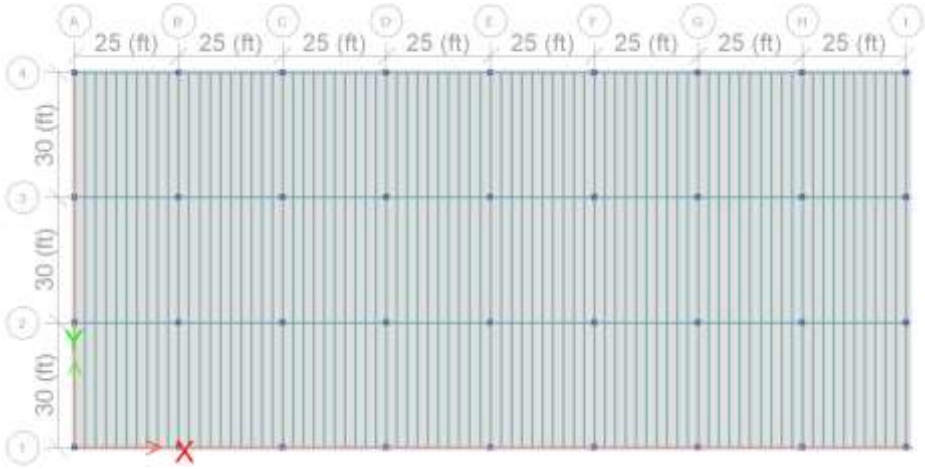

Figure 4-9 Tendon layout in ETABS 2017 Ultimate 17.0.1. (Note: 1 ft. = 304.8 mm)

The resulting tendon jacking stress calculated as the minimum between $0.8f_u$ and $0.94f_y$ was 216,000 psi (1489 MPa), and the tendon losses were set as 10% stressing losses and 5% long term losses. It was se as to be stressed from the J-end.

The vertical elements were considered as fixed on their base, to represent the analyzed floor as the lowest level, which is considered as the level with the most restriction in a building.

The dead loads considered were the self-weight of the slab and a partition load of 15 lb./ft.^{2} (718.2 Pa), the live load considered was 29 lb./ft.^{2} (1388.53 Pa). A

temperature load of -68 F° (-20 C°) was assigned to the concrete slab to account for temperature changes.

To analyze the shrinkage, creep, and temperature contribution at specific times, a new load case needs to be added under the Nonlinear Static Staged Construction option available in ETABS. To set up this special load case, first, the auto construction sequence load case must be defined as shown in **Figure 4-10**.

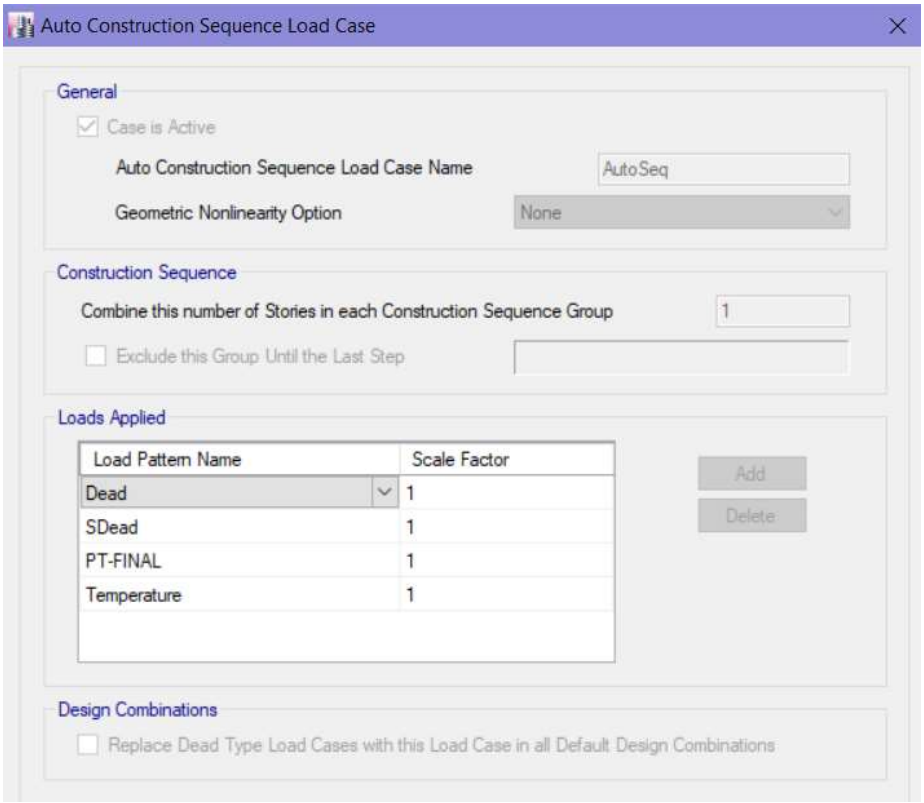

Figure 4-10 Auto construction sequence load case input on ETABS

After this new load case was defined it would appear in the Load Cases section of the software. To be able to input the sequences, it is necessary to add an additional nonlinear static staged construction case, after the previous auto

nonlinear static staged construction load case is added (**Figure 4-11**). The name of this load case corresponds to the times that are to be analyzed.

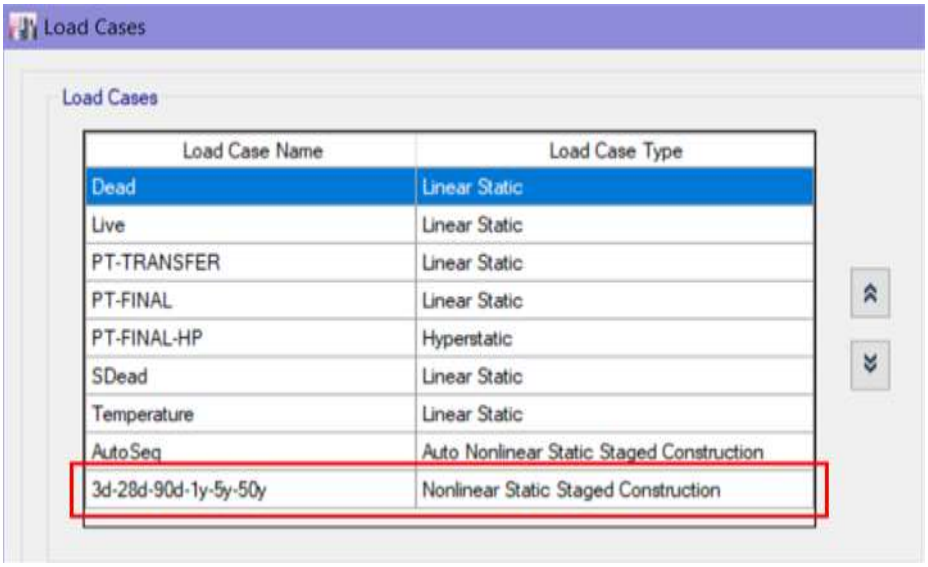

Figure 4-11 List of load cases present in the project

Before inputting these stages into ETABS the Material Properties Are Time Dependent option should be ticked for the software to take in account the previously input shrinkage and creep calculation model (**Figure 4-12**).

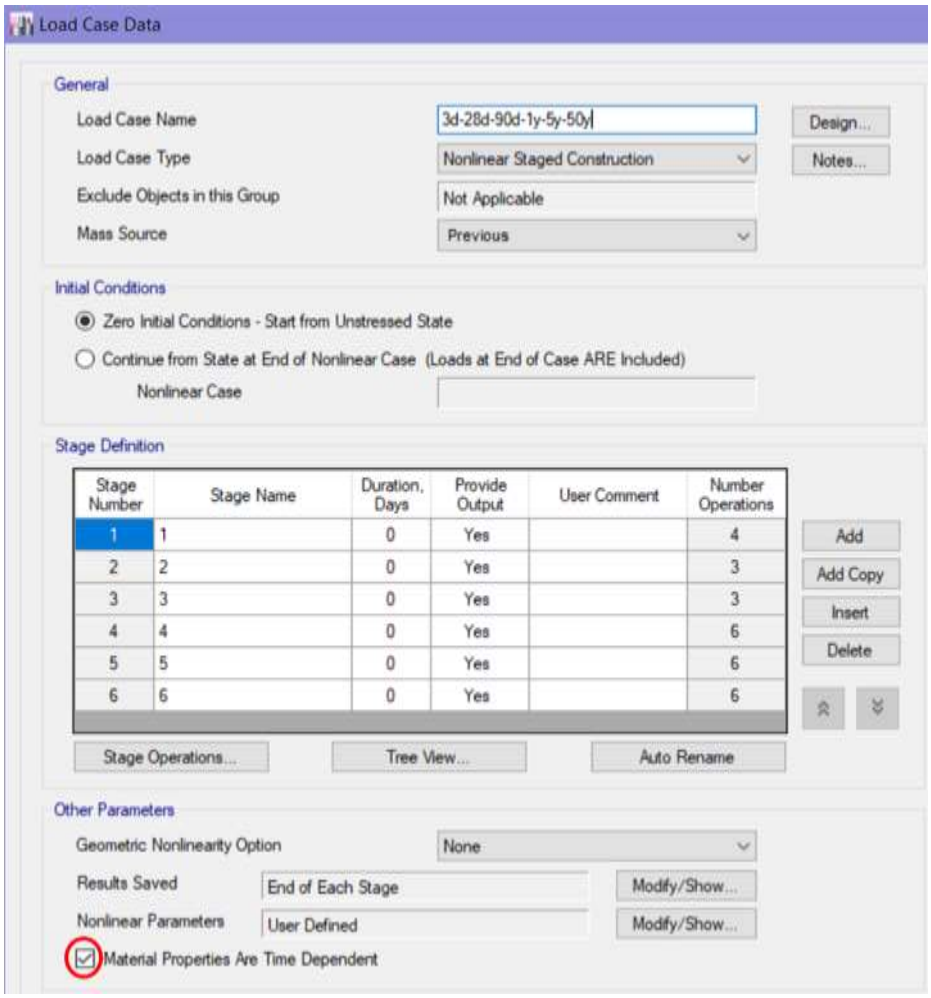

Figure 4-12 Data input for the nonlinear staged construction case

For this analysis, 6 stages were defined in this staged construction analysis, where the age of the pt-slab is changed accordingly: 1) after 3 days of concrete pouring to account for total stresses at time of tendon stressing; 2) 28 days to account for the time at which the concrete would reach its specified compressive strength, so the considered load at 3 days and 28 days is only the slab self-weight as well as the post-tensioning stresses at transfer stage; 3) 90 days to take into account the normal open pour strip time and check the stresses present, during that time the post tensioning load is changed to account for

service-stage stresses, so the live load and temperature load are added to the previously considered loads; 4) 1 year, that is the approximate time at which the building would be operational, from this stage the load consideration remains the same as the previous stage; 5) 5 years; and 6) 50 years which is usually considered as the expected lifetime of a building. The definition of each stage as input in ETABS is shown in the following figures (**Figure 4-13**, **Figure 4-14**, **Figure 4-15**, **Figure 4-16**, **Figure 4-17** and **Figure 4-18**).

Operation	Object Type	Object Name	Age at Add, days	Type	Name
Add Structure	Story	Story1	0		
Change Section & Age	Shell	4	3	Shell	Slab1
Load Objects If Added	Group	All		Load Pattern	Dead
Load Objects If Added	Group	All		Load Pattern	PT-TRANSFER

Figure 4-13 Input data of stage 1

Operation	Object Type	Object Name	Age at Add, days	Type	Name
Load Objects If Added	Group	All		Load Pattern	Dead
Load Objects If Added	Group	All		Load Pattern	PT-TRANSFER
Change Section & Age	Shell	4	28	Shell	Slab1

Figure 4-14 Input data of stage 2

Operation	Object Type	Object Name	Age at Add, days	Type	Name
Change Section & Age	Shell	4	90	Shell	Slab1
Load Objects If Added	Group	All		Load Pattern	Dead
Load Objects If Added	Group	All		Load Pattern	PT-FINAL

Figure 4-15 Input data of stage 3

Operation	Object Type	Object Name	Age at Add, days	Type	Name
Change Section & Age	Shell	4	365	Shell	Slab1
Load Objects If Added	Group	All		Load Pattern	Dead
Load Objects If Added	Group	All		Load Pattern	PT-FINAL
Load Objects If Added	Group	All		Load Pattern	SDead
Load Objects If Added	Group	All		Load Pattern	Temperature
Load Objects If Added	Group	All		Load Pattern	Live

Figure 4-16 Input data of stage 4

Operation	Object Type	Object Name	Age at Add, days	Type	Name
Change Section & Age	Shell	4	1825	Shell	Slab1
Load Objects If Added	Group	All		Load Pattern	Dead
Load Objects If Added	Group	All		Load Pattern	PT-FINAL
Load Objects If Added	Group	All		Load Pattern	SDead
Load Objects If Added	Group	All		Load Pattern	Temperature
Load Objects If Added	Group	All		Load Pattern	Live

Figure 4-17 Input data of stage 5

Operation	Object Type	Object Name	Age at Add, days	Type	Name
Change Section & Age	Shell	4	18250	Shell	Slab1
Load Objects If Added	Group	All		Load Pattern	Dead
Load Objects If Added	Group	All		Load Pattern	PT-FINAL
Load Objects If Added	Group	All		Load Pattern	SDead
Load Objects If Added	Group	All		Load Pattern	Temperature
Load Objects If Added	Group	All		Load Pattern	Live

Figure 4-18 Input data of stage 6

Chapter 5. Modeling Results and Discussion

5.1 Qualitative and Quantitative Analysis

The resulting axial stresses in the longitudinal axis **X-X** for each prototype at each of the mentioned times is presented in the following figures and the maximum and minimum stresses of all prototypes at all the calculated times can be found in **Table 5-8** at the end of this chapter section. These results do not take into account the effects of bonded reinforcement.

The tensile splitting strength f_t' as recommended in ACI Committee 363 (1992) and ACI Committee 435 (1995) for normal weight concrete of a compressive-strength ranging up to 12,000 psi (83 MPa) is: $7.4\sqrt{f'_c}$ (Nawy, 2008). Therefore, for this analysis the modulus of rupture considered is 523 psi (3.6 MPa).

The display of the stresses was limited from -530 psi (-3.65 MPa) in compression to 530 psi (3.65 MPa) in tension to take into consideration the modulus of rupture, as shown in **Figure 5-1**, where the color range goes from magenta to dark blue. This latter color indicates when the slab would initiate tensile cracking behavior. As the final slab design is expected to include punching shear reinforcement in the column area, the tensile stresses appearing in the columns can be disregarded in this analysis.

Figure 5-1 Axial stress range in psi (Note: 1 psi = 0.0068 MPa)

The results show that, although most of the shrinkage occurs during the estimated construction period, the restraint and temperature effects start

affecting the slab after the building is in its service period, and in many cases it is when the cracking appears.

In all cases it is possible to observe how, during the transfer or construction stage, the precompression starts to evenly spread throughout the slab. However, during the service stage the precompression concentrates in the extreme areas of the slab, while the tensile stresses appear in the center.

If we observe the results from prototype 1.0 at 3 days in **Figure 5-2** and at 5 years in **Figure 5-3**, versus prototype 1.1 at 3 days in **Figure 5-4** and 5 years in **Figure 5-5**, they show that the increase in length does not exert a significant cracking and tensile stresses even after time progression. This behavior is observed by the comparison of prototype 3.0 (**Figure 5-6** and **Figure 5-7**) vs. prototype 3.2 (**Figure 5-8** and **Figure 5-9**).

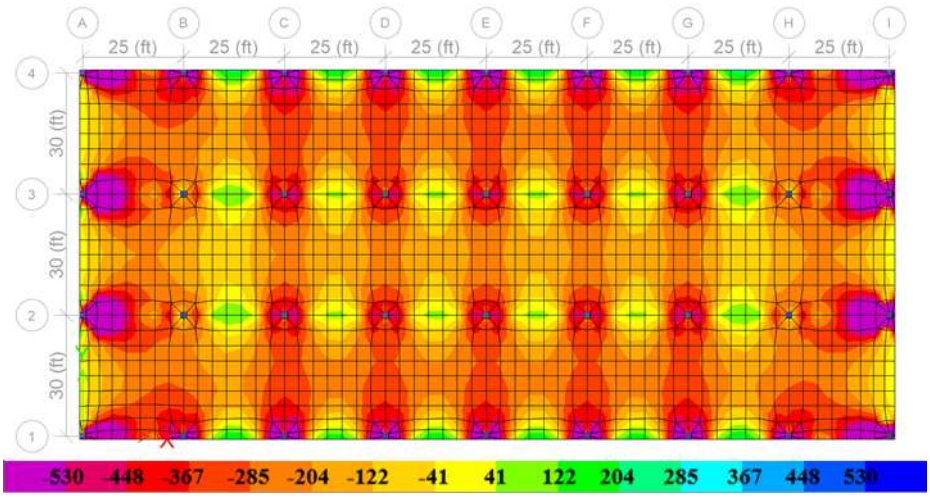

Figure 5-2 Axial stress in psi for prototype 1.0 at 3 days (Note: 1 psi = 0.0068 MPa)

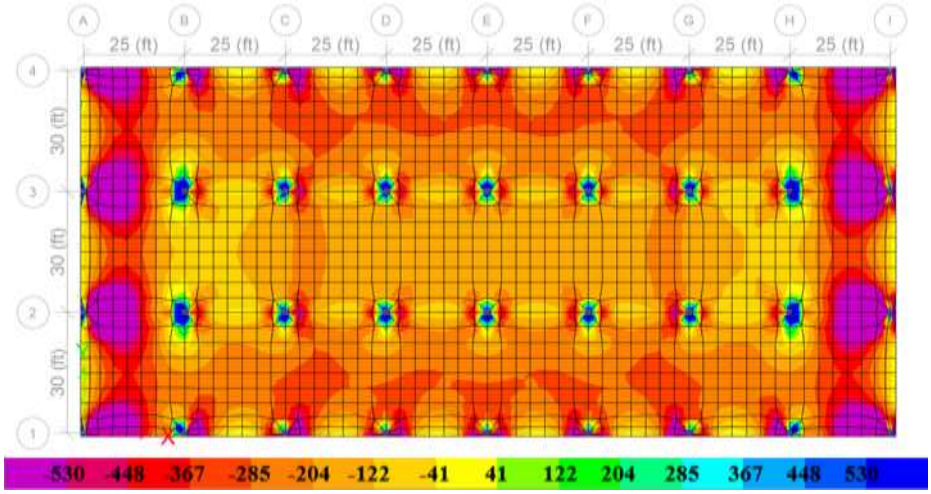

Figure 5-3 Axial stress in psi for prototype 1.0 at 5 years (Note: 1 psi = 0.0068 MPa)

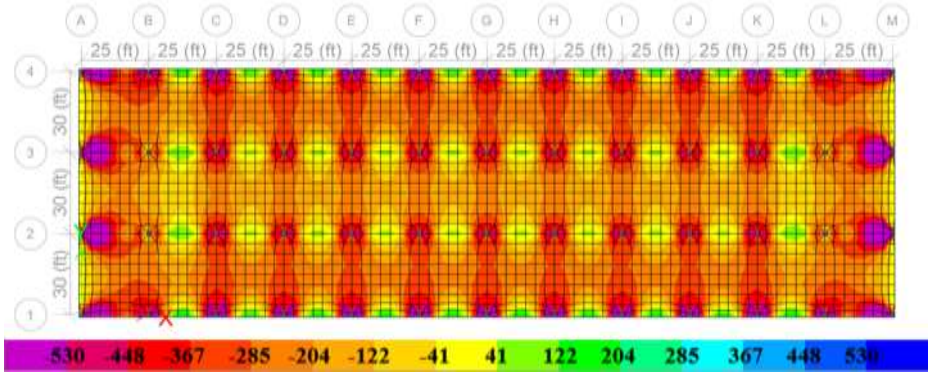

Figure 5-4 Axial stress in psi for prototype 1.1 at 3 days (Note: 1 psi = 0.0068 MPa)

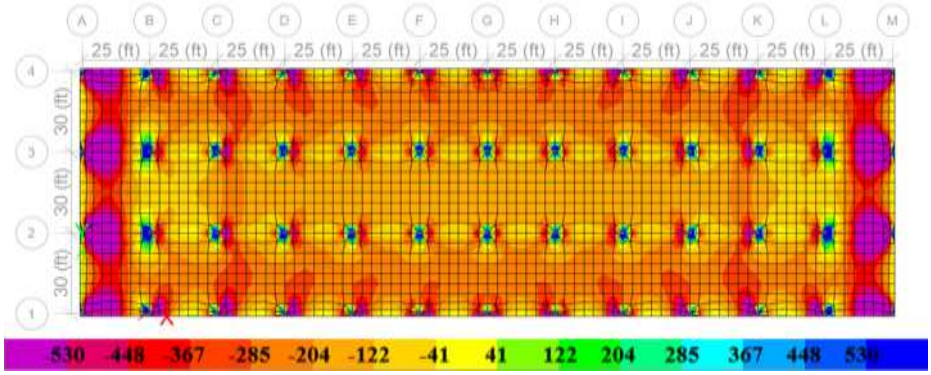

Figure 5-5 Axial stress in psi for prototype 1.1 at 5 years (Note: 1 psi = 0.0068 MPa)

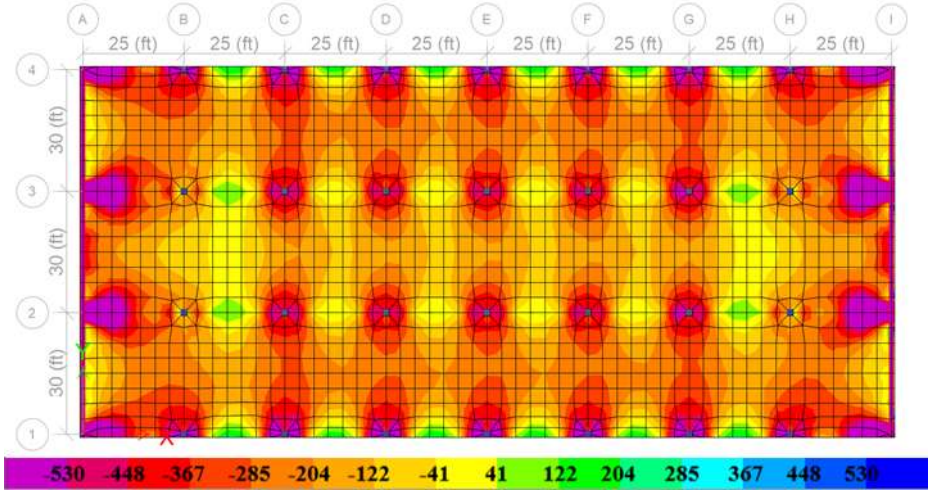

Figure 5-6 Axial stress in psi for prototype 3.0 at 3 days (Note: 1 psi = 0.0068 MPa)

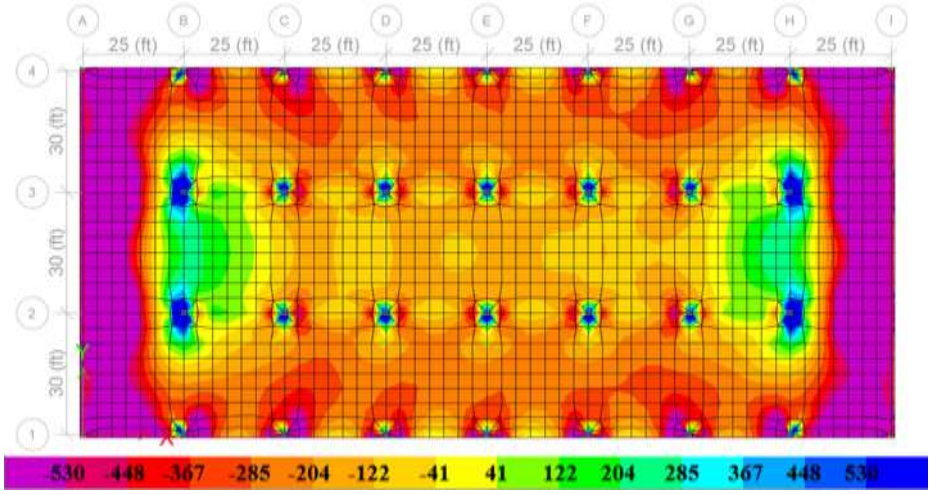

Figure 5-7 Axial stress in psi for prototype 3.0 at 5 years (Note: 1 psi = 0.0068 MPa)

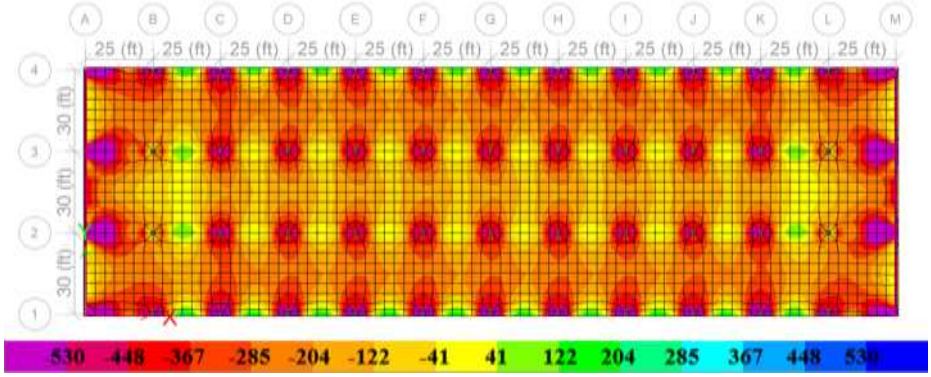

Figure 5-8 Axial stress in psi for prototype 3.2 at 3 days (Note: 1 psi = 0.0068 MPa)

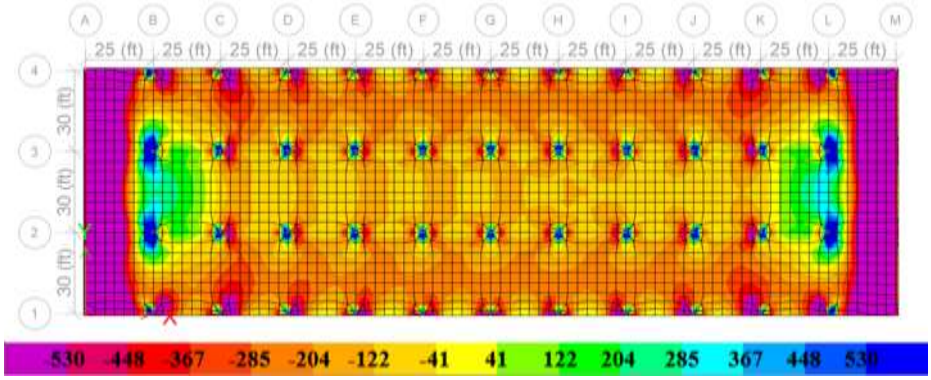

Figure 5-9 Axial stress in psi for prototype 3.2 at 5 years (Note: 1 psi = 0.0068 MPa)

However, if prototype 1.0 is compared to the models with same length but with restraining perimeter walls with a thickness of 12 in. (304.7 mm), there is an increase in tensile stresses, although not significant enough to produce cracking, as it can be observed in prototype 2.0 (**Figure 5-10** and **Figure 5-11**).

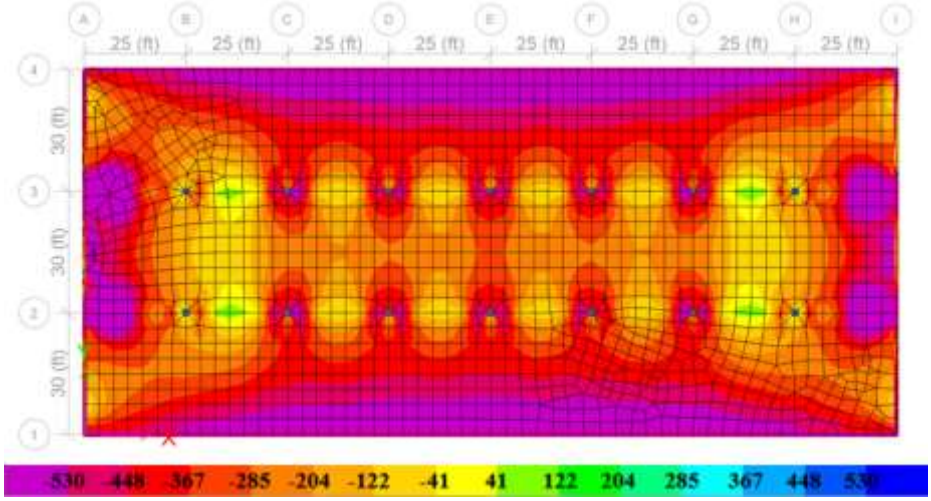

Figure 5-10 Axial stress in psi for prototype 2.0 at 3 days (Note: 1 psi = 0.0068 MPa)

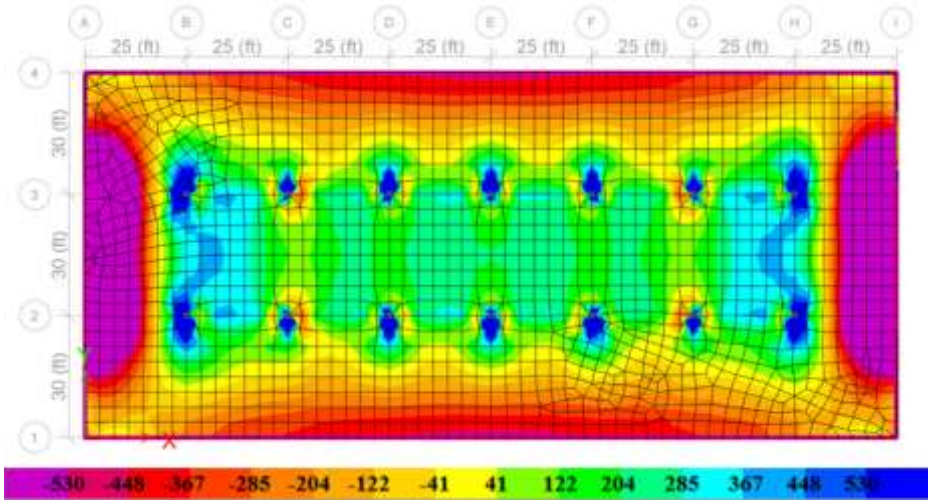

Figure 5-11 Axial stress in psi for prototype 2.0 at 5 years (Note: 1 psi = 0.0068 MPa)

But, if the wall thickness is increased to 20 in. (508 mm) cracking stresses can start at the 5-year mark as seen with the case of prototype 2.1 (**Figure 5-12** and **Figure 5-13**).

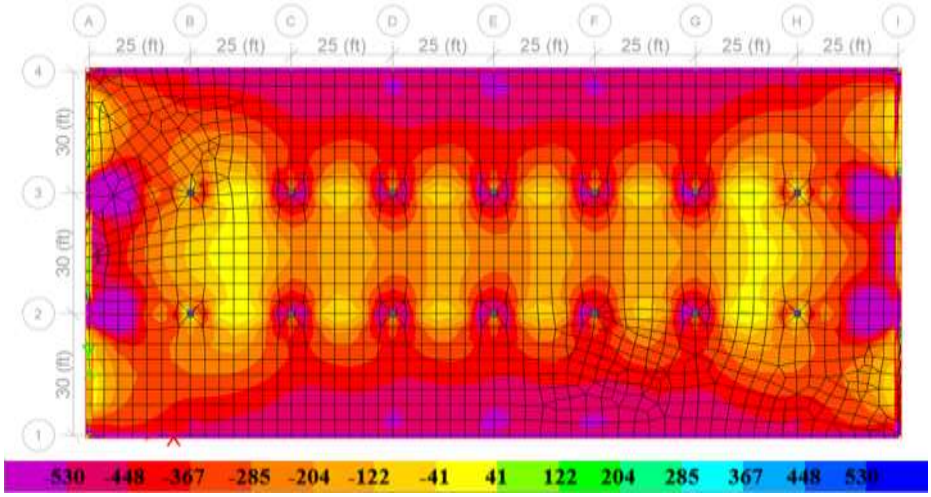

Figure 5-12 Axial stress in psi for prototype 2.1 at 3 days (Note: 1 psi = 0.0068 MPa)

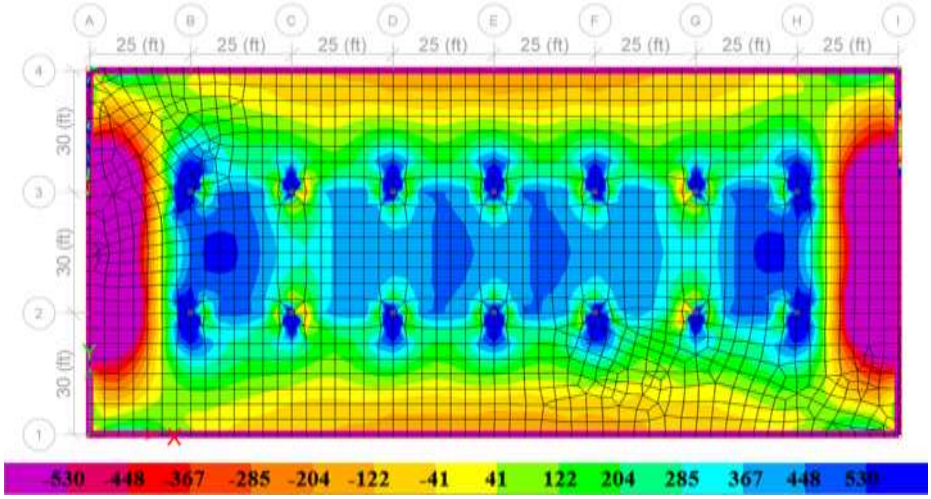

Figure 5-13 Axial stress in psi for prototype 2.1 at 5 years (Note: 1 psi = 0.0068 MPa)

Similarly, in the case of the longer slab being restrained by perimeter walls, cracking tensile stresses appear at the 5-year mark, as shown with prototype 2.2 (**Figure 5-14** and **Figure 5-15**).

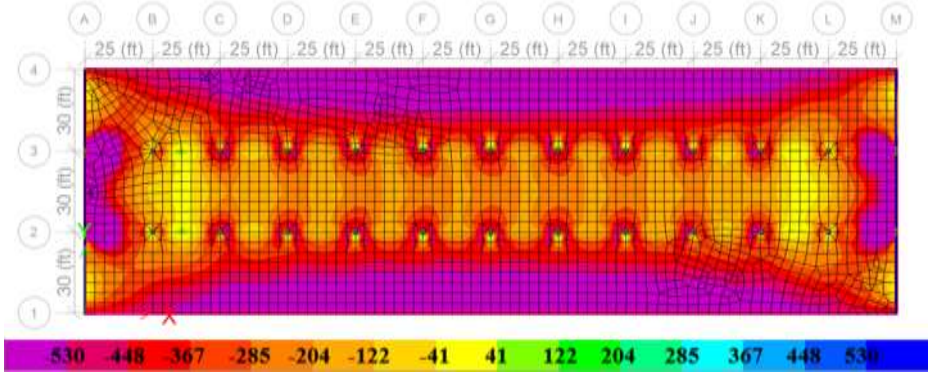

Figure 5-14 Axial stress in psi for prototype 2.2 at 3 days (Note: 1 psi = 0.0068 MPa)

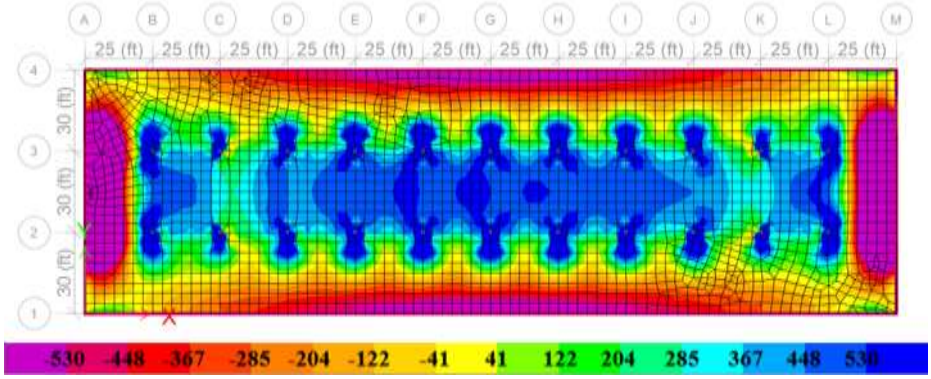

Figure 5-15 Axial stress in psi for prototype 2.2 at 5 years (Note: 1 psi = 0.0068 MPa)

Several references theorize that perimeter walls would exert a larger restraining force than walls located closer to the center of the slab; however, the analysis shows that walls located in the center could absorb large part of the precompressive stress on the slab and lead to cracking. As it can be observed in prototypes 4.0 (**Figure 5-16** and **Figure 5-17**), 5.0 (**Figure 5-18** and **Figure 5-19**), the cracking behavior could already start at 1 year vs. prototype 2.1, where cracking starts after the 5-year mark.

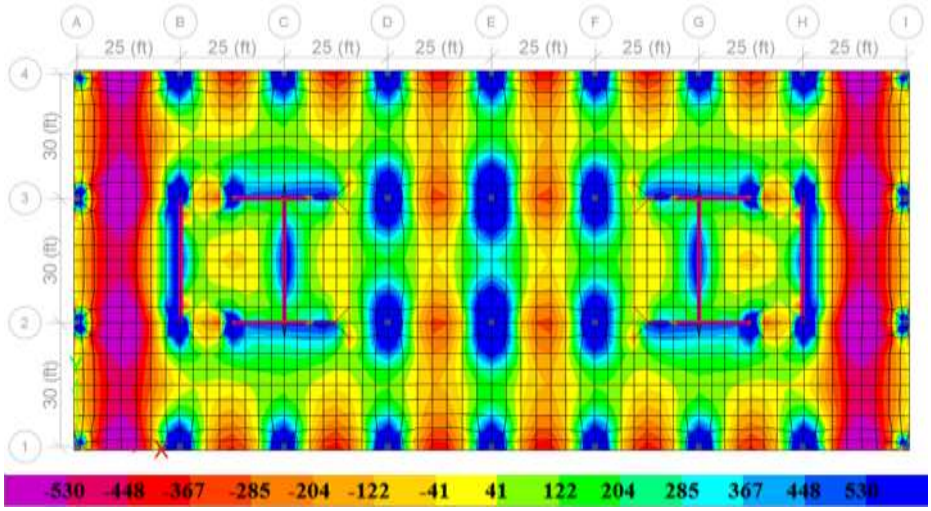

Figure 5-16 Axial stress in psi for prototype 4.0 at 1 year (Note: 1 psi = 0.0068 MPa)

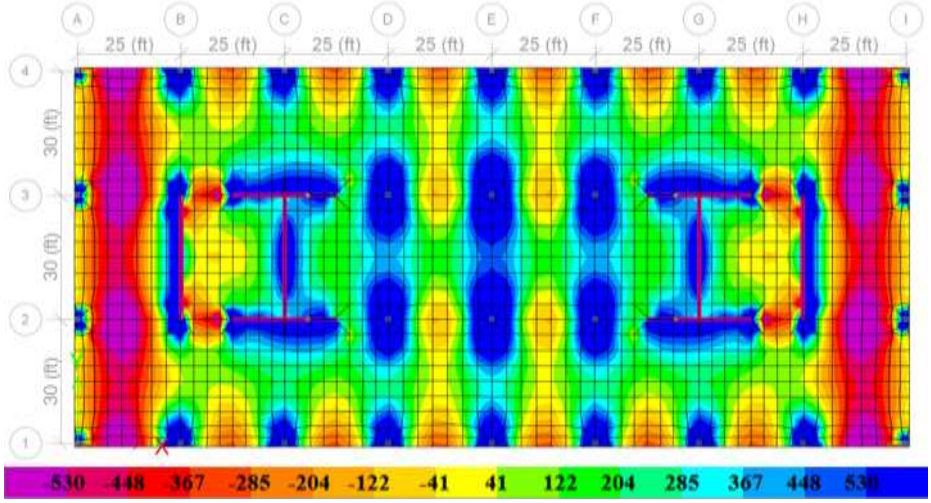

Figure 5-17 Axial stress in psi for prototype 4.0 at 5 years (Note: 1 psi = 0.0068 MPa)

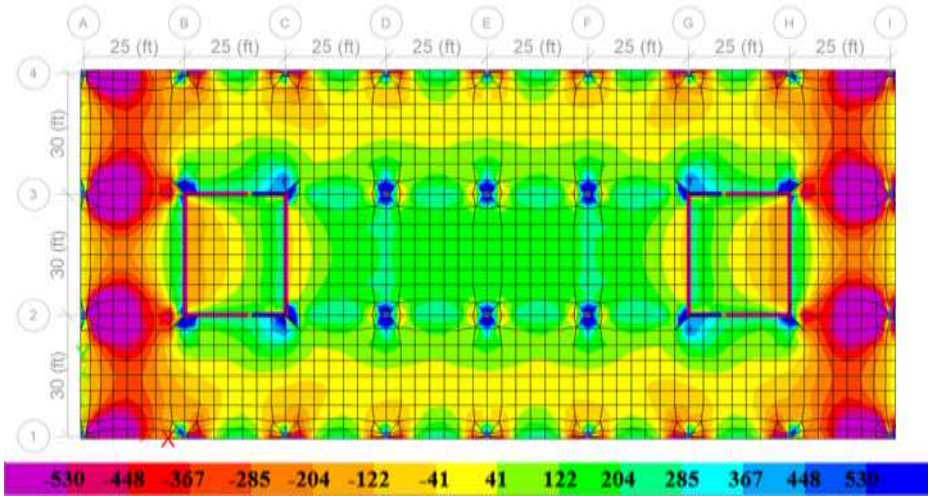

Figure 5-18 Axial stress in psi for prototype 5.0 at 1 year (Note: 1 psi = 0.0068 MPa)

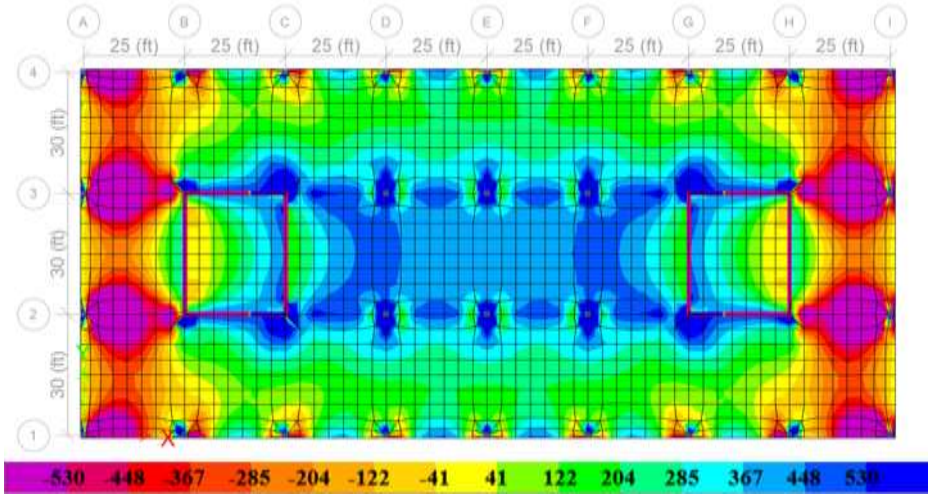

Figure 5-19 Axial stress in psi for prototype 5.0 at 5 years (Note: 1 psi = 0.0068 MPa)

Again, if there is an increase in wall thickness, as observed with prototype 5.1, a significant increase in cracking tensile stresses occurs, making this wall distribution and wall-to-slab thickness ratio not recommendable to use.

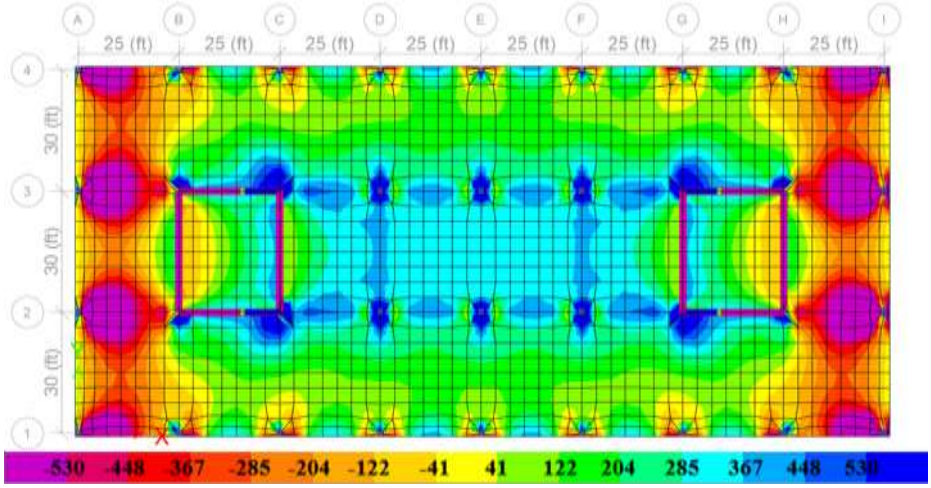

Figure 5-20 Axial stress in psi for prototype 5.1 at 1 year (Note: 1 psi = 0.0068 MPa)

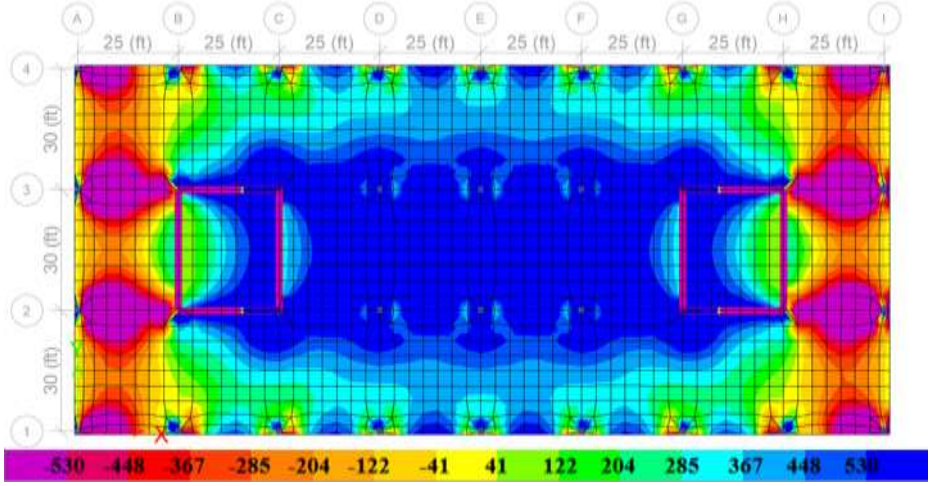

Figure 5-21 Axial stress in psi for prototype 5.1 at 5 years (Note: 1 psi = 0.0068 MPa)

The prototypes 3.0, 3.1 (**Figure 5-22** and **Figure 5-23**) and 3.2, that have walls only on the transversal sides do not present significant cracking stresses, even if there is an increase in wall thickness, as it is the case of prototype 3.1.

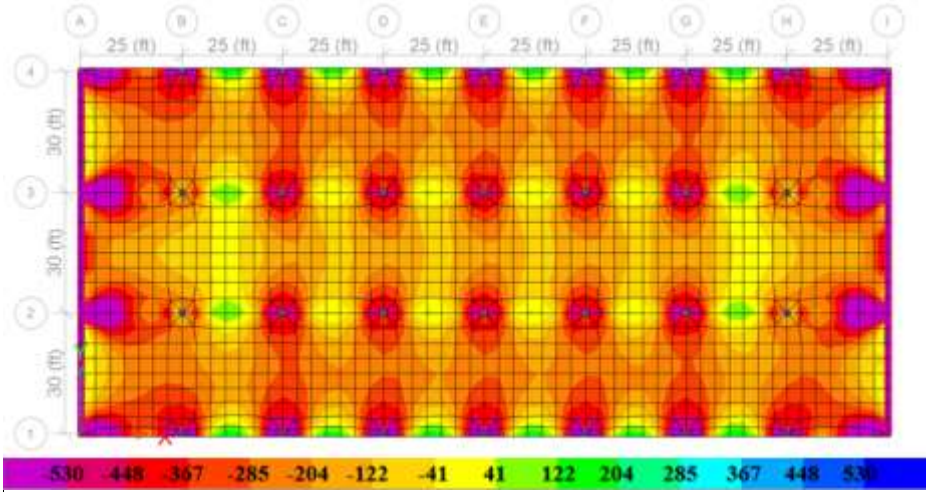

Figure 5-22 Axial stress in psi for prototype 3.1 at 3 days (Note: 1 psi = 0.0068 MPa)

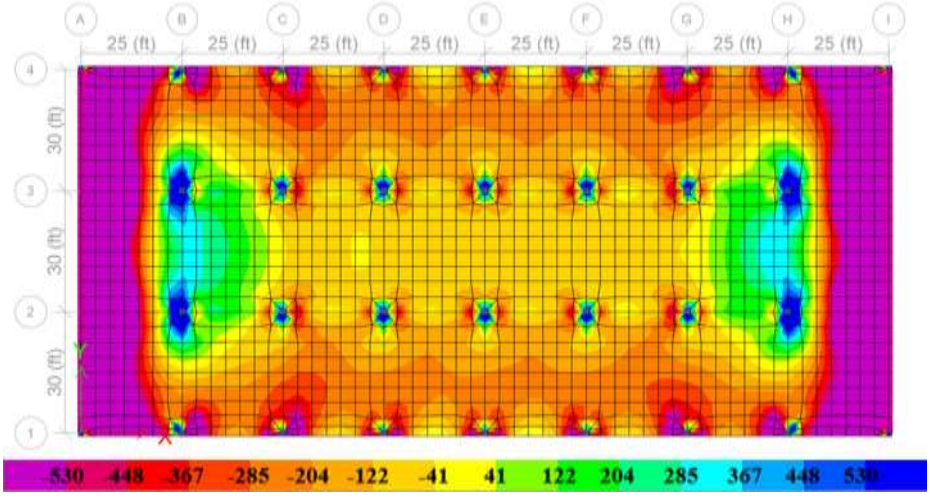

Figure 5-23 Axial stress in psi for prototype 3.1 at 5 years (Note: 1 psi = 0.0068 MPa)

An overall comparison in the effects of an increase in wall thickness can be seen through **Figure 5-24**, **Figure 5-25** and **Figure 5-26**, where an average

increase of 24% in tensile stresses and a decrease of 14% in precompression can be observed at final times (**Table 5-1**).

Table 5-1 Change in stresses caused by an increase in wall-to-slab ratio

Change in Stresses through wall-to-slab ratio increase		
	Tensile stress change	Compressive stress change
Prototype 2.0 vs. 2.1	+26%	-21%
Prototype 3.0 vs. 3.1	+21%	-5%
Prototype 7.0 vs. 7.1	+24%	-16%
Average change	**+24%**	**-14%**

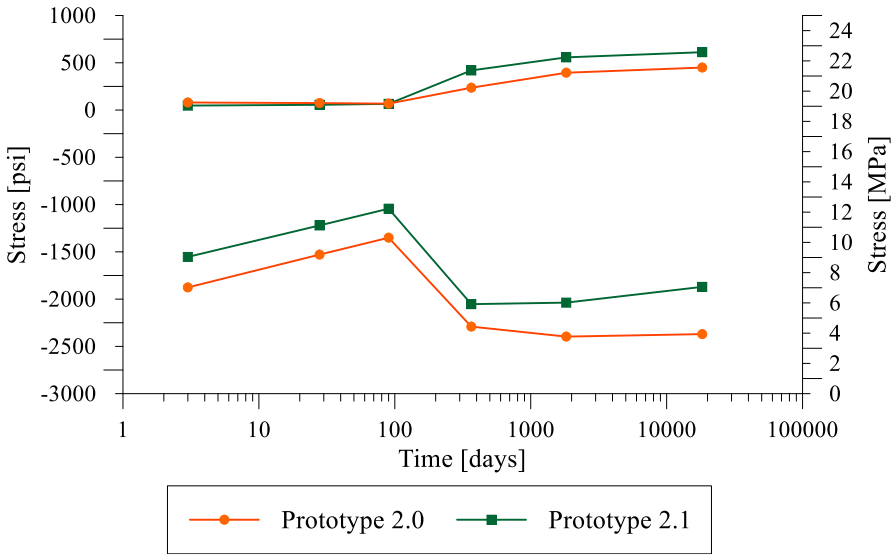

Figure 5-24 Axial stress change through time of prototype 2.0 and 2.1 (Note: 1 psi = 0.0068 MPa)

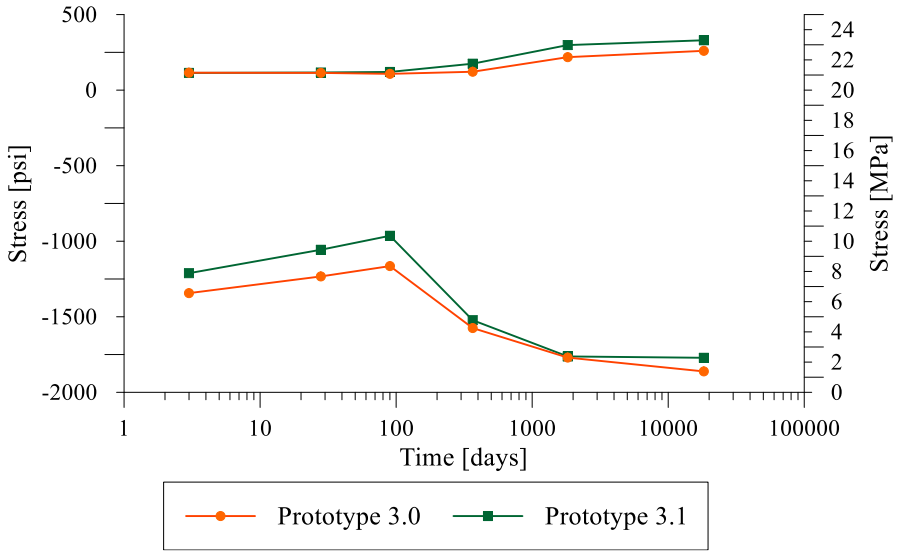

Figure 5-25 Axial stress change through time of prototype 3.0 and 3.1 (Note: 1 psi = 0.0068 MPa)

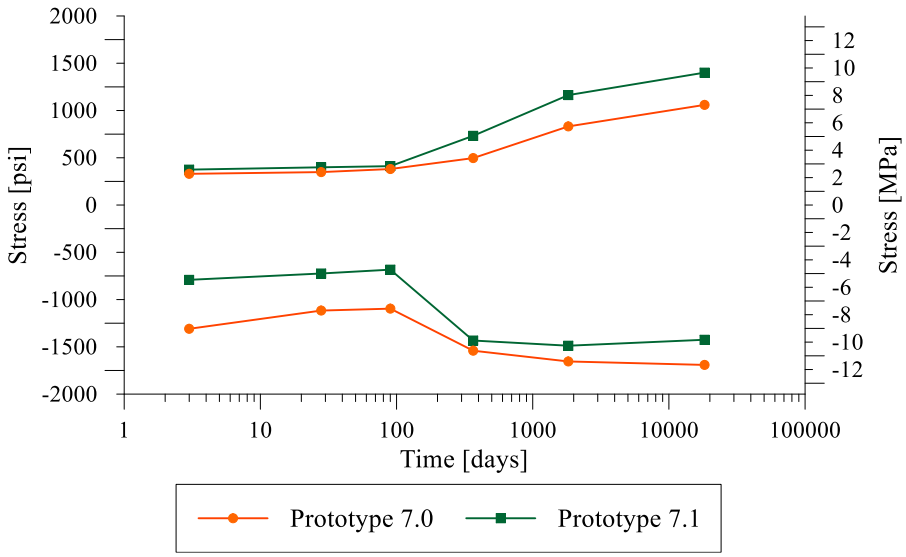

Figure 5-26 Axial stress change through time of prototype 7.0 and 7.1 (Note: 1 psi = 0.0068 MPa)

Although prototype 8.0 (**Figure 5-27** and **Figure 5-28**) has an irregular shape, it does not show significant cracking stresses. The same can be observed with prototypes 8.1 (**Figure 5-29** and **Figure 5-30**), 8.2 (**Figure 5-31** and **Figure 5-32**) and 9.0 (**Figure 5-33** and **Figure 5-34**). Even though they pass the 250 ft. (76.2 m), and have irregular shapes, they do not show significant tensile stresses due to the lack of restraint forces coming from walls.

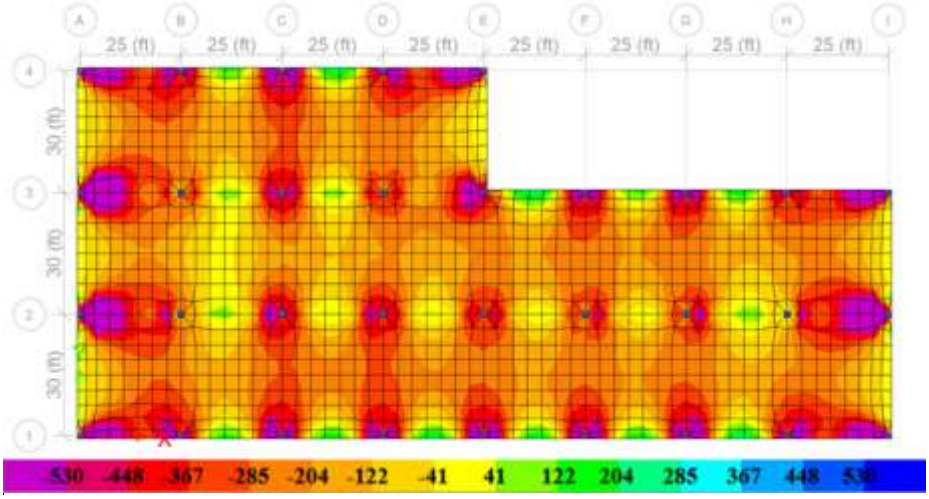

Figure 5-27 Axial stress in psi for prototype 8.0 at 3 days (Note: 1 psi = 0.0068 MPa)

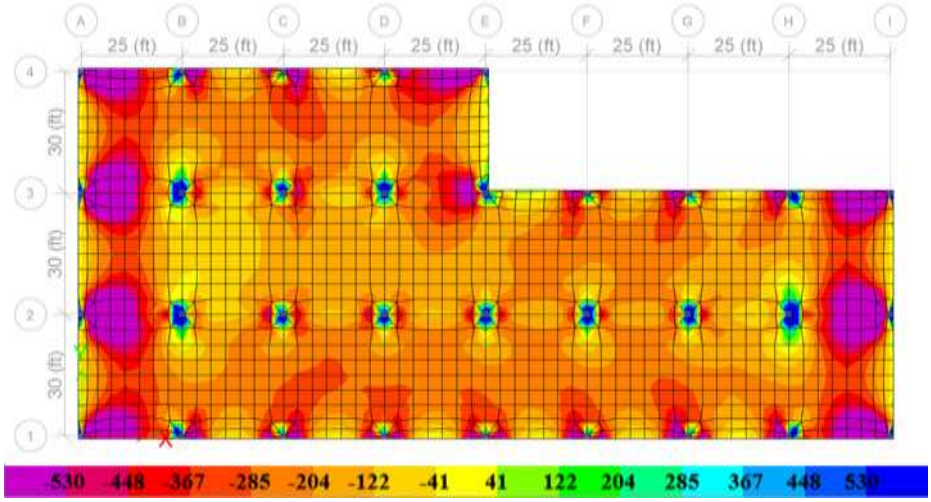

Figure 5-28 Axial stress in psi for prototype 8.0 at 5 years (Note: 1 psi = 0.0068 MPa)

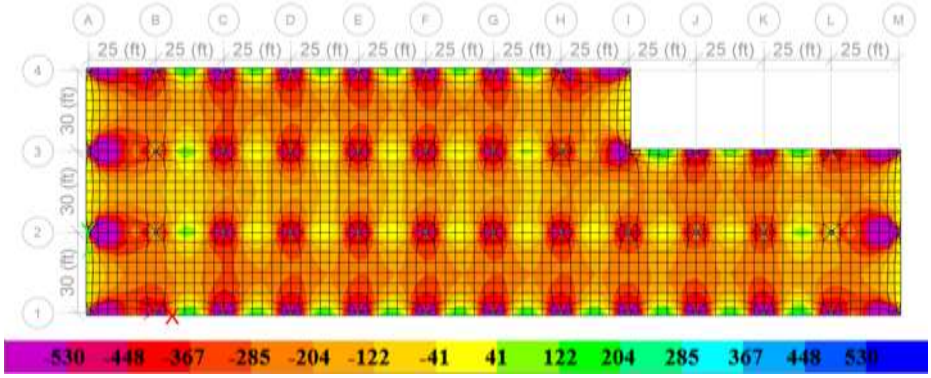

Figure 5-29 Axial stress in psi for prototype 8.1 at 3 days (Note: 1 psi = 0.0068 MPa)

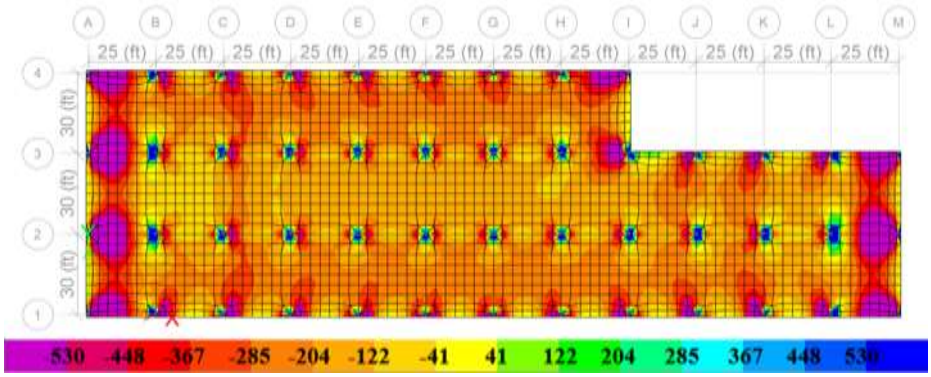

Figure 5-30 Axial stress in psi for prototype 8.1 at 5 years (Note: 1 psi = 0.0068 MPa)

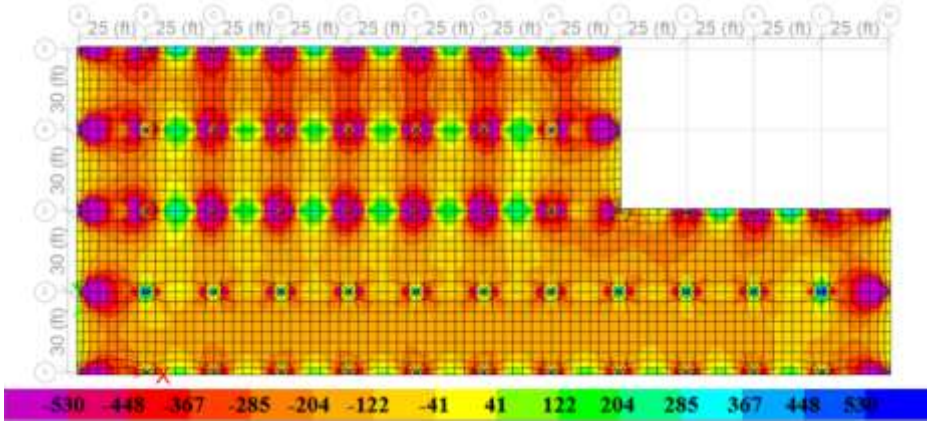

Figure 5-31 Axial stress in psi for prototype 8.2 at 3 days (Note: 1 psi = 0.0068 MPa)

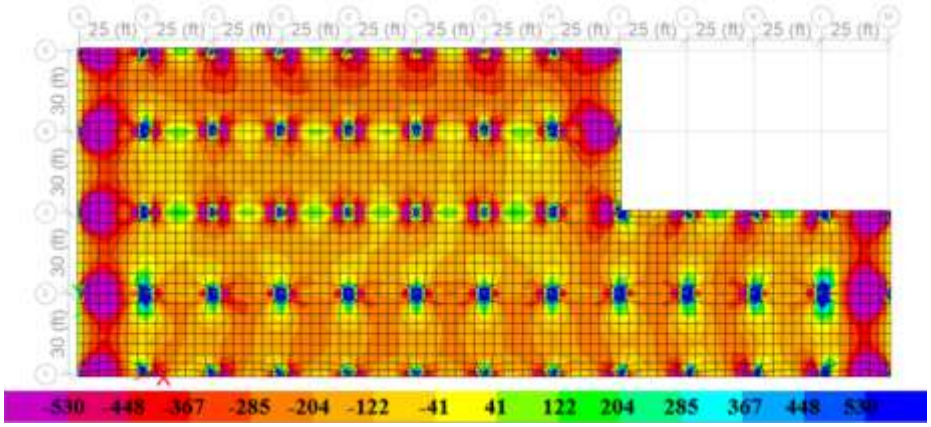

Figure 5-32 Axial stress in psi for prototype 8.2 at 5 years (Note: 1 psi = 0.0068 MPa)

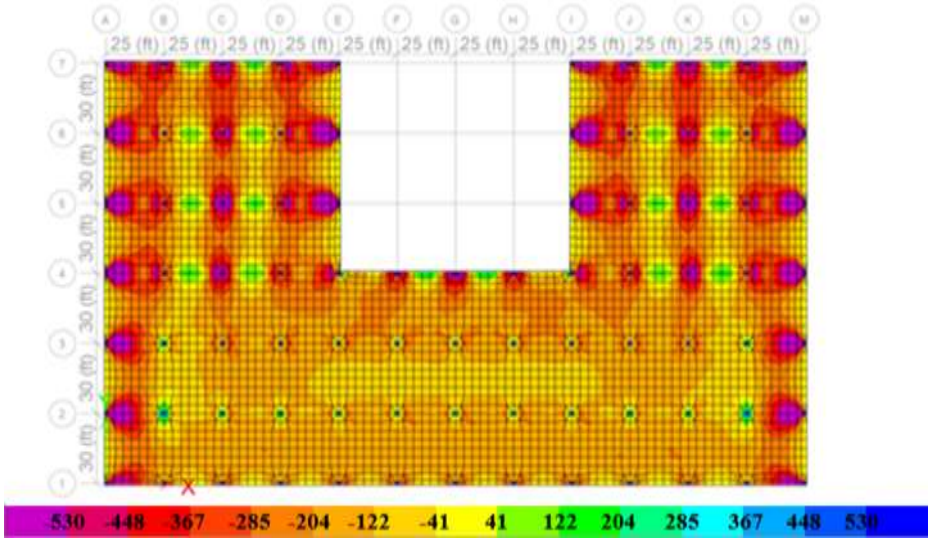

Figure 5-33 Axial stress in psi for prototype 9.0 at 3 days (Note: 1 psi = 0.0068 MPa)

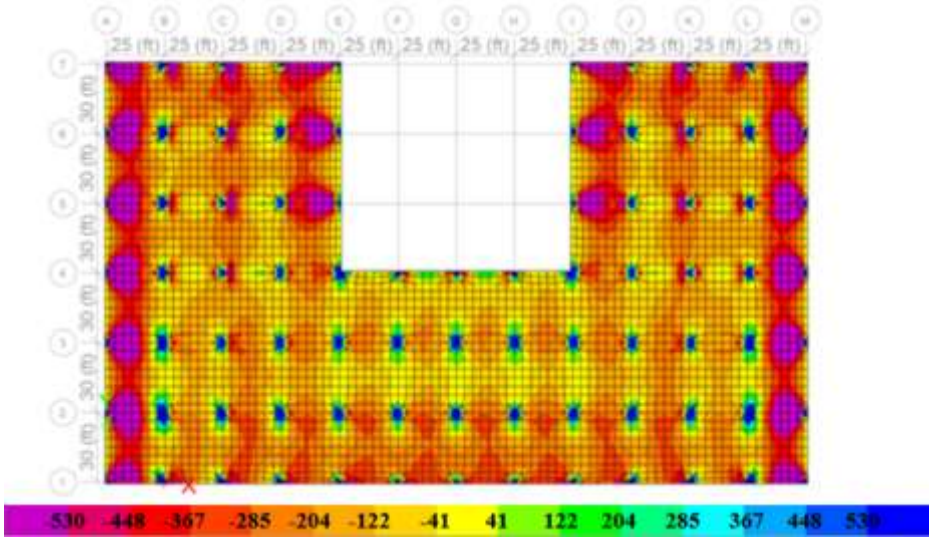

Figure 5-34 Axial stress in psi for prototype 9.0 at 5 years (Note: 1 psi = 0.0068 MPa)

According to the results, the prototype that seems to exert the most tensile stresses is the number 5.2 (**Figure 5-35** and **Figure 5-36**) which has the restraining walls in the extreme sides of the slab and center of the y-axis. By the 1-year mark, this model appears to produce a large tensile force spread throughout most of the slab.

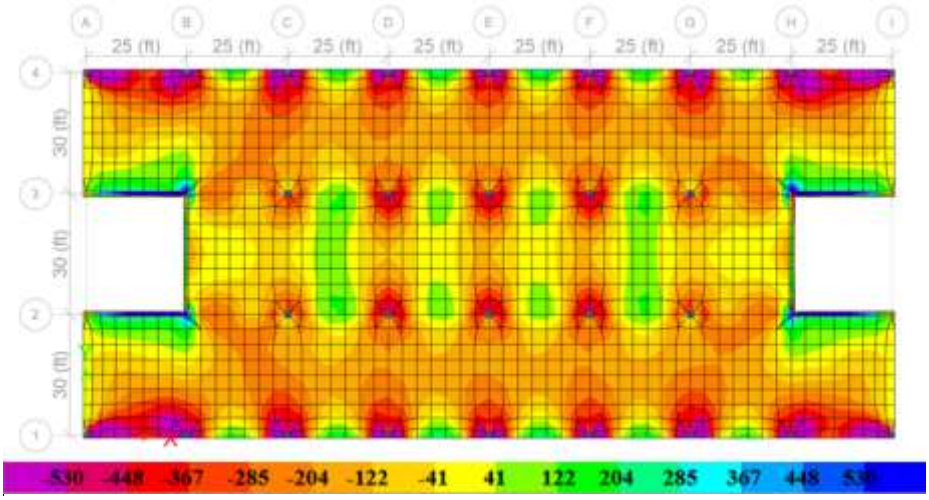

Figure 5-35 Axial stress in psi for prototype 5.2 at 3 days (Note: 1 psi = 0.0068 MPa)

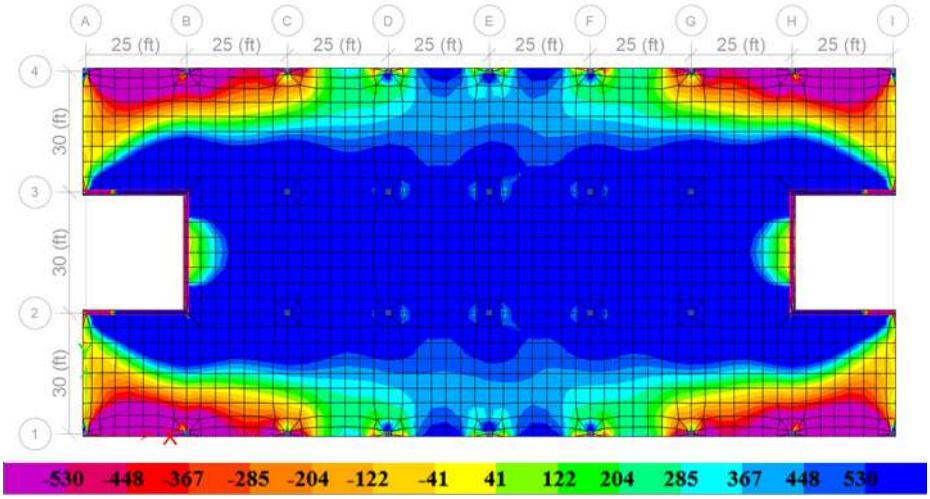

Figure 5-36 Axial stress in psi for prototype 5.2 at 1 year (Note: 1 psi = 0.0068 MPa)

Another wall configurations that seem to exert large tensile cracking stresses are the one found in prototype 6.0 (**Figure 5-37**) and that of prototype 7.1 (**Figure 5-38**), which has a wall thickness of 20 in. (508 mm).

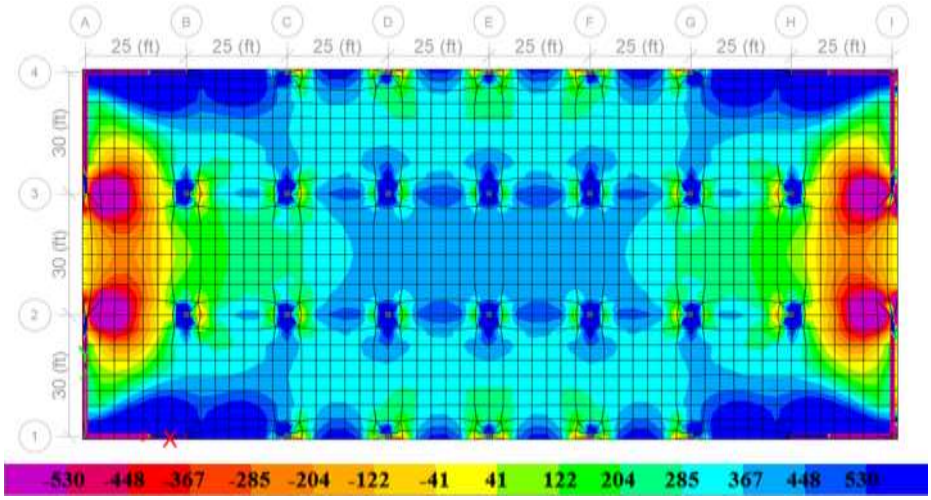

Figure 5-37 Axial stress in psi for prototype 6.0 at 5 years (Note: 1 psi = 0.0068 MPa)

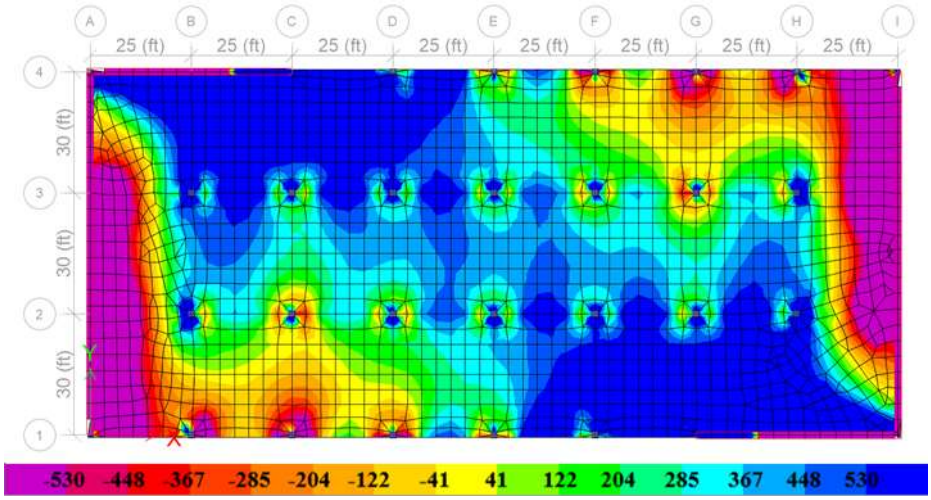

Figure 5-38 Axial stress in psi for prototype 7.1 at 5 years (Note: 1 psi = 0.0068 MPa)

According to the information in the available literature, which was developed empirically, cracking mitigation can be achieved through several methods, such as pour strips, member releases, additional bonded reinforcement in critical

locations, and structural separations. If we observe the final 50-year axial stress results for prototype 2.2 (**Figure 5-39**), which is the slab with 300 ft. (91.44 m). length and perimeter walls, a large restraint force would exert cracking. However, if a pour strip, or slab discontinuity, is added to the structure, as shown in prototype 2.2.1 (**Figure 5-40**), a large portion of the resulting stresses would be mitigated. If a partial wall release (corner release) as observed in prototype 2.2.2 (**Figure 5-41**) is added, no tensile cracking is produced. However, if instead a total release is added, which can be emulated through prototype 1.1, at the 50-year mark (**Figure 5-42**) the post-tensioning of the slab would have its best performance. In this case, nevertheless, there should be a consideration for using perimeter columns to achieve a complete detachment from the walls.

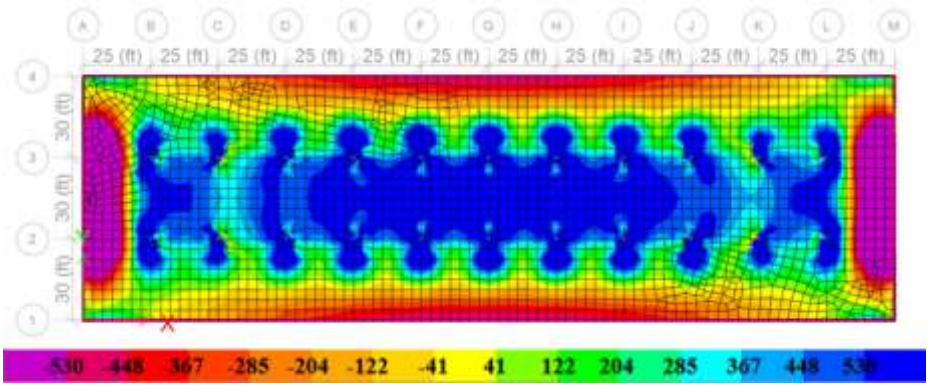

Figure 5-39 Axial stress in psi for prototype 2.2 at 50 years (Note: 1 psi = 0.0068 MPa)

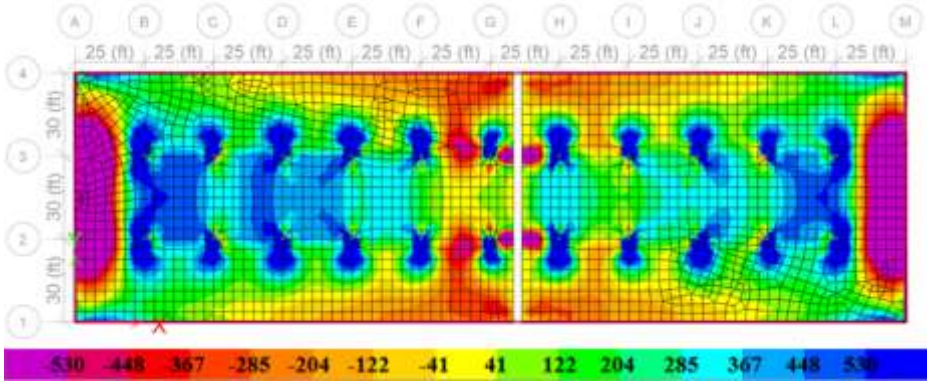

Figure 5-40 Axial stress in psi for prototype 2.2.1 at 50 years (Note: 1 psi = 0.0068 MPa)

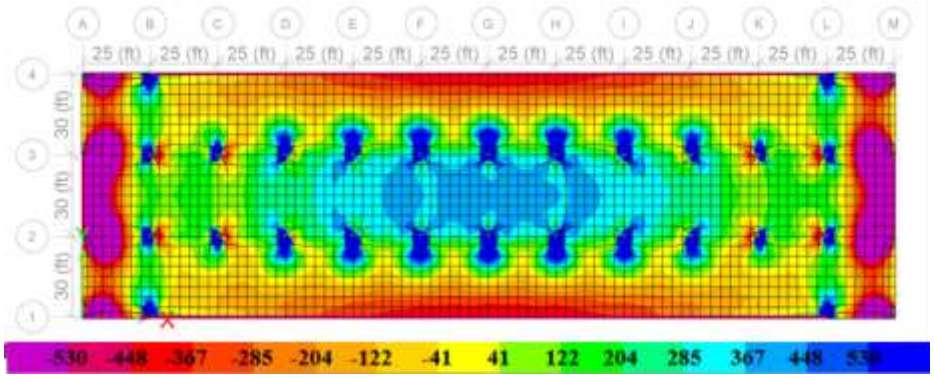

Figure 5-41 Axial stress in psi for prototype 2.2.2 at 50 years (Note: 1 psi = 0.0068 MPa)

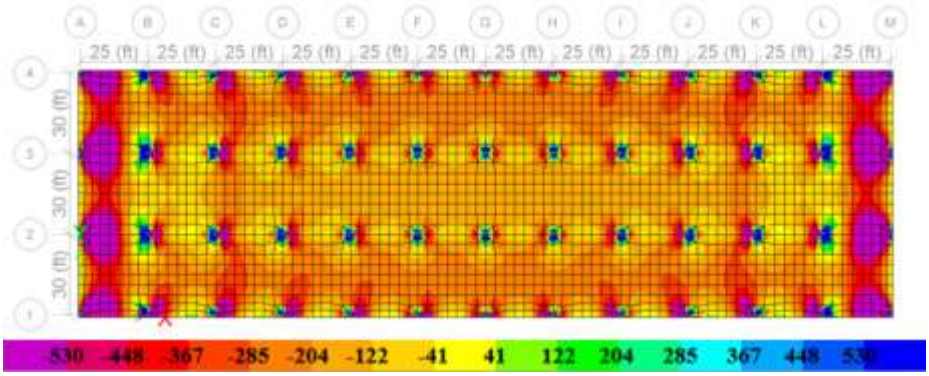

Figure 5-42 Axial stress in psi for prototype 1.1 at 50 years (Note: 1 psi = 0.0068 MPa)

Figure 5-43 shows the comparison of these prototypes' maximum tensile and compressive stresses through time, where it is possible to compare the efficiency of each mitigation strategy. **Table 5-2** shows the stress change in percentage that occurs with the use of each of these strategies.

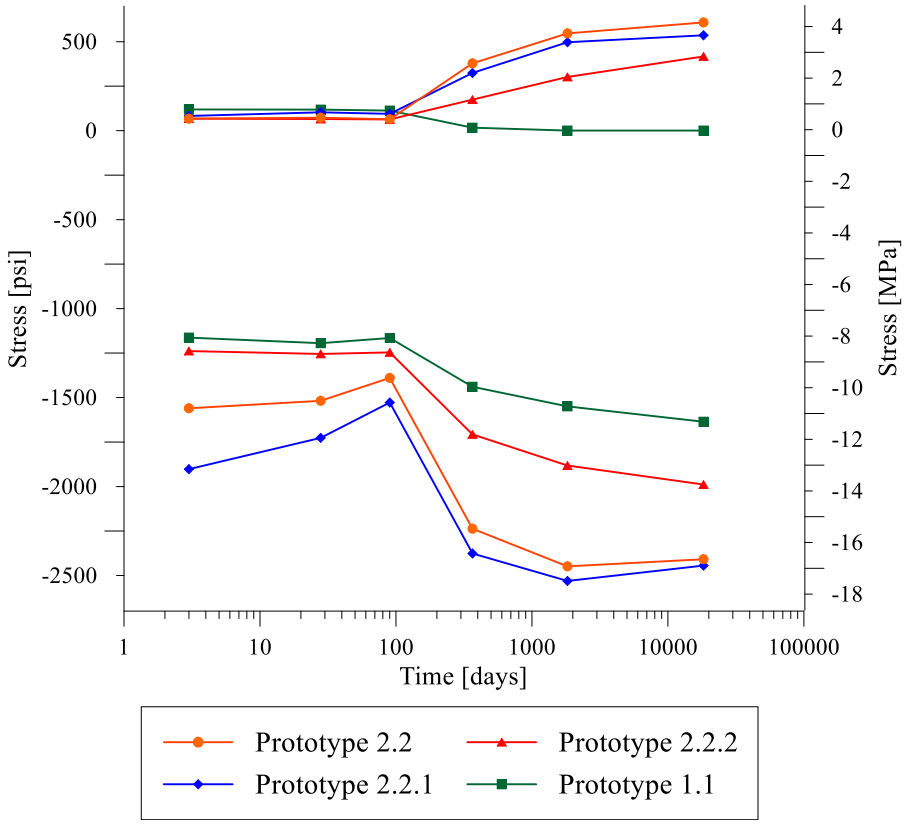

Figure 5-43 Axial stress change through time of prototype 2.2, 2.2.1, 2.2.2 and 1.1 (Note: 1 psi = 0.0068 MPa)

Table 5-2 Final axial stress reduction of prototype 2.1 vs. 2.2.1, 2.2.2 or 1.1

Change in Stresses through Mitigation Strategy		
	Tensile Stress Change	Compressive Stress Change
Prototype 2.2 vs. 2.2.1	-12%	+1%
Prototype 2.2 vs. 2.2.2	-31%	-17%
Prototype 2.2 vs. 1.1	-100%	-32%

In the case of prototype 2.0 (**Figure 5-44**), which is similar to 2.2, but with a slab length of 200 ft. (60.96 m), we can see less effective results in case of an addition of a pour strip as it shown in prototype 2.0.1 (**Figure 5-45**) although a partial wall release, which can be achieved by releasing the wall at the corners, as in prototype 6.1 (**Figure 5-46**), seems to be more effective for stress mitigation. And again, the most effective mitigation method in this comparison seems to be a total release as emulated in prototype 1.0 (**Figure 5-47**).

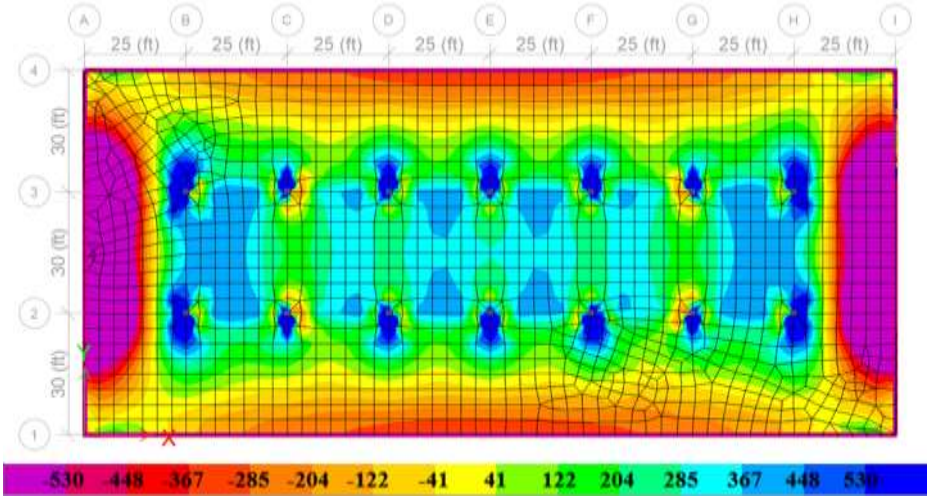

Figure 5-44 Axial stress in psi for prototype 2.0 at 50 years (Note: 1 psi = 0.0068 MPa)

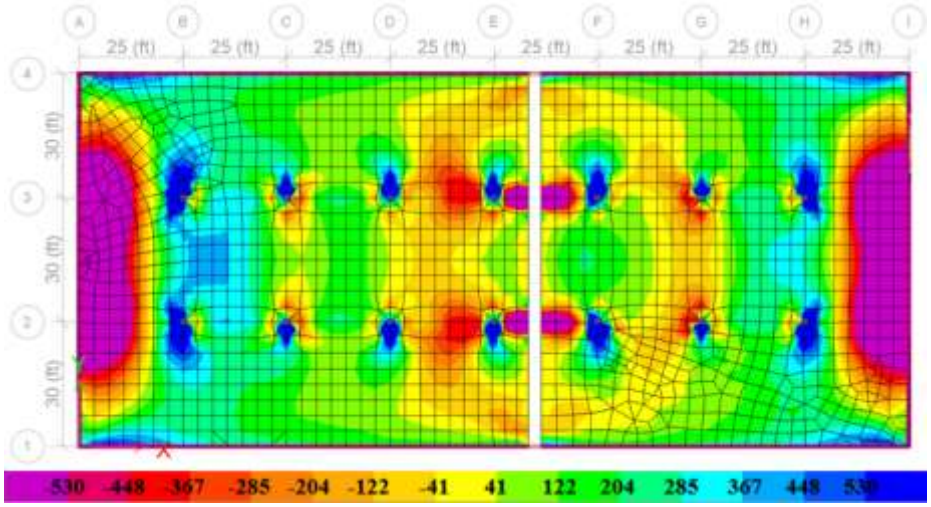

Figure 5-45 Axial stress in psi for prototype 2.0.1 at 50 years (Note: 1 psi = 0.0068 MPa)

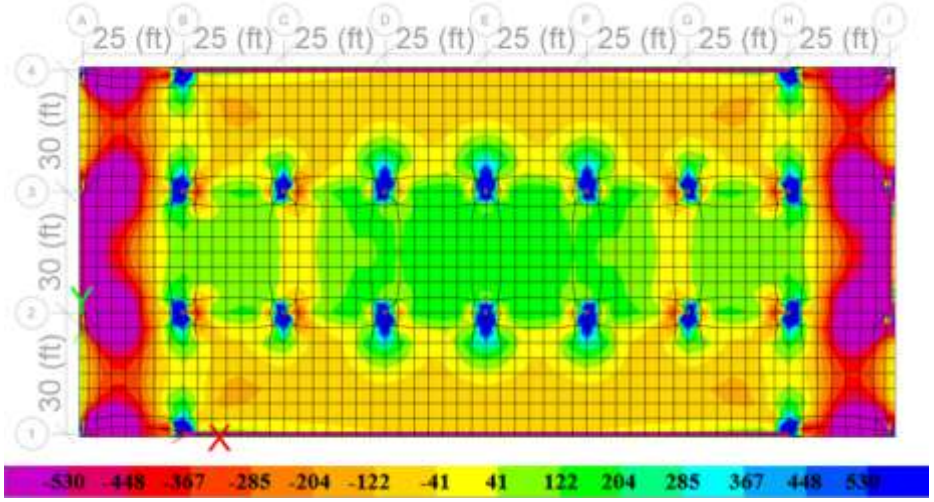

Figure 5-46 Axial stress in psi for prototype 6.1 at 50 years (Note: 1 psi = 0.0068 MPa)

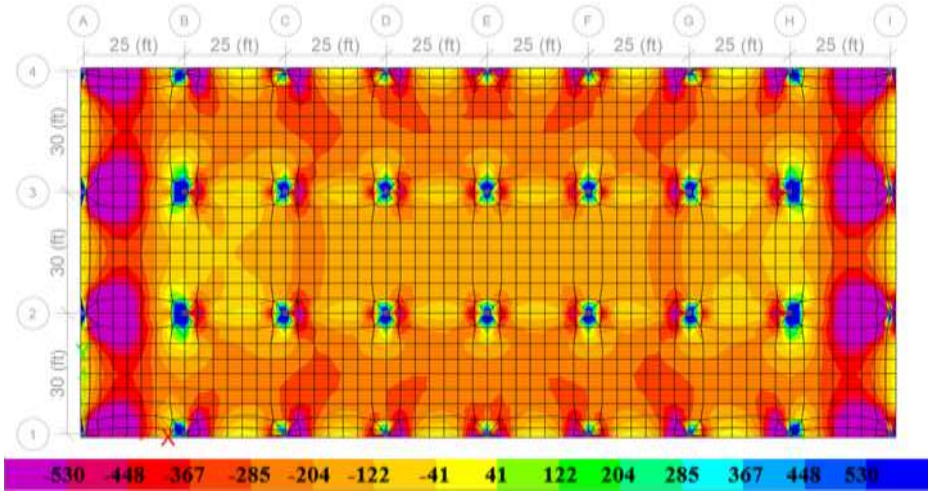

Figure 5-47 Axial stress in psi for prototype 1.0 at 50 years (Note: 1 psi = 0.0068 MPa)

Figure 5-48 shows the comparison of these prototypes' maximum tensile and compressive stresses through time, where it is possible to compare the efficiency of each mitigation strategy. **Table 5-3** shows the stress change in percentage that occurs with the use of each of these strategies.

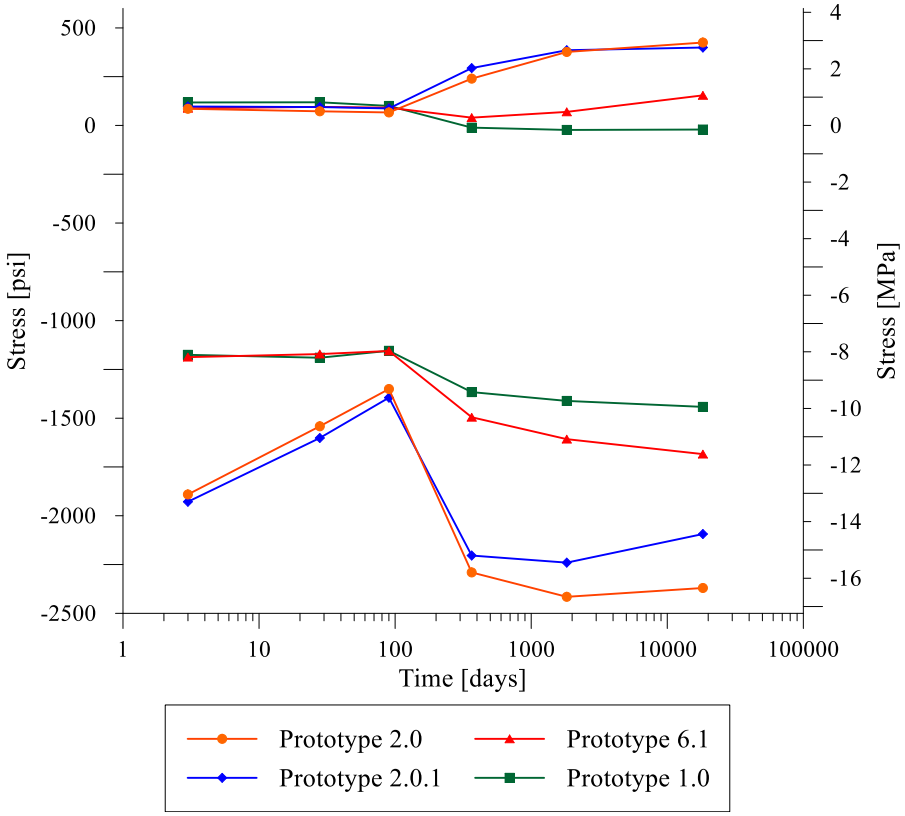

Figure 5-48 Axial stress change through time of prototype 2.0, 2.0.1, 6.1 and 1.0 (Note: 1 psi = 0.0068 MPa)

Table 5-3 Final axial stress reduction of prototype 2.0 vs. 2.0.1, 6.1 or 1.1

Change in Stresses through Mitigation Strategy		
	Tensile Stress Change	Compressive Stress Change
Prototype 2.0 vs. 2.0.1	-6%	-12%
Prototype 2.0 vs. 6.1	-64%	-29%
Prototype 2.0 vs. 1.1	-105%	-39%

A wall-to-slab connection is usually required to be maintained for earthquake-resistant structures; therefore, an analysis was made to define the minimum wall release to prevent restraint-cracking in these examples.

The reviewed literature recommends a wall release of once to twice the height of the wall to mitigate wall cracking (Nawy, 2008); however, no recommendation was found that included also the case of earthquake-resistance requirements.

Three variations of prototype 6.1 were analyzed; prototype 6.1a (**Figure 5-49**), where the transversal release was reduced to 12 ft. (3.66 m) to follow the height of the wall; prototype 6.1b (**Figure 5-50**), where there was no release from the transversal wall, but the release from the longitudinal direction was maintained as 25 ft. (7.62 m); and prototype 6.1c (**Figure 5-51**), where the release from the longitudinal direction is reduced to 12 ft. (3.66 m).

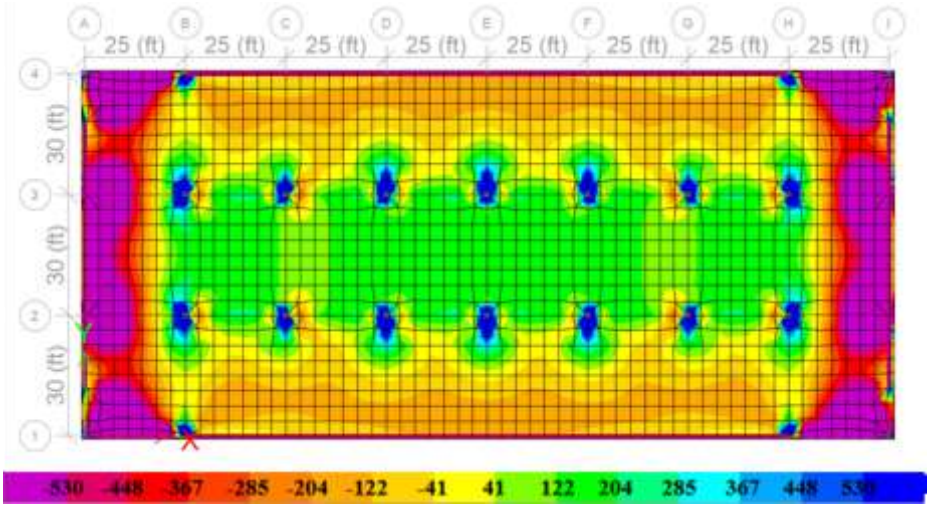

Figure 5-49 Axial stress in psi for Prototype 6.1a at 50 years (Note: 1 psi = 0.0068 MPa)

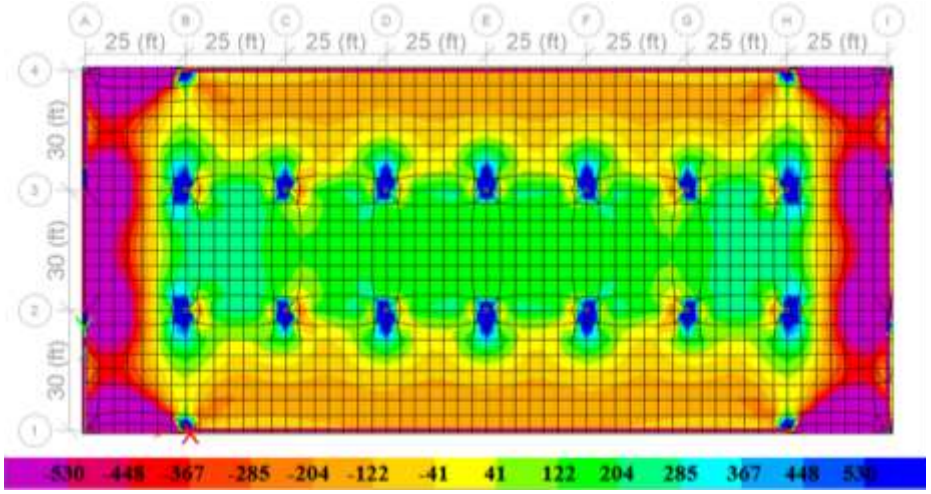

Figure 5-50 Axial stress in psi for Prototype 6.1b at 50 years (Note: 1 psi = 0.0068 MPa)

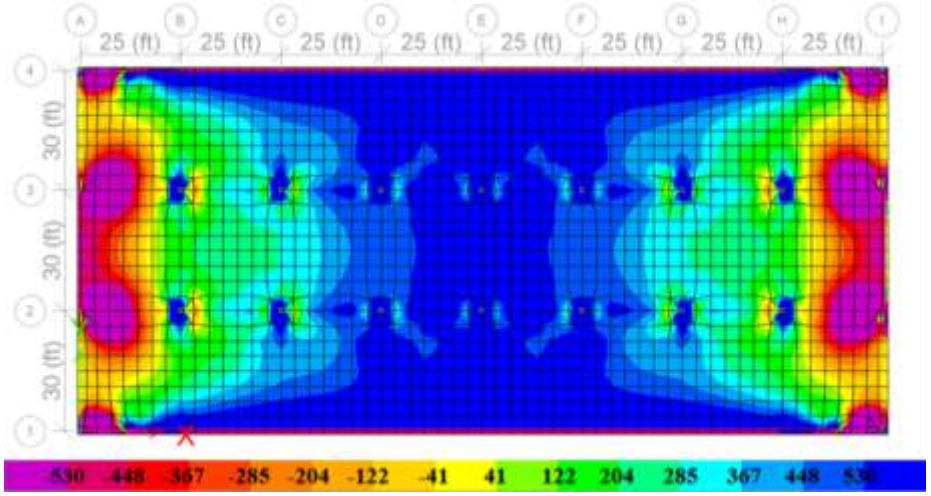

Figure 5-51 Axial stress in psi for Prototype 6.1c at 50 years (Note: 1 psi = 0.0068 MPa)

The analysis shows that, for this case, the minimum wall release allowed was 25 ft. (7.62 m) in the longitudinal direction, and no minimum release required in the transversal direction; therefore, in case of crack-prevention in the slab, it is necessary to have a release of more than twice the wall in the longest span.

In the case of the mitigation of tensile stresses exerted by walls located closer to the center of the slab, it shows that the addition of a pour strip to the design is enough to significantly reduce tensile stresses, as it is shown in the comparison of prototype 4.0 (**Figure 5-52**) vs. 4.0.1 (**Figure 5-53**) at the 50-year mark.

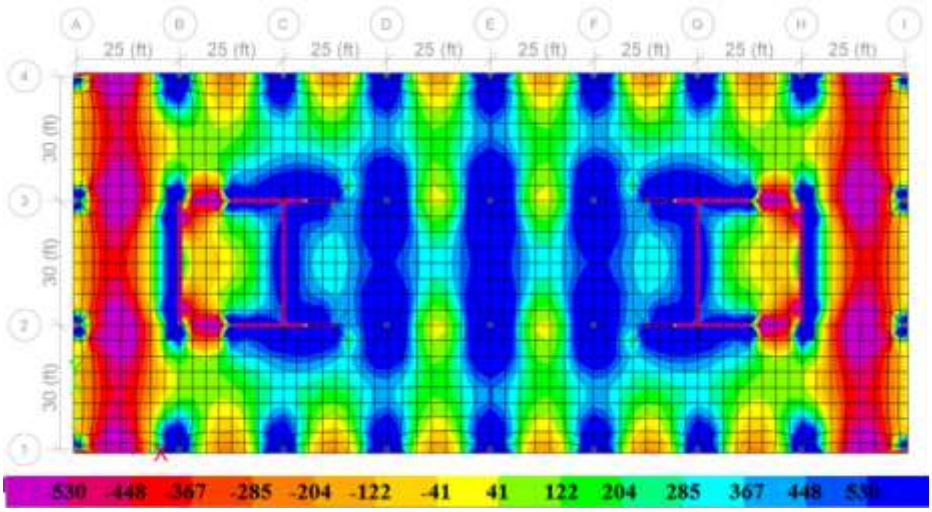

Figure 5-52 Axial stress in psi for prototype 4.0 at 50 years (Note: 1 psi = 0.0068 MPa)

In **Figure 5-54** the maximum tensile and compressive stresses through time are shown, exhibiting a significant reduction in compressive stresses and a reduction in tensile stresses at final times. Also, **Table 5-4** shows that the change in percentage produced by the use of this mitigation strategy is a 52% (decrease) in tensile stresses and a 94% (increase) in compressive stresses.

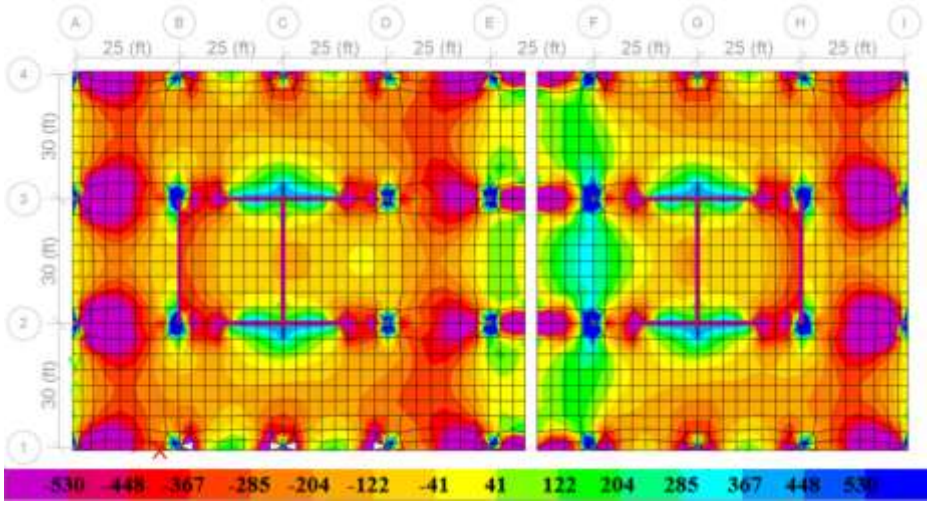

Figure 5-53 Axial stress in psi for prototype 4.0.1 at 50 years (Note: 1 psi = 0.0068 MPa)

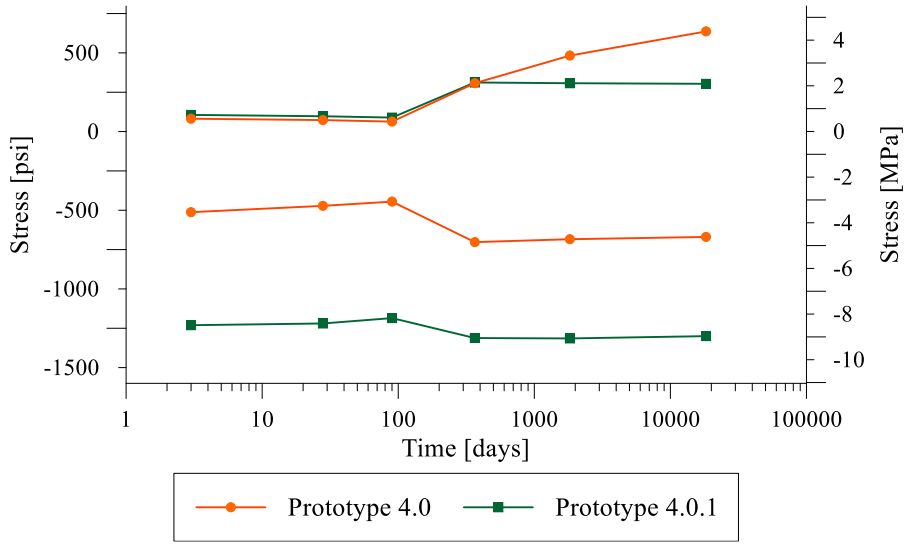

Figure 5-54 Axial stress change through time of prototype 4.0 and 4.0.1 (Note: 1 psi = 0.0068 MPa)

Table 5-4 Final axial stress reduction of prototype 4.0 vs. 4.0.1

Change in Stresses through Mitigation Strategy		
	Tensile Stress Change	Compressive Stress Change
Prototype 4.0 vs. 4.0.1	-52%	+94%

Similar behavior can be observed with prototype 5.0 (**Figure 5-55**) vs. prototype 5.0.1 (**Figure 5-56**), where the tensile stresses are effectively mitigated with the inclusion of a pour strip. Also, **Figure 5-57** shows the stress change through time of these two examples, and through this analysis a reduction of 74% in tensile stresses and 14% in compressive stresses is obtained (**Table 5-5**).

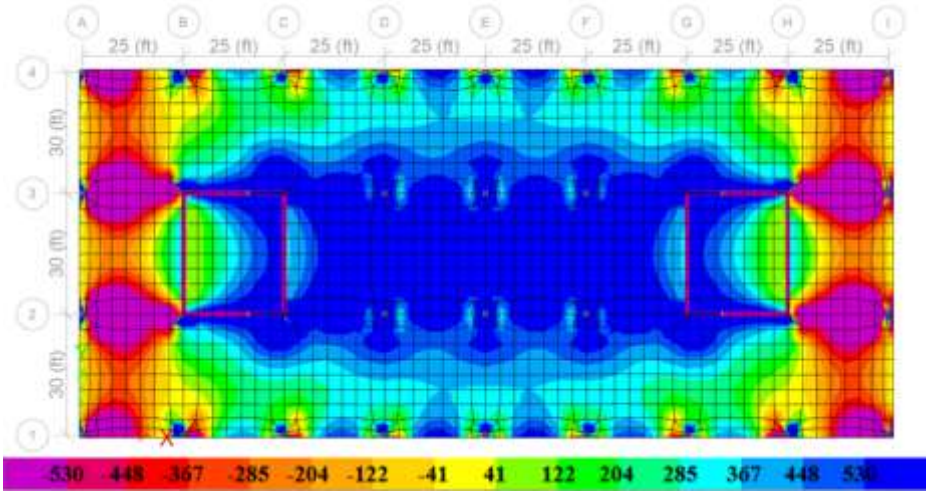

Figure 5-55 Axial stress in psi for prototype 5.0 at 50 years (Note: 1 psi = 0.0068 MPa)

Table 5-5 Final axial stress reduction of prototype 5.0 vs. 5.0.1

Change in Stresses through Mitigation Strategy		
	Tensile Stress Change	Compressive Stress Change
Prototype 5.0 vs. 5.0.1	-74%	-14%

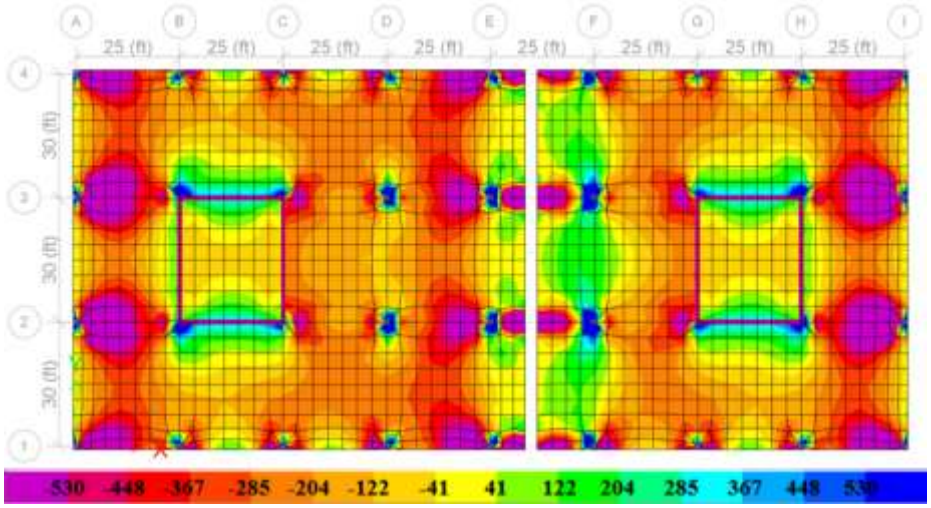

Figure 5-56 Axial stress in psi for prototype 5.0.1 at 50 years (Note: 1 psi = 0.0068 MPa)

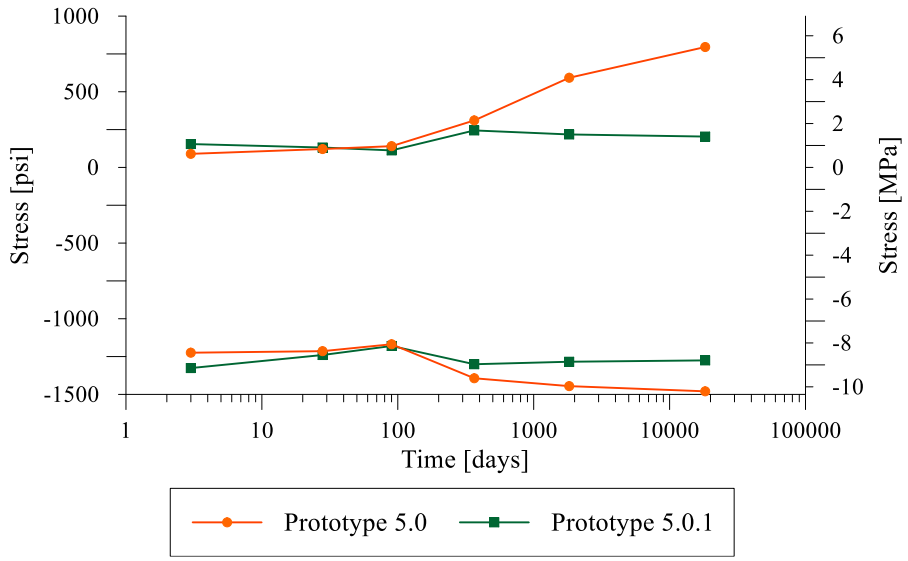

Figure 5-57 Axial stress change through time of prototype 5.0 and 5.0.1 (Note: 1 psi = 0.0068 MPa)

Instead of the case of prototype 5.3 (**Figure 5-58**), which is the one that shows the most cracking tensile stresses, the recommendation would be to structurally separate the slab as shown in prototype 5.2.1 (**Figure 5-59**), where only the center of the slab is post tensioned, and the rest of the slab could be of reinforced concrete, given the small size.

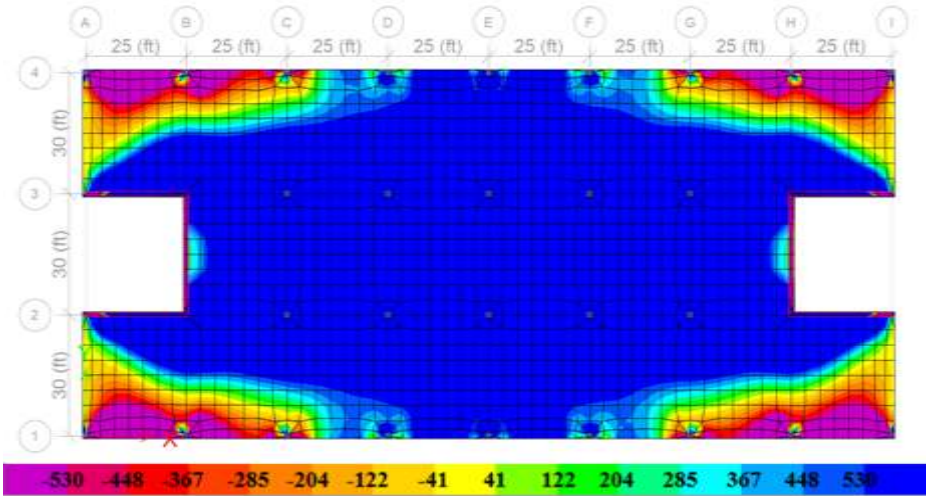

Figure 5-58 Axial stress in psi for prototype 5.2 at 50 years (Note: 1 psi = 0.0068 MPa)

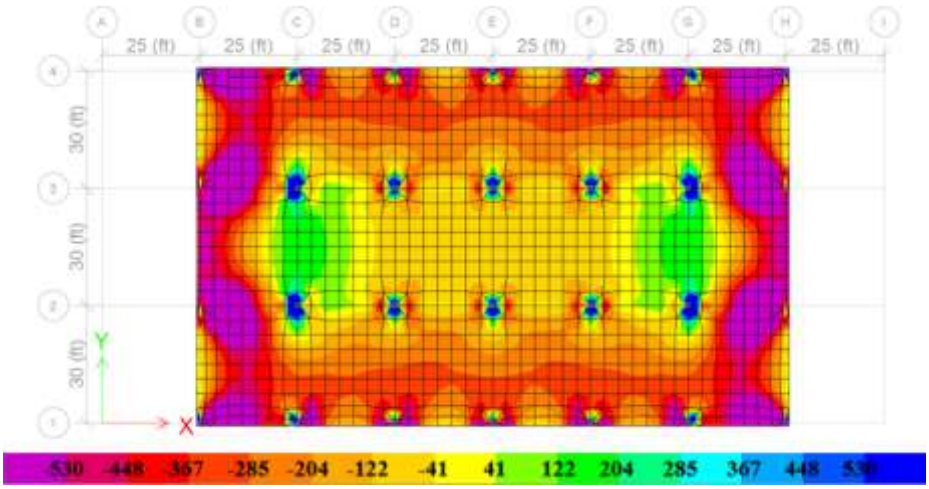

Figure 5-59 Axial stress in psi for prototype 5.2.1 at 50 years (Note: 1 psi = 0.0068 MPa)

Figure 5-60 shows the stresses through time of prototype 5.2 and 5.2.1, where a significant reduction in tensile stresses is observed. An overall reduction of 88% in tensile stresses and 10% in compressive stresses (**Table 5-6**) can be obtained from this mitigation strategy, effectively eliminating the cracking behavior.

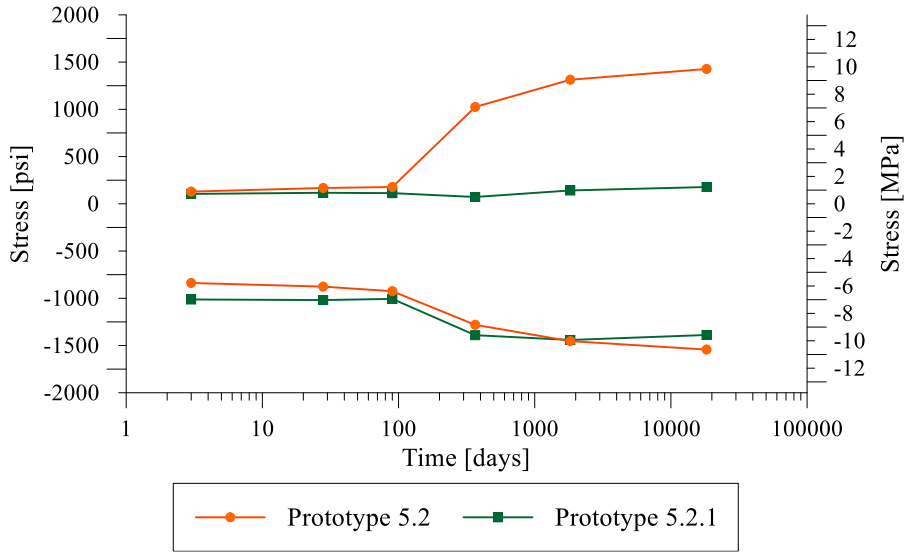

Figure 5-60 Axial stress change through time of prototype 5.2 and 5.2.1 (Note: 1 psi = 0.0068 MPa)

Table 5-6 Final axial stress reduction of prototype 5.2 vs. 5.2.1

Change in Stresses through Mitigation Strategy		
	Tensile Stress Change	Compressive Stress Change
Prototype 5.2 vs. 5.2.1	-88%	-10%

The ratio of deformed shrinkage and temperature reinforcement area to gross concrete area shall be greater than or equal to 0.0018 (ACI Committee 318, 2019) in areas where the precompression is below 100 psi (0.69 MPa), and for the examples reviewed in this analysis the minimum area of bonded

reinforcement would be 5.18 in^2 (3,341 mm^2) in the longitudinal(X-dir.) strips or 4.32 in^2 (2,787 mm^2) in the transversal (Y-dir.) strips.

Also, if the tensile stresses exceed $2\sqrt{f'_c}$ ($0.167\sqrt{f'_c}$) the minimum bonded longitudinal reinforcement should be calculated as follows (ACI Committee 318, 2019):

$$A_s = \frac{N_c}{0.5 f_y}$$

Where N_c represents the resultant tensile force and f_y represents the bonded reinforcement minimum yield stress.

In the case of the concrete specified in this analysis, the prototypes that surpass $2\sqrt{f'_c}$, calculated as 141.42 psi (0.97 MPa), in at least one area of the slab at final time (50 years) are all, except prototypes 1.0, 1.1 and 8.0.

The calculated minimum bonded reinforcement at the critical area of each prototype is presented in **Table 5-7** and it is possible to observe that the results are much lower than the minimum ratio of shrinkage and temperature reinforcement of 5.18 in^2 (3,341 mm^2) or 4.32 in^2 (2,787 mm^2).

Table 5-7 Calculated minimum area of bonded reinforcement required per prototype

Minimum Area of Bonded Reinforcement		
Prototype	in^2	mm^2
2.0	0.017	10.97
2.0.1	0.016	10.30
2.1	0.024	15.79
2.2	0.024	15.69
2.2.1	0.021	13.83
2.2.2	0.017	10.76

Minimum Area of Bonded Reinforcement		
Prototype	in^2	mm^2
3.0	0.010	6.71
3.1	0.013	8.52
3.2	0.014	8.93
4.0	0.025	16.44
4.0.1	0.012	7.85
5.0	0.032	20.54
5.0.1	0.008	5.26
5.1	0.038	24.46
5.2	0.057	36.85
5.2.1	0.007	4.57
6.0	0.047	30.09
6.0.1	0.023	14.89
6.1	0.006	3.97
7.0	0.042	27.33
7.0.1	0.008	5.08
7.1	0.056	36.15
8.1	0.008	5.11
8.2	0.011	6.81
9.0	0.011	7.12

Therefore, if the minimum ratio requirements for additional shrinkage and temperature bonded reinforcement is followed as stated in the code, it would not produce significant cracking.

Table 5-8 Calculated axial stresses in the slab over the longitudinal axis (X-axis) of each prototype

Final Axial Stresses								
Prototype Number	3 days				28 days			
	Max		Min		Max		Min	
	psi	MPa	psi	MPa	psi	MPa	psi	MPa
1.0	118	0.81	-1175	-8.10	119	0.82	-1190	-8.21
1.1	119	0.82	-1163	-8.02	118	0.81	-1194	-8.23
2.0	85	0.59	-1891	-13.04	73	0.50	-1541	-10.63
2.0.1	97	0.67	-1928	-13.30	94	0.65	-1601	-11.04
2.1	47	0.32	-1554	-10.72	56	0.39	-1220	-8.41
2.2	67	0.46	-1560	-10.76	73	0.50	-1518	-10.47
2.2.1	83	0.57	-1902	-13.12	103	0.71	-1726	-11.90
2.2.2	67	0.46	-1239	-8.54	65	0.45	-1255	-8.66
3.0	115	0.79	-1343	-9.26	114	0.79	-1233	-8.50
3.1	114	0.79	-1211	-8.35	116	0.80	-1057	-7.29
3.2	118	0.81	-1357	-9.36	115	0.79	-1252	-8.63
4.0	81	0.56	-512	-3.53	73	0.50	-472	-3.26
4.0.1	106	0.73	-1230	-8.48	97	0.67	-1219	-8.41
5.0	90	0.62	-1224	-8.44	121	0.83	-1214	-8.37
5.0.1	154	1.06	-1326	-9.14	132	0.91	-1240	-8.55
5.1	107	0.74	-1237	-8.53	146	1.01	-1210	-8.34
5.2	128	0.88	-837	-5.77	167	1.15	-877	-6.05
5.2.1	104	0.72	-1013	-6.99	116	0.80	-1019	-7.03
6.0	115	0.79	-1093	-7.54	137	0.94	-1042	-7.19
6.0.1	173	1.19	-1126	-7.77	182	1.26	-1081	-7.46
6.1	88	0.61	-1187	-8.19	95	0.66	-1171	-8.08
7.0	330	2.28	-1310	-9.03	348	2.40	-1117	-7.70
7.0.1	446	3.08	-1426	-9.83	519	3.58	-1242	-8.57
7.1	374	2.58	-792	-5.46	400	2.76	-725	-5.00
8.0	213	1.47	-1114	-7.68	198	1.37	-1097	-7.57
8.1	266	1.83	-1232	-8.50	245	1.69	-1215	-8.38
8.2	389	2.68	-1322	-9.12	404	2.79	-1291	-8.90
9.0	250	1.72	-1157	-7.98	264	1.82	-1138	-7.85

Final Axial Stresses (cont.)								
Prototype Number	90 days				1 year			
	Max		Min		Max		Min	
	psi	MPa	psi	MPa	psi	MPa	psi	MPa
1.0	100	0.69	-1155	-7.97	-11	-0.08	-1366	-9.42
1.1	113	0.78	-1165	-8.03	17	0.12	-1439	-9.92
2.0	67	0.46	-1351	-9.32	240	1.66	-2290	-15.79
2.0.1	87	0.60	-1395	-9.62	294	2.03	-2204	-15.20
2.1	65	0.45	-1043	-7.19	420	2.90	-2053	-14.16
2.2	64	0.44	-1390	-9.59	378	2.61	-2237	-15.43
2.2.1	94	0.65	-1528	-10.54	309	2.13	-2376	-16.39
2.2.2	63	0.43	-1246	-8.59	174	1.20	-1707	-11.77
3.0	108	0.74	-1165	-8.03	122	0.84	-1575	-10.86
3.1	120	0.83	-964	-6.65	175	1.21	-1522	-10.50
3.2	105	0.72	-1192	-8.22	233	1.61	-1876	-12.94
4.0	63	0.43	-445	-3.07	307	2.12	-703	-4.85
4.0.1	89	0.61	-1186	-8.18	312	2.15	-1312	-9.05
5.0	141	0.97	-1168	-8.06	310	2.14	-1393	-9.61
5.0.1	113	0.78	-1180	-8.14	244	1.68	-1301	-8.97
5.1	166	1.14	-1179	-8.13	373	2.57	-1388	-9.57
5.2	177	1.22	-925	-6.38	1024	7.06	-1281	-8.83
5.2.1	113	0.78	-1007	-6.94	72	0.50	-1390	-9.59
6.0	153	1.06	-1020	-7.03	540	3.72	-1224	-8.44
6.0.1	181	1.25	-1054	-7.27	387	2.67	-1091	-7.52
6.1	91	0.63	-1156	-7.97	40	0.28	-1495	-10.31
7.0	381	2.63	-1097	-7.57	497	3.43	-1541	-10.63
7.0.1	545	3.76	-1126	-7.77	247	1.70	-1346	-9.28
7.1	412	2.84	-683	-4.71	733	5.06	-1433	-9.88
8.0	187	1.29	-1073	-7.40	65	0.45	-1275	-8.79
8.1	238	1.64	-1203	-8.30	135	0.93	-1481	-10.21
8.2	407	2.81	-1282	-8.84	193	1.33	-1538	-10.61
9.0	278	1.92	-1142	-7.88	147	1.01	-1411	-9.73

Final Axial Stresses (cont.)								
Prototype Number	5 years				50 years			
	Max		Min		Max		Min	
	psi	MPa	psi	MPa	psi	MPa	psi	MPa
1.0	-23	-0.16	-1412	-9.74	-21	-0.14	-1442	-9.94
1.1	0.24	0.00	-1549	-10.68	0.14	0.00	-1636	-11.28
2.0	377	2.60	-2415	-16.66	425	2.93	-2370	-16.34
2.0.1	385	2.66	-2240	-15.45	399	2.75	-2094	-14.44
2.1	558	3.85	-2037	-14.05	612	4.22	-1871	-12.90
2.2	547	3.77	-2448	-16.88	608	4.19	-2409	-16.61
2.2.1	497	3.43	-2530	-17.45	536	3.70	-2444	-16.86
2.2.2	302	2.08	-1882	-12.98	417	2.88	-1989	-13.72
3.0	218	1.50	-1770	-12.21	260	1.79	-1862	-12.84
3.1	298	2.06	-1763	-12.16	330	2.28	-1772	-12.22
3.2	308	2.12	-2138	-14.74	346	2.39	-2253	-15.54
4.0	483	3.33	-684	-4.72	637	4.39	-670	-4.62
4.0.1	307	2.12	-1315	-9.07	304	2.10	-1300	-8.97
5.0	593	4.09	-1445	-9.97	796	5.49	-1480	-10.21
5.0.1	218	1.50	-1284	-8.86	204	1.41	-1275	-8.79
5.1	709	4.89	-1420	-9.79	948	6.54	-1444	-9.96
5.2	1314	9.06	-1453	-10.02	1428	9.85	-1542	-10.63
5.2.1	141	0.97	-1442	-9.94	177	1.22	-1388	-9.57
6.0	920	6.34	-1184	-8.17	1166	8.04	-1022	-7.05
6.0.1	423	2.92	-1043	-7.19	577	3.98	-1008	-6.95
6.1	70	0.48	-1607	-11.08	154	1.06	-1684	-11.61
7.0	832	5.74	-1655	-11.41	1059	7.30	-1692	-11.67
7.0.1	276	1.90	-1326	-9.14	197	1.36	-1301	-8.97
7.1	1164	8.03	-1489	-10.27	1401	9.66	-1426	-9.83
8.0	83	0.57	-1367	-9.43	84	0.58	-1373	-9.47
8.1	167	1.15	-1524	-10.51	198	1.37	-1684	-11.61
8.2	227	1.57	-1634	-11.27	264	1.82	-1713	-11.81
9.0	217	1.50	-1503	-10.37	276	1.90	-1584	-10.92

5.2 Recommendations for Crack Mitigation

Through this study several theories for restraint crack mitigation in unbonded post-tensioned slabs can be developed. In the case of the inclusion of pour strips in the design of the slab, the guideline is that if the slab length is longer than 250 ft. (76.2 m) but less than 375 ft. (114.3 m), one centrally located closure strip needs to be provided. However, the analysis presented determined that a slab of 300 ft. (91.44 m) length does not seem to require a closure strip or structural separation, if it is unrestrained by walls.

Although most available literature mentions that the walls closer to the center of the slab are more favorable than the walls in the perimeter of the slab (**Figure 5-61**), through this study it is possible to observe that centrally-located walls induce a larger restraint on the slab; therefore, it is recommended to include a pour strip in the design and a strategically placed bonded reinforcement exclusively for restraint crack mitigation.

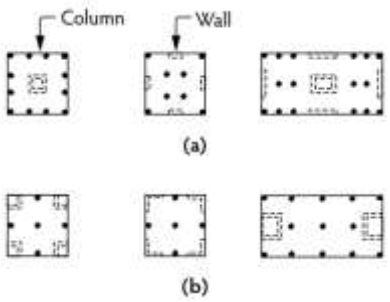

Figure 5-61 Planning in layout of shear walls to mitigate slab crack: (a) favorable arrangement of restraining walls; (b) unfavorable arrangement of restraining walls. (Nawy, 2008)

Partial wall releases at perimeter walls seem to be more efficient in restraint crack mitigation, compared to pour strips. In general pour strips are

recommended in case of having walls closer to the center of the slabs, and corner releases are recommended when having perimeter walls.

An increase in wall-to-slab ratio from 1.5 to 2.5 could exert an average increase of 24% in tensile stresses and a decrease of 14% in precompression, and in some cases it results in the difference in the appearance of restraint cracking. Therefore, it is not recommended to surpass a wall-to-slab ratio of 1.5.

Another recommendation would also be to avoid asymmetrically placed perimeter walls, because they exert larger tensile stresses than the symmetrically placed walls, as observed in the comparison of prototype 7.0 vs. prototype 6.0 (**Figure 5-37**). And in the specific case of floor plan configurations similar to prototype 5.2, it is recommended to structurally separate the slab in parts and make smaller parts conventional reinforced concrete slabs.

Chapter 6. Conclusion

In this study a series of shrinkage and creep calculation models are compared and one of these models is selected to analyze the volume-changing effects in an unbonded post-tensioned slab with different restraint configurations. The conclusions are summarized as follows:

1) The literature review suggests that for shrinkage, the B3 model is the most accurate among the available models based on the current study, while for the calculation of creep effects, the GL 2000 Model is the most appropriate.
2) According to the comparison of these models with shrinkage and creep test studies, the B3 model is the most accurate for shrinkage, while the rest overestimates the shrinkage strain, as reported by the literature. However, in the case of very high strength concretes (above 10,000 psi or 68 MPa), the AASHTO model gives the closest to the creep test results, while the other models also tend to overestimate the results.
3) The accuracy of each shrinkage and creep calculation model would depend on the type of concrete and the effect being calculated.
4) For this specific case of an unbonded post-tensioned concrete slab with a specified concrete strength of 5,000 psi (34.47 MPa), the GL 2000 model is the one that gives the largest results.
5) The results from the GL 2000 model were used for the finite element analysis in this study. The analysis shows that the precompression resulting from the prestressing is spread along the slabs at transfer stage (during construction) but tends to concentrate at the extremes with the passage of time.

6) The effects of restraints in post tensioned slabs tend to increase tension and also compression in concrete, which suggests that they reduce the efficiency and spread of prestressing forces.
7) The comparison between the prototypes indicates that the restraint effects of perimeter walls can produce more cracks, compared to having a long continuous slab without perimeter restraints.
8) However, the results also show that having walls closer to the center of the slab can still reduce the effective precompression and contribute to restraint cracking. The effects of these walls can be effectively mitigated through pour strips.
9) In a slab of 200 ft. (60.96 m) or less that is restrained by perimeter walls, if a pour strip or slab discontinuity is added to the structure, most of the resulting stresses would be mitigated. Furthermore, if a total wall release is applied, no significant stresses would be produced.
10) However, in a slab of 300 ft. (91.44 m) or more that is restrained by perimeter walls, if a pour strip or slab discontinuity is added to the structure, most of the resulting stresses would be mitigated but not entirely. And if a total wall release is applied, no significant stresses would be produced.
11) The minimum wall release allowed for the perimeter wall in the longitudinal direction needs to be more than twice the height of the wall and there is no minimum requirement for the transversal wall, at least for these cases.
12) If the recommendation of a reinforcement-to-concrete area ratio of 0.0018 is followed for temperature reinforcement, it can suffice the restraint-crack prevention.

References

1. Aalami, B. O. & Barth, F. G. (1988). *Restraint cracks and their mitigation in unbonded post-tensioned building structures*: Post-Tensioning Institute.

2. ACI Committee 209. (1992). ACI 209 R-92: Prediction of Creep, Shrinkage, and Temperature Effects in Concrete Structures. *American Concrete Institute Committee*, 47.

3. ACI Committee 209. (2008). ACI 209.2 R-08: Guide for Modeling and Calculating Shrinkage and Creep in Hardened Concrete. *American Concrete Institute Committee*.

4. ACI Committee 211. (2002). ACI 211.1-91: Standard Practice for Selecting Proportions for Normal Heavyweight and Mass Concrete. *American Concrete Institute Committee*, 120-121.

5. ACI Committee 318. (2019). 318-19: Building Code Requirements for Structural Concrete and Commentary. *Technical Documents*. doi:10.14359/51716937

6. Al-Omaishi, N., Tadros, M. K. & Seguirant, S. J. (2009). Elasticity Modulus, Shrinkage, and Creep on High-strength Concrete as Adopted by AASHTO. *PCI journal, 54*(3).

7. Bazant, Z. P. & Baweja, S. (1995). Creep and Shrinkage Prediction Model for Analysis and Design of Concrete Structures: Model B3. *Materials and structures, 28*(6), 357-365. doi:10.1007/BF02473152

8. Bazant, Z. P., Jirásek, M., Hubler, M. & Carol, I. (2015). RILEM draft recommendation: TC-242-MDC multi-decade creep and shrinkage of concrete: material model and structural analysis. Model B4 for creep, drying shrinkage and autogenous shrinkage of normal and high-strength concretes with multi-decade applicability. *Materials and structures, 48*(4), 753-770.

9. CEB-FIP. (1999). Structural concrete-Textbook on behaviour, design and performance updated knowledge of the CEB-FIP model code 1990 Volume 2, basis of design. *Bulletin-FIB*(2).

10. Fanourakis, G. (2017). Validation of the fib 2010 and RILEM B4 models for predicting creep in concrete. *Architecture Civil Engineering Environment, 10*, 95-101.

11. Fanourakis, G. & Ballim, Y. (2003). *Predicting Creep Deformation of Concrete: A Comparison of Results from Different Investigations.* Paper presented at the 11th FIG Symposium on Deformation Measurements, Santorini, Greece.

12. Gardner, N. (2004). Comparison of prediction provisions for drying shrinkage and creep of normal-strength concretes. *Canadian Journal of Civil Engineering, 31*(5), 767-775.

13. Gardner, N. J. & Lockman, M. J. (2001). Design Provisions for Drying Shrinkage and Creep of Normal-Strength Concrete. *ACI Materials Journal, 98*(2). doi:10.14359/10199

14. Goel, R., Kumar, R. & Paul, D. K. (2007). Comparative Study of Various Creep and Shrinkage Prediction Models for Concrete. *Journal of Materials in Civil Engineering, 19*(3), 249-260. doi:10.1061/(ASCE)0899-1561(2007)19:3(249)

15. Guo, G. & Joseph, L. M. (2013). Shortening Estimation for Post-Tensioned Concrete Floors-Part I: Model Selection. *ACI Structural Journal, 110*(1), 8. doi:10.14359/51684326

16. Guo, G., Joseph, L. M. & Bieberly, G. E. (2009). Restraint Design of Cast-in-Place Post-Tensioned Underground Parking Structures. *PTI Journal, 7*(1), 5-18.

17. Le Roy, R., Le Maou, F. & Torrenti, J. M. (2016). Long term basic creep behavior of high performance concrete: data and modelling. *Materials and structures, 50*(1), 85. doi:10.1617/s11527-016-0948-8

18. Nawy, E. G. (2008). *Concrete Construction Engineering Handbook*: Taylor & Francis.

19. Post-Tensioning Institute. (2006). *Post-Tensioning Manual*. Phoenix, Arizona, USA: Post-Tensioning Institute.

20. Precast/Prestressed Concrete Institute. (2004). *PCI Design Handbook: Precast and Prestressed Concrete*. Chicago, Illinois, U.S.A.: Precast/Prestressed Concrete Institute.

21. Shadravan, S., Ramseyer, C. & Kang, T. H.-K. (2015). A long term restrained shrinkage study of concrete slabs on ground. *Engineering structures, 102*, 258-265.

Appendix A. Architectural Configuration Prototypes Selected for Finite Element Analysis

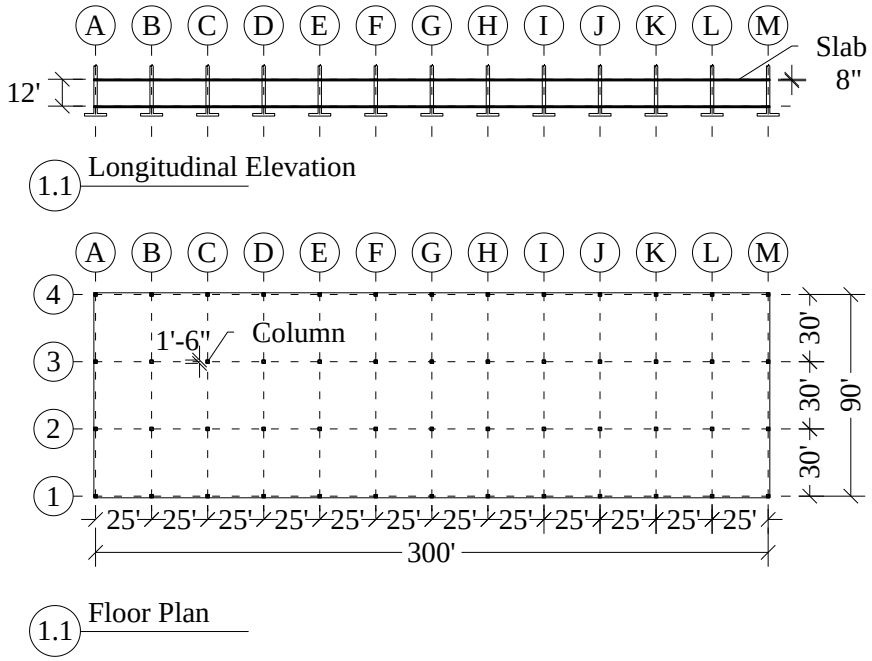

Figure A-1 Prototype 1.1 reference drawings (Note: 1 in. = 25.4 mm; 1 ft. = 304.8 mm)

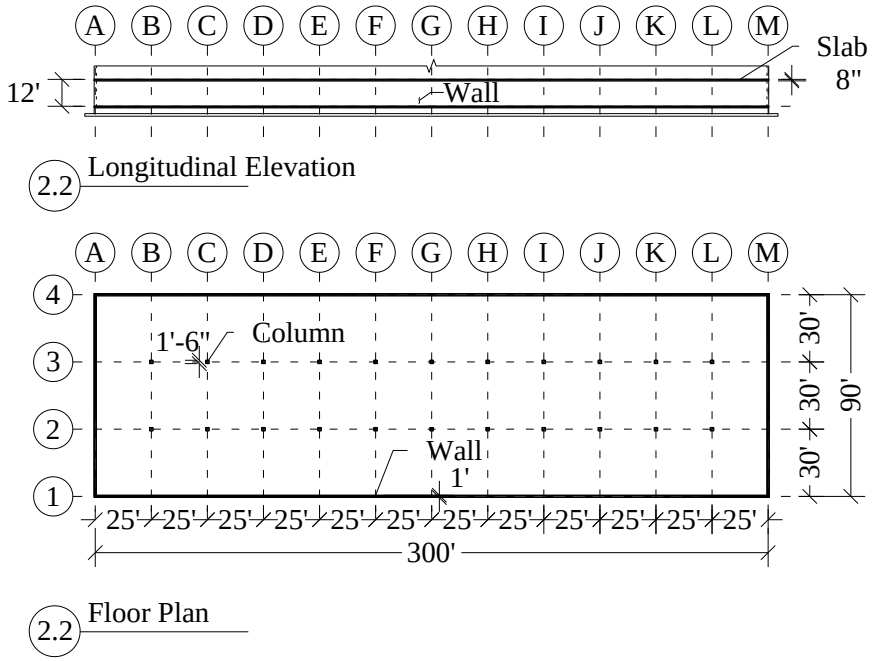

Figure A-2 Prototype 2.2 reference drawings (Note: 1 in. = 25.4 mm; 1 ft. = 304.8 mm)

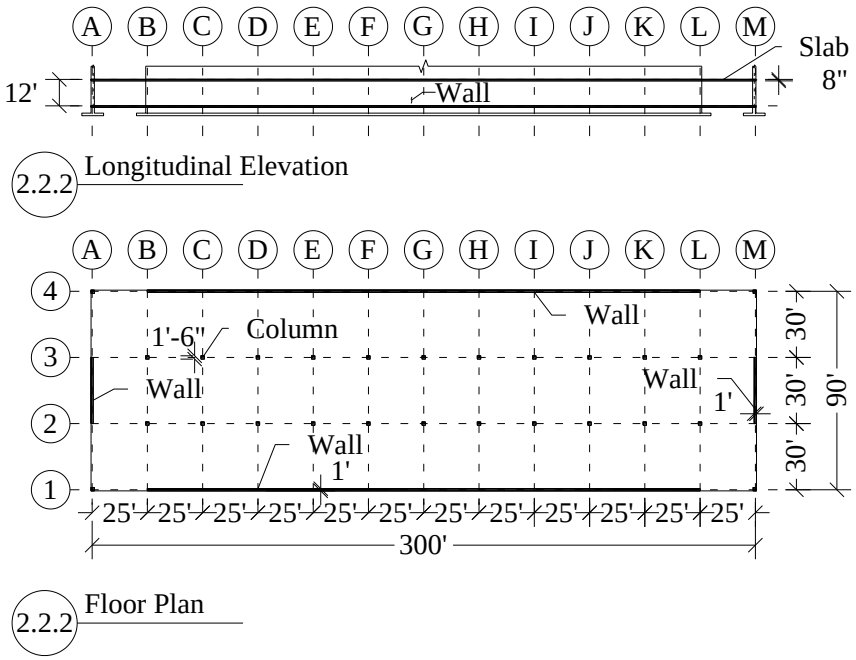

Figure A-3 Prototype 2.2.2 reference drawings (Note: 1 in. = 25.4 mm; 1 ft. = 304.8 mm)

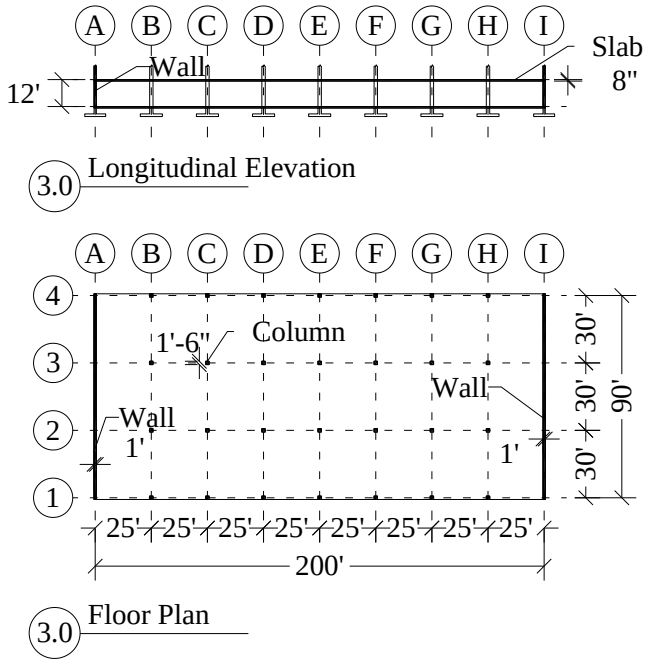

Figure A-4 Prototype 3.0 reference drawings (Note: 1 in. = 25.4 mm; 1 ft. = 304.8 mm)

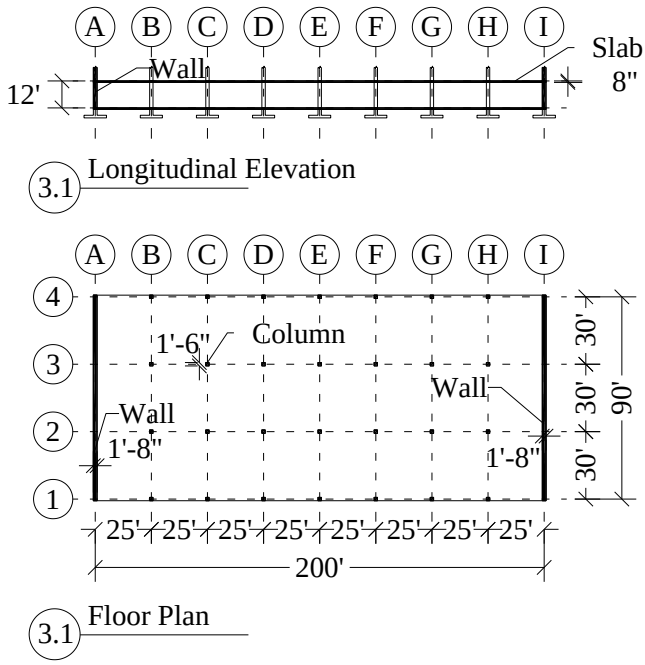

Figure A-5 Prototype 3.1 reference drawings (Note: 1 in. = 25.4 mm; 1 ft. = 304.8 mm)

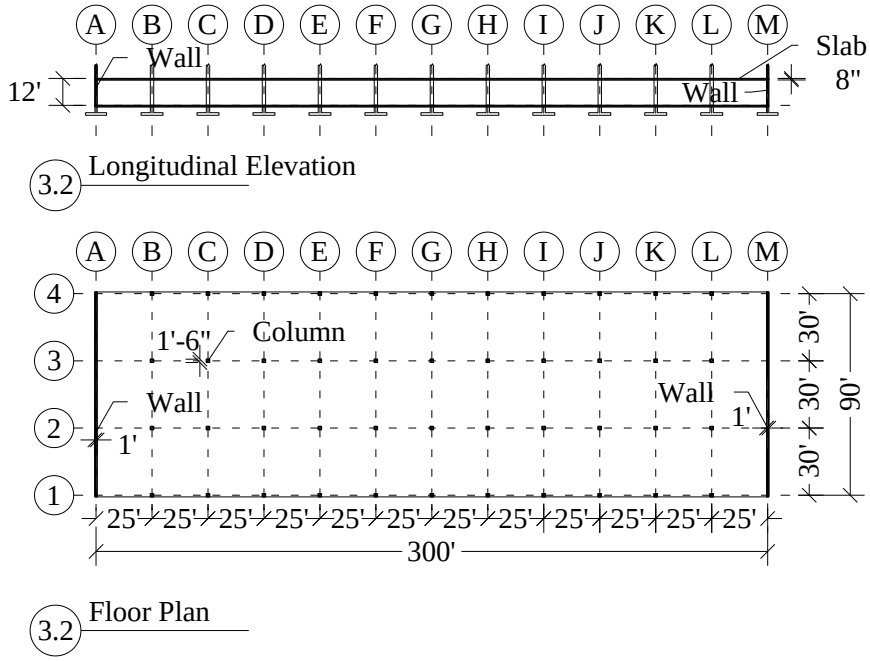

Figure A-6 Prototype 3.2 reference drawings (Note: 1 in. = 25.4 mm; 1 ft. = 304.8 mm)

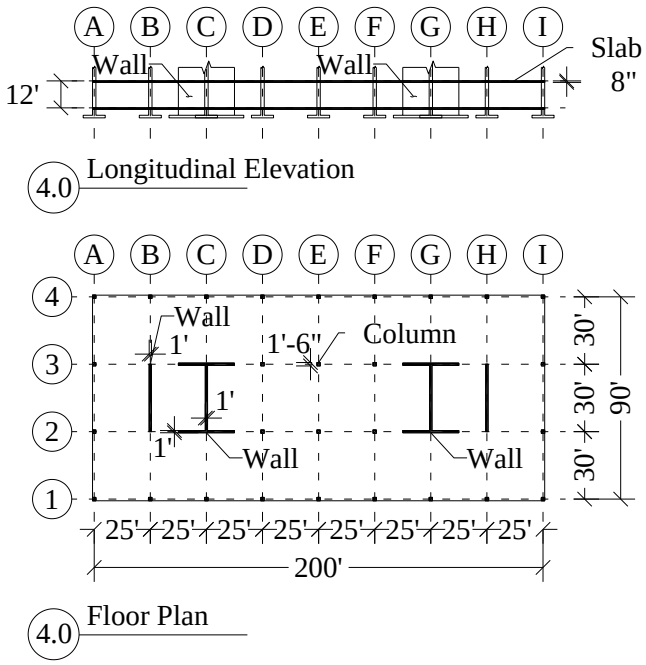

Figure A-7 Prototype 4.0 reference drawings (Note: 1 in. = 25.4 mm; 1 ft. = 304.8 mm)

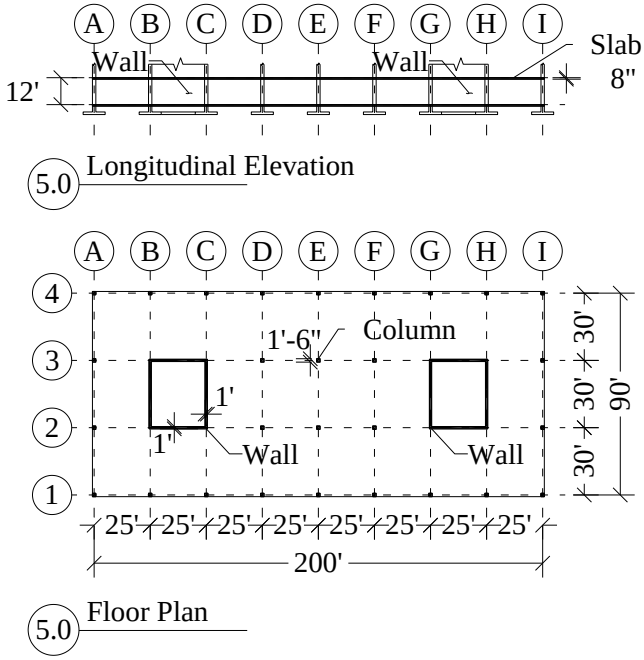

Figure A-8 Prototype 5.0 reference drawings (Note: 1 in. = 25.4 mm; 1 ft. = 304.8 mm)

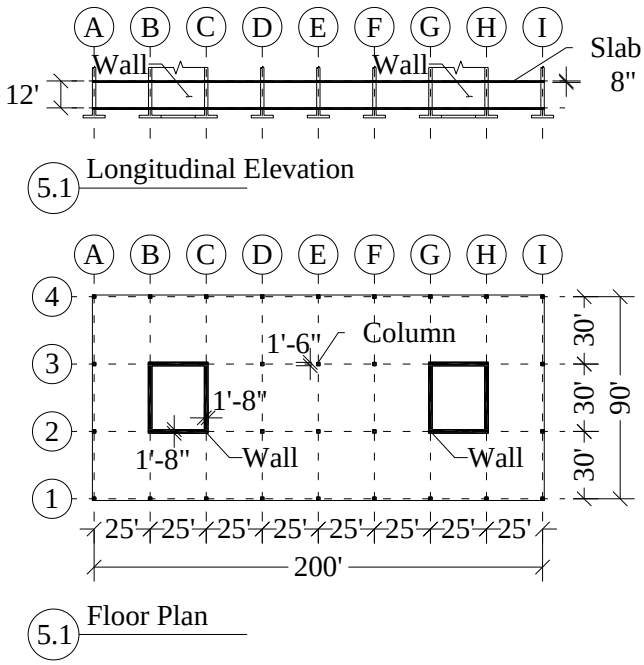

Figure A-9 Prototype 5.1 reference drawings (Note: 1 in. = 25.4 mm; 1 ft. = 304.8 mm)

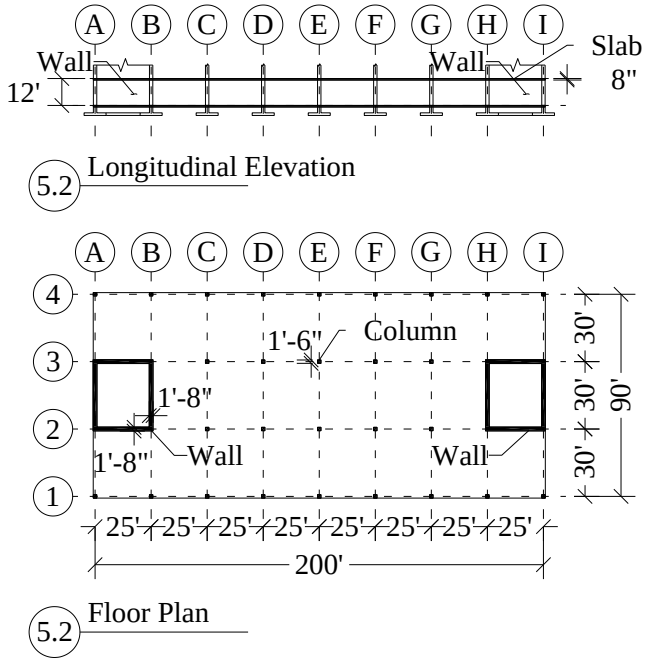

Figure A-10 Prototype 5.2 reference drawings (Note: 1 in. = 25.4 mm; 1 ft. = 304.8 mm)

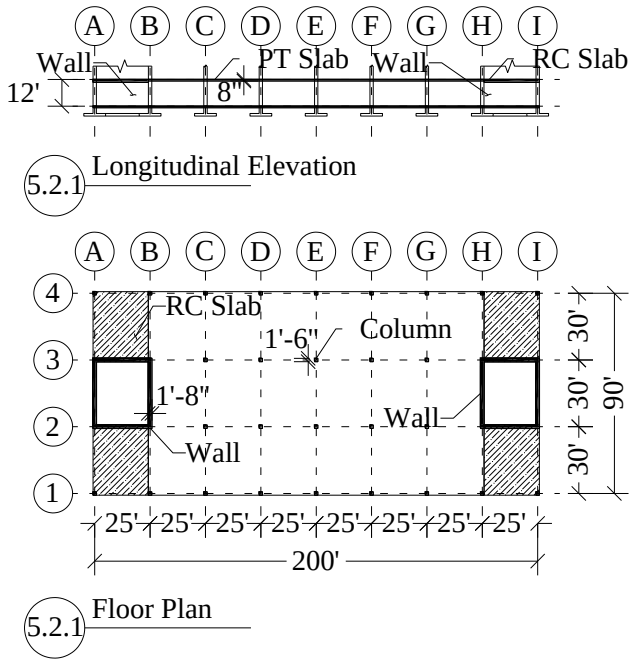

Figure A-11 Prototype 5.2 reference drawings (Note: 1 in. = 25.4 mm; 1 ft. = 304.8 mm)

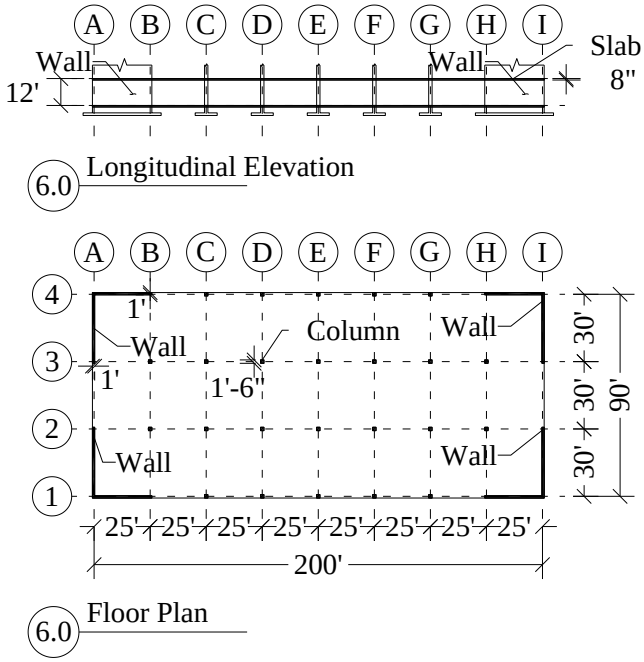

Figure A-12 Prototype 6.0 reference drawings (Note: 1 in. = 25.4 mm; 1 ft. = 304.8 mm)

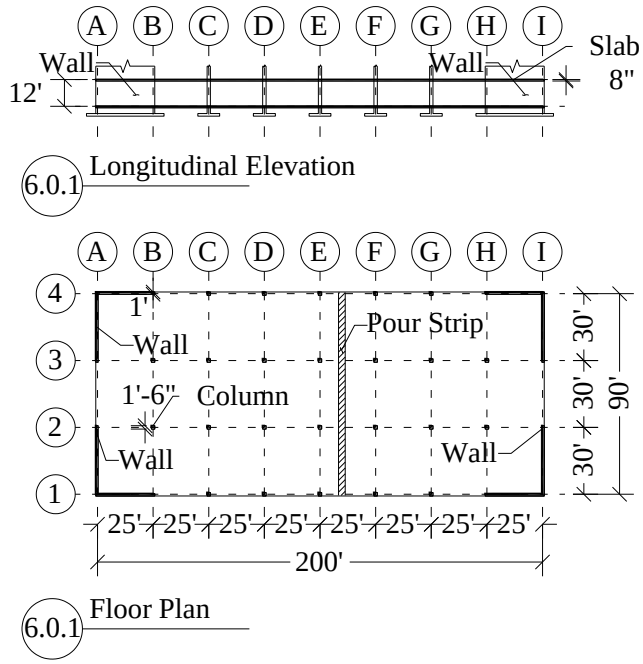

Figure A-13 Prototype 6.0.1 reference drawings (Note: 1 in. = 25.4 mm; 1 ft. = 304.8 mm)

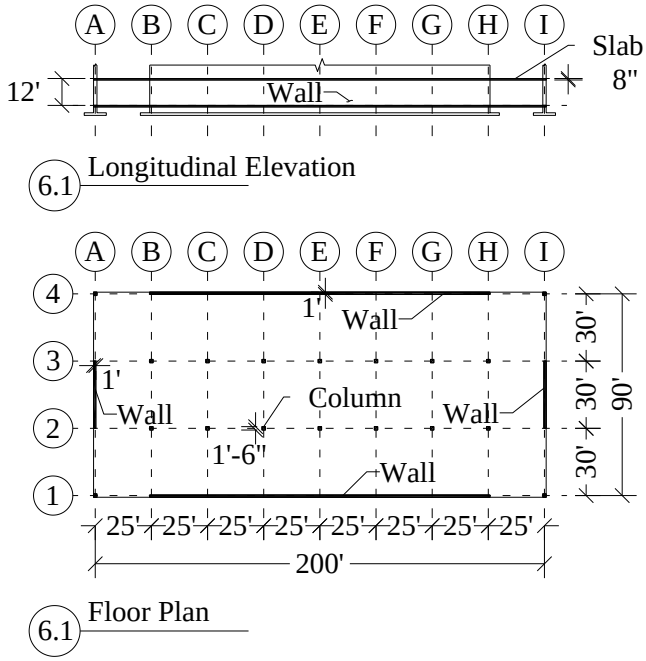

Figure A-14 Prototype 6.1 reference drawings (Note: 1 in. = 25.4 mm; 1 ft. = 304.8 mm)

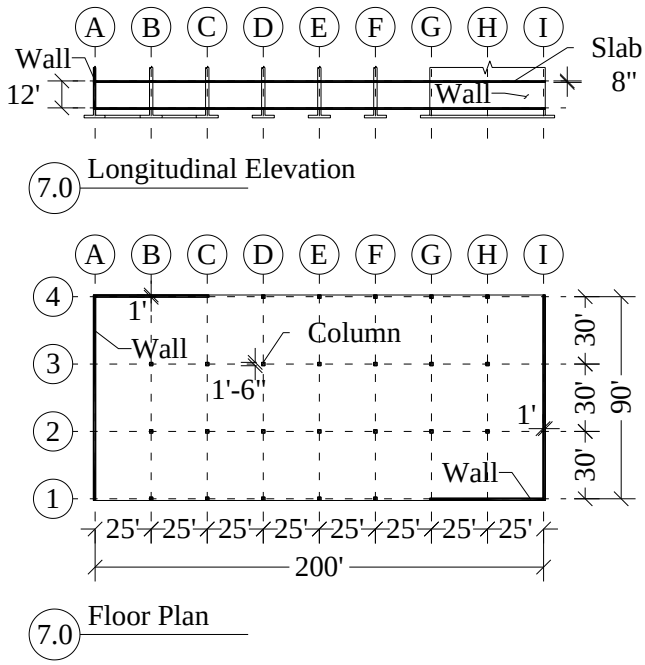

Figure A-15 Prototype 7.0 reference drawings (Note: 1 in. = 25.4 mm; 1 ft. = 304.8 mm)

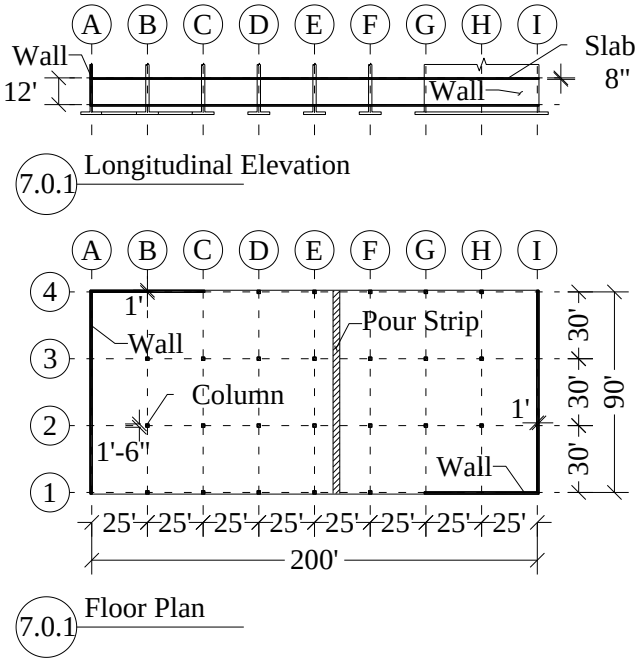

Figure A-16 Prototype 7.0.1 reference drawings (Note: 1 in. = 25.4 mm; 1 ft. = 304.8 mm)

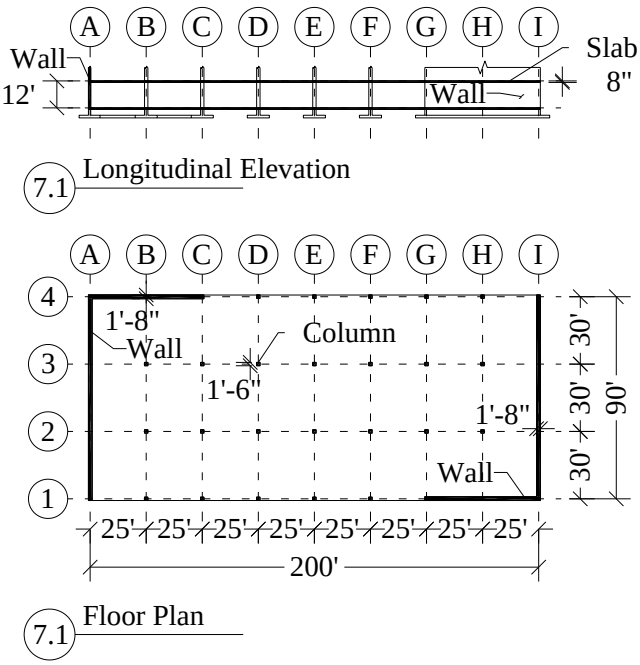

Figure A-17 Prototype 7.1 reference drawings (Note: 1 in. = 25.4 mm; 1 ft. = 304.8 mm)

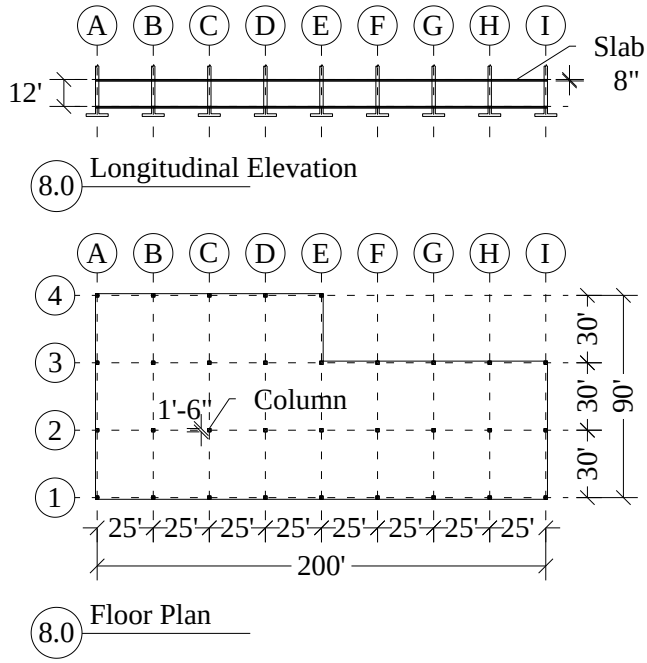

Figure A-18 Prototype 8.0 reference drawings (Note: 1 in. = 25.4 mm; 1 ft. = 304.8 mm)

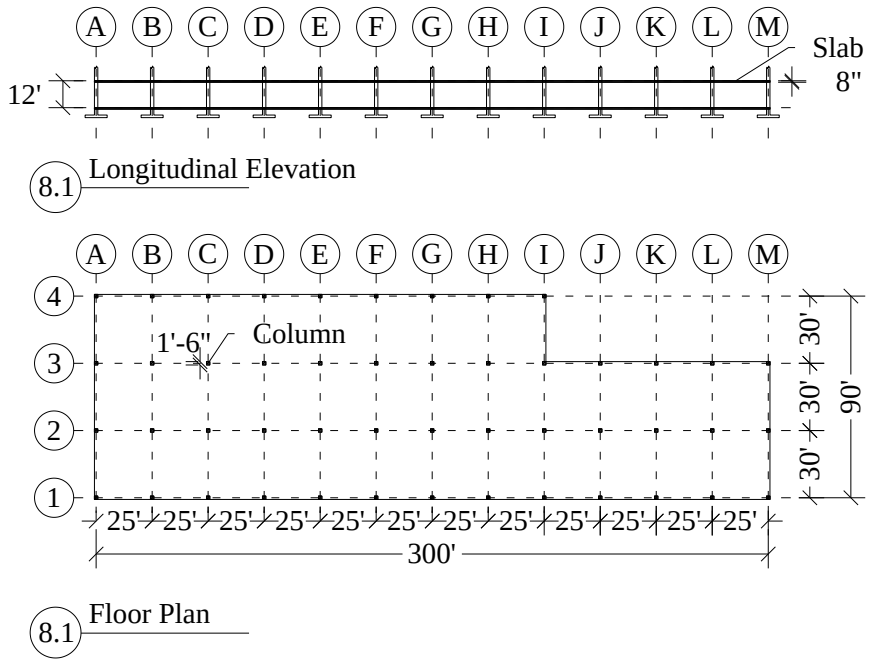

Figure A-19 Prototype 8.1 reference drawings (Note: 1 in. = 25.4 mm; 1 ft. = 304.8 mm)

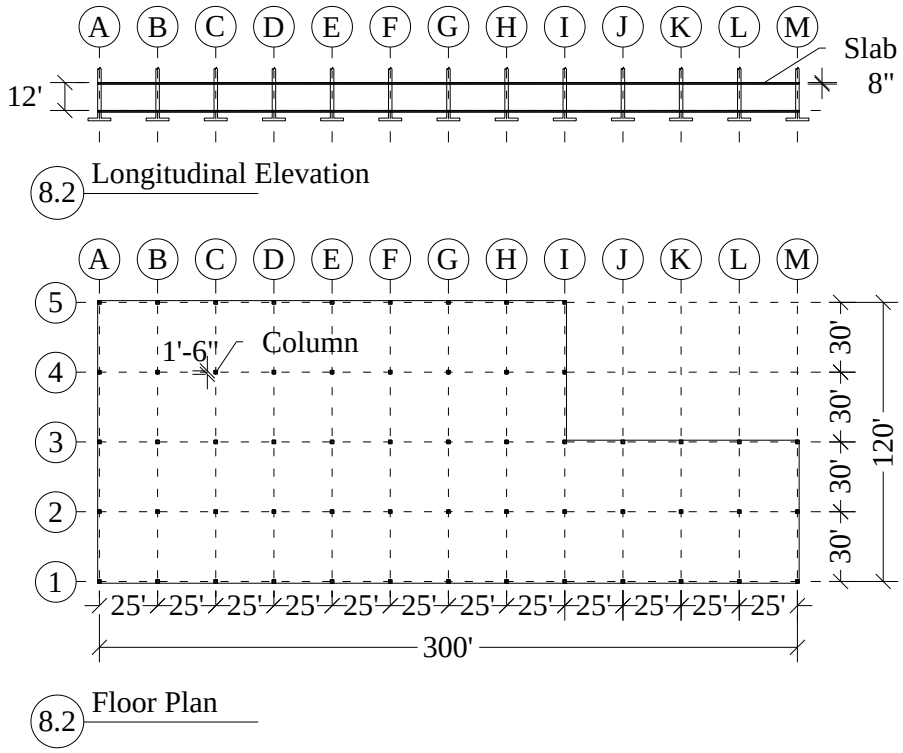

Figure A-20 Prototype 8.2 reference drawings (Note: 1 in. = 25.4 mm; 1 ft. = 304.8 mm)

국 문 초 록

비부착 포스트텐션 슬래브의 수축 예측모델과 구속균열형성에 관한 연구

콘크리트 슬래브는 장·단기 처짐으로 인해 균열이 발생할 가능성이 높으며, 이는 미관상 안좋을 뿐만 아니라 장기 내구성을 저하시킬 우려가 있다. 이에 균열은 사용성 설계에 매우 중요한 고려사항이며 균열 폭을 허용치 이내로 제어해야 한다. 콘크리트 슬래브의 균열은 처짐에 의해서만 발생하는 것이 아니라, 시간 경과와 환경적 요인에 따라 발생하는 콘크리트 크리프, 수축, 체적 변화가 슬래브의 구속조건과 상호작용하여 균열을 야기할 수도 있다. 그러므로, 콘크리트 크리프와 수축에 의한 균열, 이를 저감하기 위한 상세를 구조설계 단계에서 고려해야 한다.

이에 본 연구의 전반부에서는 콘크리트 크리프와 수축에 관한 문헌조사를 통해, 일곱 가지 크리프/수축 예측모델을 기존 실험 연구와 비교하여 각 예측모델의 정확성을 비교·분석하였다. 후반부에서는 크리프/수축 예측모델 계산 결과와 유한요소해석(FEA)을 활용하여

벽체, 기둥, 지연 줄눈 등 구속조건에 따른 비부착 포스트텐션 슬래브의 응력 분포와 균열 발생 양상을 분석하였다.

검토한 일곱 가지 예측 모델 중 GL 2000 모델(Gardner and Lockman, 2001)이 가장 합리적인 크리프/수축 예측 결과를 보여 후반부의 유한요소해석에 적용하였다. 해석 결과, 슬래브의 수축을 방해하는 구속요소가 많을수록 슬래브의 인장응력과 압축응력이 증가하는 경향을 보였으며, 이는 프리스트레스에 의한 압축력의 고른 분포를 방해하고 프리스트레스 효과를 저해한다는 것을 의미한다. 또한, 슬래브 길이는 슬래브를 구속하는 벽체의 유무보다 콘크리트 인장응력에 덜 영향을 주는 것으로 드러났으며, 이는 슬래브가 테두리벽으로 구속되어 있을 때 슬래브 내에 지연줄눈을 두는 것 보다 부분적으로 벽체 구속을 해제하는 것이 슬래브 균열 제어에 더 효과적일 수 있다는 것을 의미한다.

핵심용어: 수축 예측 모델, 포스트텐션 콘크리트 슬래브, 균열 제어, 슬래브 구속효과

학번: 2019-28364